

**LABORATORY SPECTROSCOPIC STUDY OF ACETYLENE AND CARBON
DIOXIDE FOR ATMOSPHERIC REMOTE SENSING PURPOSES**

ABDULLAH AL MASHWOOD
Master of Science (Physics)
Shahjalal University of Science and Technology, 2014

A Thesis
Submitted to the School of Graduate Studies
of the University of Lethbridge
in Partial Fulfillment of the
Requirements for the Degree

MASTER OF SCIENCE

Department of Physics and Astronomy
University of Lethbridge
LETHBRIDGE, ALBERTA, CANADA

© Abdullah Al Mashwood, 2016

LABORATORY SPECTROSCOPIC STUDY OF ACETYLENE AND CARBON
DIOXIDE FOR ATMOSPHERIC REMOTE SENSING PURPOSES

ABDULLAH AL MASHWOOD

Date of defense: January 11, 2017

Dr. Adriana Predoi-Cross Supervisor	Professor	Ph.D.
Dr. Michael Gerken Co-supervisor	Professor	Ph.D.
Dr. Brant Billingham Committee Member	Adjunct Assistant Professor	Ph.D.
Dr. David Naylor Committee Member	Professor	Ph.D.
Dr. Steve Patitsas Chair, Thesis Examination Committee	Associate Professor	Ph.D.

Dedication

This thesis is dedicated to my parents.

Abstract

This thesis presents line-shape studies of carbon dioxide and acetylene, found as trace constituents in planetary atmospheres. The $\nu_1 + \nu_3$ band of acetylene broadened by CO₂ was recorded using a tunable diode laser spectrometer at different pressures (50-750 Torr) and temperatures (216-333 K) to retrieve pressure induced line-shape parameters as well as their temperature dependences.

A second study was carried out to analyze line shapes of the Q-branch transitions of three weak bands (12201-03301, 11101-10002 and 12201-11102) of pure CO₂ recorded at room temperature and different pressures (0.2-140 Torr) using a Fourier transform spectrometer.

For both of these studies a non-linear least squares fitting software was used. A constraint analysis was performed in the CO₂ study in order to reduce correlations between the retrieved line-shape parameters. Furthermore, theoretical calculation of line mixing parameters corresponding to the three bands of CO₂ was performed using Exponential Power Gap (EPG) law.

Acknowledgement

I would like to express my gratitude to everyone who helped and supported me during my graduate studies at University of Lethbridge. I am especially grateful to Dr. Adriana Predoi-Cross for her teachings and supervision during my academic research. At the beginning of my M.Sc. program I took several courses taught by Dr. Adriana. Her lecture sessions helped me to develop a good understanding of the theoretical and experimental aspects of molecular spectroscopy.

I would also like to thank my co-supervisor Dr. Michael Gerken for his encouragement and guidance during my graduate research work period. He always checked my research progress, which helped me to keep track of the timeline of my research and writing the thesis.

I would also like to thank my committee members Dr. Brant Billingham and Dr. David Naylor. Their comments and suggestions during each of my committee meetings gradually developed my presentation skills and helped me to improve my academic performance. I am also thankful to Dr. Malathy Devi of College of William and Mary, Williamsburg, VA, USA, for her advice in carrying out my CO₂ study. Dr. Chris Benner of College of William and Mary is thanked for allowing us to use his spectroscopic analysis software Labfit [74] in our study of carbon dioxide.

During my M.Sc. program, I was supported by the University of Lethbridge and Advanced Methods, Education and Training in Hyperspectral Science and Technology (AMETHYST) program initiated by the Natural Sciences and Engineering Research Council (NSERC) of Canada.

I would like to mention the support and inspiration of my family members during every phase of my graduate life, without which I would not be able to accomplish my thesis.

I consider myself very lucky to have two very helpful co-workers: Hoimonti Rozario, a Ph.D. student and Md. Nazrul Islam, a M.Sc. student of University of Lethbridge.

Last but not least I thank almighty God for giving me the strength and ability to take on this journey towards obtaining a Master degree in Physics.

Table of contents

Dedication	iii
Abstract	iv
Acknowledgement.....	v
List of Figures	ix
List of Tables.....	xii
List of Abbreviations.....	xiii
Chapter 1. Introduction.....	1
1.1. Historical development	1
1.2. Applications of Molecular spectroscopy.....	2
1.3. Tunable diode laser spectroscopy	3
1.4. Fourier Transform Spectroscopy (FTS).....	4
1.5. The acetylene and carbon dioxide molecules.....	4
1.5.1. Acetylene.....	5
1.5.2. Carbon dioxide	6
1.6. Previous laboratory studies on C ₂ H ₂ and CO ₂	8
1.7. Goal and purpose.....	13
Chapter 2. Theoretical background	15
2.1. Electromagnetic radiation	15
2.2. Pure rotation.....	16
2.3. Pure vibration.....	19
2.4. Rotation-vibration transitions.....	22
2.4.1. Dependence of Rotational Constants on Vibration.....	22
2.4.2. Vibrational angular momentum.....	23
2.4.3. Parallel and perpendicular bands.....	24
2.5. Theory of line shapes	25
2.5.1. Spectral line intensity	27
2.5.2. Einstein-A coefficient.....	28
2.5.3. Transition dipole moment	29
2.5.4. Natural broadening of spectral lines.....	29
2.6. Line-shape profiles.....	30
2.6.1. Doppler line profile	30
2.6.2. Lorentz profile.....	31
2.6.3. Voigt profile:	32

2.6.4. Speed-dependent Models	33
2.7. Line mixing	36
2.7.1. Exponential Power Gap (EPG) calculations for line mixing	37
2.7.2. Energy Corrected Sudden (ECS) approximation	39
2.8. Temperature dependence of line parameters.....	40
Chapter 3. Experimental details	41
3.1. TDLS facility at the University of Lethbridge.....	41
3.1.1. Temperature- and pressure-controlled gas cell	44
3.1.2. Reference gas cell.....	45
3.1.3. Detectors.....	46
3.2. Data processing and analysis	46
3.3. Fourier transform spectrometers	48
3.3.1. Working Mechanism of a Michelson Interferometer	49
3.3.2. Fourier transform spectroscopy facility at CLS	51
3.4. Brief description of the Labfit software	52
3.4.1. Implementing Rozenkranz line mixing in Labfit	54
Chapter 4. Line-shape study of Q branches of three weak bands of CO ₂	56
4.1. Data retrieval for CO ₂ spectra:	56
4.2. Retrieved line parameters.....	62
Chapter 5. Line-shape study of the $\nu_1+\nu_3$ band of acetylene broadened by CO ₂	83
5.1. Asymmetry in line-shape parameters.....	96
5.2. Discussion on measurement accuracy.....	97
5.3. Error budget	99
Chapter 6. Conclusion	101
6.1. Summary	101
6.2. Future directions.....	103
References	104

List of Figures

- Fig. 1.1. Fundamental vibrational modes of CO₂ molecule. Here the red (bigger) balls represent Oxygen atoms whereas the black (smaller) ones correspond to Carbon atoms in the molecule. [Photo: <http://chemistry.stackexchange.com/>]7
- Fig. 1.2. Change of CO₂ abundance in terrestrial atmosphere over time. [Photo: <http://climate.nasa.gov/>]8
- Fig. 2.1. Electromagnetic spectrum showing different spectral regions in spectroscopy [57].15
- Fig. 2.2. Classical picture of the molecular vibrations and rotation [57].....23
- Fig. 2.3. Intensity of the incident light is reduced by the sample molecules. [<http://www.brighthub.com/>].....26
- Fig. 2.4. Two main characteristic features of absorption line shapes: the half width at half maximum (γ) and line shift (δ) [56].27
- Fig. 2.5. Spontaneous emission of a photon.28
- Fig. 3.1. Configuration of 3-channel TDLS instrument: (A) Photo of the lab set-up, (B) 1. Vacuum pump, 2. Neslab temperature controller, 3. Gas cylinder, 4 & 5. Fabry Perot interferometer and controller, 6. Detector pre-amplifiers and power source, 7. Wavenumber, 8 & 9. Laser head and controller, 10. Pressure gauge. L₁, L₂ and L₃ are lenses for the detectors. M₁ and M₂ are beam guiding mirrors. D₁, D₂ and D₃ are detectors used. C₁, C₂, C₃ and C₄ correspond to the collimators. S₁, S₂, S₃ and S₄ are the beam splitters [51].43
- Fig. 3.2. Configuration of the temperature and pressure controlled cell: 1. MKS Pressure gauge, 2. Pirani pressure reader, 3. vacuum points, 4. CaF₂ glass windows for the outer chamber, 5. Windows for the gas cell, 6. Thermometers, 7. Body of the gas cell, 8. gas inlet point, 9. Vacuum valve points, 10. Gas outlet point, 11. Air flow port for the outer chamber [51].45
- Fig. 3.3. Layout of a Michelson interferometer. [Photo: <http://www.muelaner.com/laser-interferometers/>]49
- Fig. 3.4. Photo of the high-resolution spectrometer located at the far-infrared beamline at CLS.....51
- Fig. 4.1. (A). Non-linear least squares fit of spectra from 12201-03301 band. The narrowest line represents spectrum recorded at 0.26 Torr pressure and room temperature (296 K). The gradually broadened lines were recorded at increasing pressures up to 140 Torr.....60
- Fig. 4.1. (B). Non-linear least square fit of spectra from 11101-10002 band. The narrowest line represents spectrum recorded at 0.26 Torr pressure and room temperature (296 K). The gradually broadened lines were recorded at increasing pressures up to 140 Torr.....61
- Fig. 4.1. (C). Non-linear least square fit of spectra from 12201-11102 band. The narrowest line represents spectrum recorded at 0.26 Torr pressure and room temperature

(296 K). The gradually broadened lines were recorded at increasing pressures up to 140 Torr.....	62
Fig. 4.2. (A). Difference between line positions from 12201-03301 band and the HITRAN 2012 [77] and GEISA 2015 [88] dataset plotted against m ($m = J$ for Q branch transitions).....	70
Fig. 4.2. (B). Difference between line positions from 11101-10002 band and the HITRAN 2012 [77] and GEISA 2015 [88] dataset plotted against m ($m = J$ for Q branch transitions).....	70
Fig. 4.2. (C). Difference between line positions from 12201-11102 band and the HITRAN 2012 [77] and GEISA 2015 [88] dataset plotted against m ($m = J$ for Q branch transitions).....	71
Fig. 4.3. (A). Line intensities from 12201- 03301 band of CO ₂ . The uncertainties shown as error bars are smaller than the size of the symbols.	72
Fig. 4.3. (B). Line intensities from the 11101-10002 band of CO ₂ . The uncertainties shown as error bars are much larger than the symbols used.....	72
Fig. 4.3. (C). Line intensities from the 12201-11102 band of CO ₂ . The uncertainties shown as error bars are much larger than the symbols used.....	73
Fig. 4.4. Ratio of measured line intensities and the (HITRAN & GEISA) dataset for the three bands.....	74
Fig. 4.5. Broadening coefficients from the three bands of CO ₂ with the associated uncertainties shown as error bars.	75
Fig. 4.6. (A). Comparison of self-broadening coefficients between observed, HITRAN 2012, GEISA 2015 and calculated (EPG) values from 12201-03301 band.	76
Fig. 4.6. (B). Comparison of self-broadening coefficients between observed, HITRAN 2012, GEISA 2015 and calculated (EPG) values from 11101-10002 band.	76
Fig. 4.6. (C). Comparison of self-broadening coefficients between observed, HITRAN 2012, GEISA 2015 and calculated (EPG) values from 12201-11102 band.	77
Fig. 4.7. (A). Calculated (EPG, ECS) self-line mixing coefficients from 12201-03301 band. Uncertainties associated with the observed self-line-mixing values are shown as error bars.....	80
Fig. 4.7. (B). Observed and calculated (EPG, ECS) self-line-mixing coefficients from 11101-10002 band. Uncertainties associated with the observed self-line mixing values are shown as error bars.....	80
Fig. 4.7. (C). Calculated (EPG, ECS) self-line-mixing coefficients from 12201-11102 band.	81
Fig. 5.1. Photo of on-linear fit of P14 line done by applying the Voigt profile in Labfit [74, 75].....	86
Fig. 5.2. Photo of 46 overlaid spectra of P14 line with an overall standard deviation of 0.30.	87

Fig. 5.3. Line position of transitions corresponding to the $\nu_1+\nu_3$ band of acetylene broadened by CO ₂ plotted against index m ($m = -J$ for P branch lines, where J is a rotational quantum number).The uncertainties shown as error bars are much smaller than the size of the symbols.....	88
Fig. 5.4. Residuals of measured line positions and database results for the P branch of $\nu_1+\nu_3$ band of acetylene plotted against m ($m = -J$ for P branch lines, where J is a rotational quantum number [See section 2.4.3]).	89
Fig. 5.5. Comparison of line intensities between experimentally observed and collected values from HITRAN 2012 and GEISA 2015 database. Uncertainties shown as error bars are much smaller than the size of the symbols.	90
Fig. 5.6. Broadening coefficients of absorption lines from $\nu_1+\nu_3$ band of acetylene broadened by CO ₂ . Error bars show uncertainties associated with the retrieved broadening parameters from non-linear least squares fit.	91
Fig. 5.7. Comparison between broadening coefficients from acetylene broadened by CO ₂ study and other studies using different perturbing gases.	92
Fig. 5.8. Shift coefficients of absorption lines from $\nu_1+\nu_3$ band of acetylene broadened by CO ₂ . Uncertainties shown by error bars are much smaller than the symbols used.	93
Fig. 5.9. Comparison between pressure-induced shift coefficients from acetylene broadened by CO ₂ study and other studies using different perturbing gases. ...	94
Fig. 5.10. Temperature-dependence exponents from CO ₂ (present study) and N ₂ [7] broadened Acetylene study, and HITRAN values for air-broadened acetylene (calculated). The observed values are shown with error bars representing uncertainties associated with the non-linear least squares fit.....	95
Fig. 5.11. Temperature-dependence exponent of shift coefficients for CO ₂ and N ₂ perturber. The observed values from the present CO ₂ study are shown with error bars. ..	96
Fig. 5.12. Intensities of all the absorption lines in the spectral region (6471.75 - 6554.11 cm ⁻¹) of P branch of $\nu_1+\nu_3$ band of acetylene. [Photo: www.hitran.org].....	99

List of Tables

Table 1.1. Fundamental modes of vibration of acetylene.	5
Table 1.2. Summary of literature review on the acetylene studies perturbed by different molecules.	11
Table 3.1. Details of the experimental set-up.	52
Table 3.2. Experimental details of the recorded spectra for pure CO ₂ recorded at the CLS using the globar source and a 72.15 m path length. The standard deviation of the recorded temperature was 0.16. The accuracy of the pressure readings was up to 0.05%.	52
Table 4.1. Ro-vibrational and band intensity parameters of the 12201-03301 band of CO ₂ . The error in bracket is one standard deviation.	58
Table 4.2. Ro-vibrational and band intensity parameters of the 11101-10002 band of CO ₂	59
Table 4.3. Ro-vibrational and band intensity parameters of the 12201-11102 band of CO ₂	59
Table 4.4. (a). Line parameters retrieved using Labfit for Q branch lines from 12201-03301 band of CO ₂	65
Table 4.4. (b). Line parameters retrieved for Q branch lines from 11101-10002 band of CO ₂	67
Table 4.4. (c). Line parameters retrieved for Q branch lines from 12201-11102 band of CO ₂	68
Table 4.5. Measured and calculated (EPG) line-mixing coefficients of the three bands. This parameter has a unit atm ⁻¹	78
Table 4.6. Average values of uncertainties associated with the line-shape parameters corresponding to the three band transitions.	82
Table 5.1. Line parameters obtained from the P branch of $\nu_1+\nu_3$ band of acetylene. The errors quoted in parentheses are one standard deviation.	84
Table 5.2. Temperature-dependence exponents for broadening and shift coefficients. The errors quoted in parentheses are one standard deviation.	85
Table 5.3. Average values of uncertainties for each retrieved line-shape parameter.	97

List of Abbreviations

TDLS	Tunable Diode Laser Spectrometer
FTS	Fourier Transform Spectrometer
VI	Virtual Instrument
RMS	Root Mean Squared
SNR	Signal-to-Noise Ratio
ILS	Instrumental Line Shape
ECS	Energy Corrected Sudden Approximation
EPG	Exponential Power Gap Law
IOS	Infinite Order Sudden Approximation
PRT	Platinum Resistance Thermometer
InGaAs	Indium Gallium Arsenide
HITRAN	High Resolution Transmission
GEISA	Gestion et Etude des Informations Spectroscopiques Atmosphériques
OPD	Optical Path Difference
CLS	Canadian Light Source
AER	Atmospheric and Environmental Research

Chapter 1. Introduction

The interaction between light and matter gives information about the identity and structure of the molecules studied. Molecular spectroscopy is one of the most efficient measuring tools in experiments involving light-matter interaction. The basic principle of this technique is straight forward. A light beam of specific frequencies is transmitted through a homogeneous medium of molecular species of interest. Due to the refractive index of the medium some of the incident light is dispersed. At the same time, some of the light frequencies get absorbed by the molecular vibrational and rotational transitions. The spectra of the transmitted light can be studied to extract valuable information about different physical properties (absorbance, concentration etc.) of the medium as well as its molecular structure. With the advent of cutting-edge technologies, the spectroscopic measurements have improved dramatically in terms of signal-to-noise ratio as well as the resolution of the recorded spectra. Molecular spectra recorded at very high resolution can provide signatures of inter-molecular collisional effects (e.g. line mixing, speed-dependent collisions etc.), which were never noticed before.

1.1. Historical development

The very first spectroscopic observations were made by Newton in 1665. He demonstrated that white light disperses into different colors after passing through a prism [1]. But the first use of spectroscopy as an analytical tool was initiated by Bunsen and Kirchhoff in 1860 [2]. Their efforts were mostly concentrated on identifying the elements from the emission spectra of different flammable compounds. In 1885, Balmer first established a mathematical formula that could fit the spectra observed from atomic

hydrogen [3]. This was the very first attempt to relate the experimental observations to theory in the field of spectroscopy. But the theory developed by Balmer could not predict the experimental observations for any other atom or molecule because it was based upon the formulas of classical mechanics. After the development of quantum mechanics by Einstein, Schrödinger, Max Born and many other scientists, theories began to generate more accurate predictions of observed molecular spectra. After 1960, both theoretical computations and experimental techniques improved significantly due to the invention of lasers and computers [4].

1.2. Applications of Molecular spectroscopy

Different experimental techniques have been invented to record and interpret molecular spectra. For example, infrared spectroscopy, Raman spectroscopy and fluorescence spectroscopy are well known techniques in the field of molecular spectroscopy. My present study focuses on the study of absorption spectra of acetylene and carbon dioxide recorded in the near and mid infrared regions, respectively.

Infrared spectroscopy has a broad range of applications in research and development in the areas such as clinical chemistry and disease diagnosis, food science, agriculture, environmental research etc. In clinical chemistry, the diagnosis of disease heavily depends upon the accurate analyses of glucose, blood and urine, generally carrying out by infrared tests [5, 6]. Near infrared spectroscopy (NIR) is used in pharmaceutical laboratories to ensure the manufacture of medicines which meet specifications of best quality [7, 8]. It is also used in the food industry for inspecting the quality and quantity of water, protein, fat and carbohydrates in food samples [9, 10]. In agricultural applications, the commercially grown food grains such as sesame, sun flower, wheat and barley are

analysed using NIR spectroscopic techniques [11, 12]. In environmental research, infrared spectroscopy is used in monitoring pollutants and contaminants in air, water and soil [13]. Atmospheric remote sensing is one of the most advanced fields of science with its far reaching applications in both terrestrial and planetary atmospheric research. Infrared spectroscopy is one of the most efficient methods for measuring the concentrations of major greenhouse gases (CO_2 , CH_4 , N_2O , CO) in the terrestrial atmosphere [14].

1.3. Tunable diode laser spectroscopy

Semiconductor diode lasers play an important role in absorption spectroscopy of molecules in the infrared region. The first semiconductor laser was invented in 1962 by the research group of Robert N. Hall [15]. Previously, scientists had to use spectrographic techniques to generate light frequencies of a desired wavelength range. The first-generation lasers were not very efficient because they had to be kept at a very low operating temperature (~ 77 K) and required very high injection current ($\sim 10^4$ A/cm²) in order to produce a high intensity light beam. But due to the advent of new technologies modern lasers do not have those disadvantages.

Diode lasers have the advantage of tunability over a large frequency range and high output power required for obtaining high-resolution spectra. Usually, in the mid infrared region (2-25 μm) lasers capable of producing 100 mW power are used whereas 10 mW lasers are implemented for near infrared (< 2 μm) spectroscopic measurements. Example of some of the diode lasers include antimonide diode lasers, lead salt diode lasers, monolithic semiconductor lasers etc. High-resolution spectra recorded by tunable diode lasers can help us to understand the complex structure of molecules and the quantum mechanical dynamics of different vibrational and rotational levels.

1.4. Fourier Transform Spectroscopy (FTS)

Fourier transform spectroscopy is a technique for obtaining emission or absorption spectra of a sample, usually in a liquid or gaseous state, by using an interferometer. In case of solids, due to higher concentration of molecules, the absorption spectra becomes saturated. The primary data obtained from an interferometer is called the interferogram, which is converted to a spectrum by performing a Fourier transform.

Although the first interferometer was invented by Michelson in 1881 [16, 17], the very first infrared spectrum using a Fourier-transform interferometer was obtained by Peter Fellgett in 1949 [18]. But this method of spectroscopy only became popular after the invention of fast Fourier-transform algorithm by Cooley and Tukey in 1966 [19]. An FTS instrument has many advantages over other dispersive techniques used in spectroscopy.

The whole spectral region corresponding to the frequency range of the light source is recorded in a single scan. This is called the Fellgett or multiplex advantage [20]. Fourier-transform spectrometers also have the advantage of obtaining the spectrum without any significant throughput or etendue known as the Jacquinot or throughput advantage [21]. A laser is used to accurately determine the displacement of the moving mirror, which in turn generates a highly accurate measurement of frequencies from the spectrum. This is known as the Connes advantage [22]. A detailed description of the Fourier-transform spectrometer used in our study is given in section 3.3.2.

1.5. The acetylene and carbon dioxide molecules

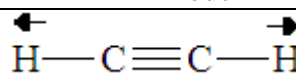
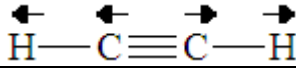
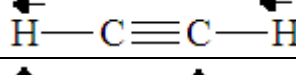
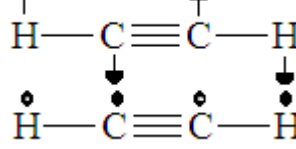
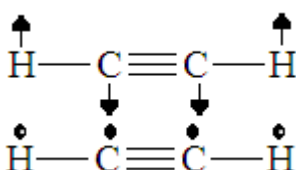
My thesis is based on two projects: (1) Accurate measurement of line-shape parameters and the temperature dependences of the $\nu_1+\nu_3$ band of acetylene broadened by

CO₂ and (2) Theoretical calculation and analyses of line-shape parameters extracted from the 3 weak bands of CO₂ located at around 15 μm.

1.5.1. Acetylene

Acetylene (C₂H₂) is an odorless compound commonly found in gaseous form in the terrestrial atmosphere (up to 0.5 ppb) [23]. It has a C-C triple bond and two C-H single bonds with bond lengths of 106 pm and 120 pm, respectively. It was first discovered by scientist Edmund Davy in 1836 [24]. Acetylene is a linear polyatomic molecule which belongs to the *D_{∞h}* point group. Therefore, it has (3×4)-5 = 7 fundamental modes of vibration. Table 1.1 shows all the different modes with their corresponding location in the electromagnetic spectrum.

Table 1.1. Fundamental modes of vibration of acetylene.

mode		comments	frequency (cm ⁻¹)
	ν_1	Symmetric CH stretching	3372.8
	ν_2	Symmetric CC stretching	1974.3
	ν_3	Anti-symmetric CH stretching	3294.8
	ν_4	'Symmetric' bending	612.9
	ν_5	'Anti-symmetric' bending (Black and white dotted circles represent out-of and into the paper respectively)	730.3

Among the 5 fundamental vibrational (2 of them are degenerate) modes of acetylene, 3 modes (ν_1 , ν_2 and ν_4) are infrared inactive. Only the anti-symmetric stretching

mode (ν_3) and the degenerate anti-symmetric bending mode (ν_5) can be observed using infrared light. Although the symmetric C-H stretching mode (ν_1) is infrared inactive, a combination of ν_1 and ν_3 modes denoted as $\nu_1+\nu_3$, can be excited using infrared light. The resultant vibrational band is located at around $1.5 \mu\text{m}$ (6666.67 cm^{-1}) in the near infrared region of the electromagnetic spectrum.

Acetylene is the second most abundant trace gas constituent after methane found in the upper atmosphere of giant planets (Jupiter: 110 ppb, Saturn: 300 ppb, Uranus: 10 ppb and Neptune: 60 ppb). For methane the concentrations are as follows: Jupiter: 3 ppt, Saturn: 4.5 ppt, Uranus: 20 ppm, Neptune: 0.6 – 5 ppm and Titan: 0.1 - 0.3 ppt) [25]. Acetylene has also been observed in the atmospheres of many stellar and interstellar medium. It is found in the Earth's troposphere [26] and is considered to be a pollutant gas in the urban and industrial environments [27, 28]. Automobile emission causes of air pollution. It is also the main source of acetylene in the atmosphere [28]. The total amount of pollution caused by the automobile exhaustion can be measured by finding the ratio of the total hydrocarbons to acetylene in the atmosphere [29].

1.5.2. Carbon dioxide

Carbon dioxide is a triatomic linear molecule. It is naturally found in gaseous form in the Earth's atmosphere with an average abundance of 405 ppm (increases by an average 1.66 ppm each year). Like acetylene, CO_2 is also a linear molecule and belong to the $D_{\infty h}$ point group. CO_2 has $(3 \times 3) - 5 = 4$ fundamental modes of vibration. All of these vibrational modes are shown in the following figure.

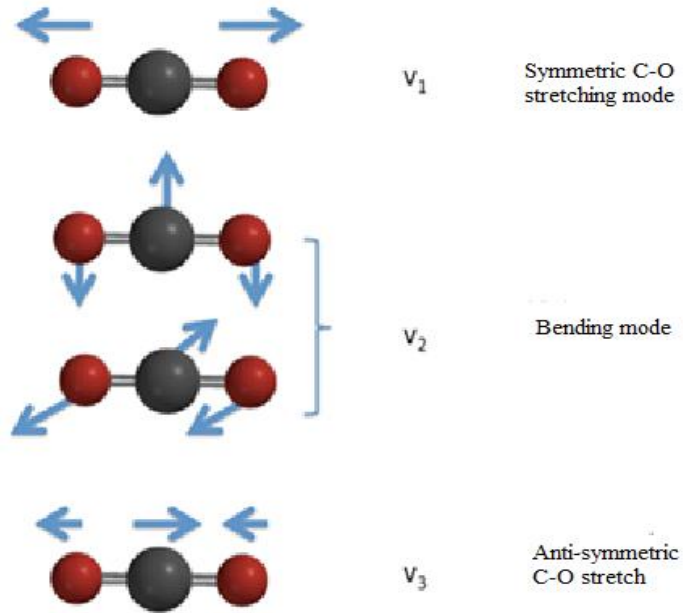


Fig. 1.1. Fundamental vibrational modes of CO₂ molecule. Here the red (bigger) balls represent Oxygen atoms whereas the black (smaller) ones correspond to Carbon atoms in the molecule. [Photo: <http://chemistry.stackexchange.com/>]

The first fundamental vibration is the C-O stretching mode which is located at around 1388 cm⁻¹. The second mode is a degenerate pair of bending vibrations located at 667 cm⁻¹. The third one is the anti-symmetric C-O stretching mode observed at 2349 cm⁻¹.

CO₂ is one of the major greenhouse gases considered to be responsible for global warming. The advent of fossil fuel use in the pre-industrial period has resulted in a gradual increase of CO₂ concentration in the atmosphere (more than 30% increase) and has been one of the most important contributing factors to global warming [30].

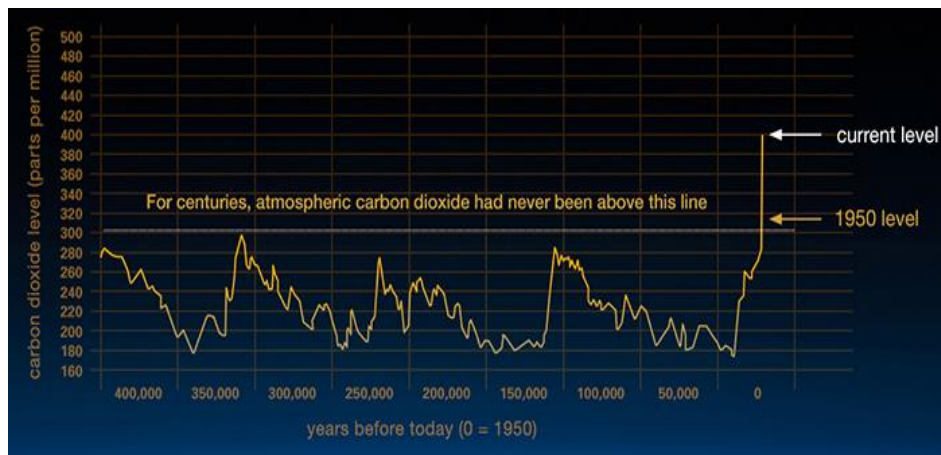


Fig. 1.2. Change of CO₂ abundance in terrestrial atmosphere over time. [Photo: <http://climate.nasa.gov/>]

In the Kyoto protocol the United Nations agreed upon the necessity for monitoring industrial CO₂ emission around the globe [31]. Satellite-based remote-sensing devices such as SCIAMACHY/ENVISAT and TANSO/GOSAT were developed to monitor the CO₂ concentration in air to help identify its impact and take necessary initiatives accordingly [29]. Also, CO₂ can be found in the atmosphere of many other planets. Atmospheres of Mars and Venus have 95.3% and 96.5% CO₂, respectively.

Therefore, CO₂ is considered to be of interest to the spectroscopic community that focuses on atmospheric research of different planets. CO₂ is considered to be a key element in making an atmosphere habitable for any kind of life form [32]. Therefore, spectroscopic studies of CO₂ and CO₂-rich planets like Mars can yield information on how the atmosphere of a habitable planet may evolve due to changes in the CO₂ concentration.

1.6. Previous laboratory studies on C₂H₂ and CO₂

Different bands of acetylene have been studied in laboratories around the globe for the purpose of accurate interpretation of remotely extracted spectral data from terrestrial

and C₂H₂-enriched atmospheres of giant planets (Jupiter, Saturn, Uranus and Neptune) or planets like Mars and Venus.

Two fundamental vibrational modes of acetylene (ν_3 and ν_5) were studied by several research groups for measuring accurate line parameters. The ν_3 band has been studied by Vander Auwera *et al.* [33] and Rinsland *et al.* [34] using two different FTS set ups. They measured the line positions and intensities corresponding to 62 and 86 lines of this band respectively. The pathlengths of the gas cells used in those two studies were different. In case of the study carried out by Vander Auwera *et al.* [33], the length of the gas cell only allowed recording of 62 lines from the ν_3 band of acetylene. Lambot *et al.* [35] first studied the ν_5 band of self-broadened acetylene using a diode laser spectrometer. They also reported calculated values for self-broadened halfwidths obtained using semi-classical impact theories [36]. Varanasi *et al.* [37] also studied this same band using a tunable diode spectrometer. They measured the line intensities and self-broadened halfwidths of several band lines at temperatures ranging from 147 to 295 K using the Voigt profile.

Apart from the fundamental bands, different combination bands of acetylene have been studied by many research groups. Among these bands, the $\nu_1+\nu_3$ has been studied most extensively. The first laboratory study of pressure broadening of the $\nu_1+\nu_3$ band transitions of acetylene mixed with Kr and Xe was carried out by Rank *et al.* [38] in 1960. They observed that the lines corresponding to lower J values had higher broadening coefficients than the lines with higher J . Varanasi and Bangaru [39] also studied this band under temperatures ranging from 171 to 295 K for self-broadening as well as broadening by H₂ gas. Minutolo *et al.* recorded few lines from $\nu_1+\nu_3$ band of pure and foreign-broadened acetylene by using a tunable diode laser spectrometer [40]. Li *et al.* measured the self-broadened halfwidths corresponding to ten P- branch lines from the $\nu_1+\nu_3$ band by using

both Voigt and the Rautian model [41]. Arteaga *et al.* [42] reported an extensive study of the $\nu_1+\nu_3$ band of acetylene broadened by N_2 , D_2 , H_2 , air and different noble gases. They measured the foreign broadening and shift coefficients at room temperature. These authors claimed that the broadening coefficients did not change for different vibrational bands, whereas the shift coefficients vary significantly.

Many other combination bands have also been investigated. The $\nu_1+\nu_5$ band of acetylene broadened by N_2 and air was studied by Pine who used a tunable laser spectrometer for his recordings [43]. Lucchesini *et al.* [44] recorded and analyzed self-broadened acetylene transitions belonging to the 11800 to 12700 cm^{-1} spectral region. Martin *et al.* [45] studied the line-shape parameters corresponding to the $\nu_4+\nu_5$ band transitions of acetylene using the Rautian and Galatry line-shape models. Biswas *et al.* [46] measured line-shape parameters corresponding to the $\nu_1+3\nu_3$ band of pure and N_2 -mixed acetylene using a diode laser spectrometer. They did not find any evidence of velocity-dependent pressure-induced effects in their study. Velocity dependence of intermolecular collisions arise from diffusion or Brownian motion of the molecules. But another study of the same band done by Herregodts *et al.* [47] showed the effect of Dicke narrowing (narrowing of spectral lines due to velocity changing intermolecular collisions) in line shapes recorded at low pressure. Sharma [48] carried out a laboratory study on the same $\nu_1+3\nu_3$ band of pure acetylene gas to measure broadening and shift coefficients.

Few research publications have reported the temperature dependence of line-shape parameters for self- or foreign-broadened acetylene transitions. Two separate spectroscopic studies have been conducted by Hoimonti *et al.* [49] and Campbell *et al.* [50] to measure the temperature-dependent exponents of pressure broadening and shift coefficients

corresponding to the $\nu_1+\nu_3$ band transitions of acetylene broadened by N_2 . The temperature dependence for self-broadening and self-shift coefficients belonging to the $\nu_1+\nu_2+\nu_4+\nu_5$ band has been reported by Povey *et al.* [51].

Table 1.2. Summary of literature review on the acetylene studies perturbed by different molecules.

Band	Brodener	Temperature	Branches	Line shape model	Ref.
ν_3	-	-	R	Voigt	[33]
ν_3	-	RT, 433K	Q	-	[34]
ν_5	C_2H_2	RT (room temperature)	P,R	-	[35]
ν_5	C_2H_2	173K	P,R	Theoretical(semi-classical impact theories)	[36]
ν_5	He, Ar, H_2 , N_2	147-295K	P,Q,R	Voigt	[37]
$\nu_1+\nu_3$	Kr, Xe	-	-	-	[38]
$\nu_1+\nu_3$	C_2H_2	171-295K	P,R	-	[39]
$\nu_1+\nu_3$	C_2H_2 , N_2 , O_2 , CO_2	-	-	-	[40]
$\nu_1+\nu_3$	C_2H_2	RT	P	Voigt, Rautian	[41]
$\nu_1+\nu_3$	N_2 , D_2 , H_2 , air	RT	P,R	Voigt	[42]
$\nu_1+\nu_3$	N_2	213-333K	P,R	Voigt, Hard Collision	[49]
$\nu_1+\nu_3$	N_2	195,373,473K	P,R	Voigt	[50]
$\nu_1+\nu_5$	C_2H_2 , N_2 , Ar	296K	Q,R	Rautian	[43]
$\nu_1+\nu_5$	C_2H_2	-	-	-	[44]
$\nu_4+\nu_5$	CO_2	RT	P,R	Voigt, Rautian, Galatry	[45]
$\nu_1+3\nu_3$	C_2H_2 , N_2	-	-	Voigt	[46]
$\nu_1+3\nu_3$	C_2H_2	-	-	Voigt, Soft and Hard Collision	[47]
$\nu_1+3\nu_3$	C_2H_2	-	P,R	Voigt	[48]
$\nu_1+\nu_2+\nu_4+\nu_5$	C_2H_2	213-350K	R	Voigt, Speed Dependent Voigt	[51]

Several previous studies have been reported that discussed line parameters extracted from the Q branch transitions belonging to numerous bands of CO₂. L. Larrabee Strow and Bruce M. Gentry reported calculations of line-mixing parameters using a fitting law model for Q branch lines in the (11¹0, 03¹0)₁₁-00⁰0 band located at 1932.47 cm⁻¹ [52]. They recorded their spectra with a TDLS (Tunable diode laser spectrometer) instrument at pressures from 100 to 745 Torr. They calculated line-mixing coefficients for up to $J = 50$ using a relaxation matrix formulation. The calculated results agreed with the experiments within a few percent.

A similar study was done by the same group for CO₂ broadened by N₂ for the (11¹0-03¹0)₁-00⁰0 band at 2076 cm⁻¹ [53]. The absorption coefficients measured from their recordings were 65% lower compared to the ones computed from the Lorentzian line-shape approximation. Similar to the previous study, line-mixing coefficients were calculated and used to reproduce the absorption coefficients which agreed well with the observations.

Another study was carried out by M. V. Tonkov *et al.* for pure and mixed CO₂ gas (CO₂-He & CO₂-Ar) in the 580-850 cm⁻¹ range [54]. The spectra were recorded at pressures ranging from 2 Torr to 50 atm. At higher pressures the line shapes of the Q branch lines change significantly which deviates from the Lorentzian approximation. As the study suggests taking into account line-mixing parameter can provide an explanation for such asymmetry.

Predoi-Cross *et al.* reported results from the spectroscopic analyses of pure CO₂ for the Q branch transitions in the three bands 12²0 ← 01¹0, 20⁰0 ← 01¹0 and 11¹0 ← 00⁰0 [55]. A scaling law based on the Energy Corrected Sudden approximation (ECS) was implemented in this study to take into account weak line-mixing effects and to predict transformations of line shapes in these three bands at higher pressures. This is a semi-

empirical method of calculating line mixing parameters, which assumes that intermolecular collisions are not instantaneous. But they have a finite duration. It also considers population transfer due to intermolecular collisions between different rotational levels in a vibrational level. They also described the Exponential Power Gap (EPG) law which has also been implemented in my present study for theoretical computations.

1.7. Goal and purpose

My goal was to study the shape parameters of CO₂ and C₂H₂ spectra in the mid and near-infrared spectral region. I have chosen the $\nu_1+\nu_3$ band of acetylene because of its high intensity or band strength, which makes it an ideal candidate to be used for interpretation of remote sensing observations. In this study CO₂ has been chosen as a perturbing gas, because, in order to accurately measure the concentration of acetylene in an atmosphere, we have to consider how its absorption lines are influenced by the presence of other gases. In planets like Mars or Venus, CO₂ is found as the most abundant gas whereas acetylene is found as a trace constituent. In order to accurately measure acetylene concentration in these planets, we need to study how the lineshapes of acetylene bands are transformed due to the presence of CO₂ molecules as perturbing species.

CO₂ is a linear polyatomic molecule found almost everywhere in the Earth's atmosphere [56]. My second goal was to study three weak bands of CO₂ located at around 15 μm . These bands have very little or no overlapping bands in the electromagnetic spectrum which makes them ideal candidates for accurate measurement of temperature in the terrestrial atmosphere. In order to monitor the concentration of other gases in the air, one needs to know the temperature profiles accurately. So, a careful approach had been

adopted to accurately retrieve and analyze line-shape parameters of pure CO₂ gas for the three bands 12201-03301, 11101-10002 and 12201-11102 (only Q branches).

Sophisticated software capable of fitting several spectra simultaneously (Labfit) was chosen for analyzing both CO₂ and C₂H₂ spectra. It can fit spectral lines using parameters such as position, intensity, broadening, shift as well as their temperature dependence exponents.

I also planned to calculate mixing parameters for the three weak Q branches of CO₂. The principles of semi-empirical exponential energy gap approximation have been implemented to carry out this calculation. The calculated and experimentally measured values have been reported in my thesis in order to demonstrate the suitability of such calculations for similar future studies.

Chapter 2. Theoretical background

[The following discussion is based on the books *Molecular Spectra and Molecular Structure* by Gerhard Herzberg [90], *Fundamentals of Quantum Chemistry* by M. Mueller [57], *Spectra of Atoms and Molecules* by P. F. Bernath [58] and *Collisional Line Broadening and Shifting of Atmospheric Gases* by Jeanna Buldyreva *et al.* [56]]

2.1. Electromagnetic radiation

Every molecular species has the property of absorbing light of different frequencies. Depending on the type of absorption these frequencies may fall into different spectral regions of the electromagnetic spectrum. For example, absorption of light from the visible and ultraviolet region is associated with transition of energy between electronic states of the molecule. Similarly, infrared light is absorbed due to transitions between different vibrational states. Also absorption of microwave radiation corresponds to interaction of light with the rotational states of the molecule.

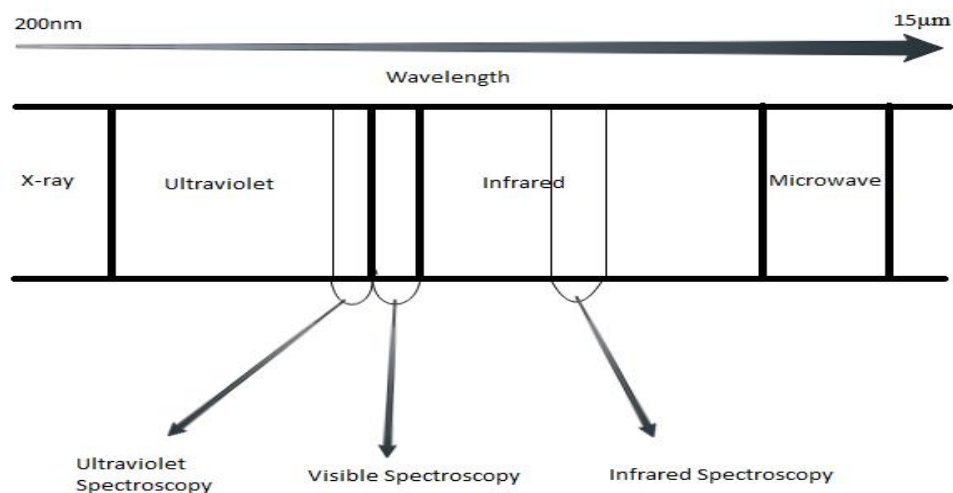


Fig. 2.1. Electromagnetic spectrum showing different spectral regions in spectroscopy [57].

The energy of a photon is related to its wavelength by the following expression,

$$E_{\text{photon}} = \frac{hc}{\lambda}, \quad 2-1$$

with h as Planck's constant and c as the speed of light in cm s^{-1} . λ is the wavelength of the light (cm). The frequency of the radiation is expressed as,

$$\nu = \frac{c}{\lambda} \text{ Hz}. \quad 2-2$$

Thus equation 2-1 can be rewritten as,

$$E_{\text{photon}} = h\nu J. \quad 2-3$$

The absorbed photon energy during any transition between two levels is equal to the energy difference between those levels,

$$\Delta E_{\text{transition}} = E_{\text{photon}}. \quad 2-4$$

Each electronic state in a molecule has many vibrational levels whereas each vibrational state may have rotational states. When a transition occurs between two rotational states of the same vibrational level it is called a rotational transition. On the other hand, when energy is transferred from one rotational state of an initial vibrational level to another rotational state of a final vibrational level, this is called a rotation-vibration transition.

In infrared spectroscopy, molecules can rotate and vibrate simultaneously. But it is often beneficial to start theoretical discussions considering them as independently occurring phenomena and subsequently discussing the rotation-vibration coupling.

2.2. Pure rotation

Pure rotational spectra occur in the microwave frequency region. Any molecule that has a permanent dipole moment will exhibit this type of transitions. CO_2 and C_2H_2 are polyatomic linear molecules, whose rotational transitions are mechanically equivalent to

those of simple diatomic molecules [57]. However the moment of inertia, I in the case of a polyatomic molecule has to be determined considering more than two atoms. The expression for I is,

$$I = \frac{\sum_{i<j} m_i m_j r_{ij}^2}{\sum_i m_i}, \quad 2-5$$

where m_i and m_j are masses of each pair of atoms in the molecule and r_{ij} represents the distance between them. For the purpose of quantum mechanical treatment, the rotation in a diatomic molecule can be compared with the motion of a rigid rotor. For a rigidly rotating diatomic molecule the Schrödinger equation can be written as

$$\frac{\hat{j}^2 \Psi}{2I} = E \Psi, \quad 2-6$$

which can be rewritten as

$$\frac{\hat{j}^2 \Psi}{2I} = \frac{J(J+1)\hbar^2 \Psi}{2I} = BJ(J+1)\Psi, \quad 2-7$$

where \hat{j} is the angular momentum operator and I is the moment of inertia associated with the rotational axis of the molecule. B is called the rotational constant. Thus the rotational energy levels are quantized and can be expressed as

$$F(J) = BJ(J+1), \quad 2-8$$

where,

$$B = \frac{h}{8\pi^2 c I} \times 10^{-2} \text{ (cm}^{-1}\text{)}. \quad 2-9$$

The rotational selection rule which ensures non-zero intensity of the transitions is given as

$$\Delta J = \pm 1, \quad 2-10$$

where $\Delta J = +1$ corresponds to absorption of energy during transition whereas $\Delta J = -1$ represents emission of radiation.

The transition frequency is calculated from the difference of energy between two rotational levels. For instance, the frequency of an absorbed photon in a transition from J to $J+1$ level can be calculated as,

$$\nu_{J+1 \leftarrow J} = F(J') - F(J'') = B(J+1)(J+2) - BJ(J+1) = 2B(J+1) \text{ cm}^{-1}, \quad 2-11$$

where, J'' represents the lower state and J' represents the upper state energy level. $2B$ is the spacing between consecutive transitions. Whether the transition is occurring in the microwave or the millimeter or far-infrared region, depends on the values of B and J . The value of B corresponding to most polyatomic linear molecules is very small. For example, CO_2 has an experimentally measured rotational constant of 0.39021 cm^{-1} . Therefore, the rotational transitions of these molecules occur in millimeter wave or microwave frequency region.

But the rigid-rotor approximation does not completely model the rotational motion of molecules. The bonds between atoms in a molecule are not rigid. They behave more like springs. As a result, we have to consider the effect of centrifugal distortion in rotational motion of molecules. The speed of rotational motion increases as we consider higher J levels. Due to centrifugal distortion, the higher J levels move radially outward. Therefore, the higher J levels gradually get closer to each other, making the value of B smaller. To take into account this J -dependence of the rotational constant, a correction term is added to the right hand side of equation 2-8 and 2-11 as,

$$F(J) = BJ(J+1) - D[J(J+1)]^2, \quad 2-12$$

$$\nu_{J+1 \leftarrow J} = F(J') - F(J'') = 2B(J+1) - 4D(J+1)^3, \quad 2-13$$

where, D is called the centrifugal distortion constant. The consequence of considering this constant is that the rotational transitions in the molecule are no longer equidistant. This is

a better approximation than the rigid rotor one, thus allowing us to predict the position of the rotational transitions more accurately.

2.3. Pure vibration

In order to describe the theoretical aspects of vibrational motion of the molecules, it is helpful to understand first the different degrees of freedom that molecules have. Any molecule with N atoms has up to $3N$ degrees of freedom, among which, 3 are due to the translational motion of the molecule. Another 3 (for non-linear molecules) or 2 (for linear molecules) degrees of freedom are associated with rotational motion. Thus, for linear polyatomic molecules, $3N-5$ degrees of freedom correspond to vibrational motion. These are often called normal modes of vibration of the molecule.

In case of a diatomic molecule the vibrational motion can be modeled with a ball and spring approximation, i.e., as a simple harmonic oscillator. The quantum mechanical approach towards finding vibrational energy level eigenvalues is by solving the time-independent Schrödinger equation expressed as,

$$\hat{H}\Psi = E\Psi . \quad 2-14$$

In order to solve this equation we consider the Born-Oppenheimer approximation which assumes that the electrons move much faster than the vibrating nuclei. Thus, their corresponding energy states can be treated independent of each other which enable us to write the wavefunction as the product of the nuclei and electronic state functions.

$$\Psi = \Psi_{el} \Psi_n . \quad 2-15$$

Using the one-dimensional case of a simple harmonic oscillator we can solve the above equation. The derived energy-level expression for the vibrational motion of a diatomic molecule is as follows,

$$E(v) = hf\left(v + \frac{1}{2}\right), \quad 2-16$$

where, h is Planck's constant, f is the frequency of vibration corresponding to the oscillator and v is the quantum number for vibration. The above expression shows that the vibrational energy levels are separated from each other by an equal distance.

During each vibrational transition the molecule must undergo a change in the total dipole moment. This leads to the selection rule for vibrational transition, which is the condition for allowed transitions.

$$\Delta v = \pm 1. \quad 2-17$$

Like the rigid-rotor approximation, the simple harmonic oscillator model also does not accurately describe the vibrational motion of the molecule. The simple harmonic model cannot explain the dissociation of a molecule into its constituent atoms. In order to explain dissociation, a molecule can be modeled as an anharmonic oscillator.

The solutions to the Schrödinger equation using the anharmonic oscillator model yield a new energy level expression for vibrational motion of molecules

$$E(v) = hv_e\left(v + \frac{1}{2}\right) - hv_e x_e\left(v + \frac{1}{2}\right)^2 + \dots \quad 2-18$$

where x_e is the anharmonicity constant whereas the subscript e represents equilibrium state of the molecule. A consequence of taking into account anharmonicity is that the vibrational energy levels are no longer equidistant. In fact, they tend to get closer to each other with increasing v . It is a tradition in molecular spectroscopy to express terms in the units of cm^{-1} . Therefore equation 2-18 can be rewritten as,

$$G(v) = \frac{E(v)}{hc} = \tilde{\nu}_e\left(v + \frac{1}{2}\right) - \tilde{\nu}_e x_e\left(v + \frac{1}{2}\right)^2 + \dots \quad 2-19$$

The above equation can be modified to implement the case of a polyatomic linear molecule. For a polyatomic linear molecule, the wavefunction can be expressed as the product of $(3N-5)$ state functions each corresponding to a specific mode of vibration

$$\Psi = \Psi_1(Q_1)\Psi_2(Q_2)\dots\Psi_{3n-5}(Q_{3n-5}). \quad 2-20$$

The total energy of vibration in the molecule can be expressed as the sum of all the energies corresponding to the 3N-5 vibrational modes

$$G(v_1, v_2, \dots) = \tilde{\nu}_1(v_1 + \frac{1}{2}) + \tilde{\nu}_2(v_2 + \frac{1}{2}) + \dots + \tilde{\nu}_{3n-5}(v_{3n-5} + \frac{1}{2}). \quad 2-21$$

Polyatomic linear molecules can have degenerate energy levels (e.g., bending motion of a molecule in a horizontal or a vertical plane). This degeneracy of different vibrational modes can be taken into account by rewriting the above expression as,

$$G(v_1, v_2, \dots) = \sum_1^{3n-5} \tilde{\nu}_i(v_i + \frac{d_i}{2}), \quad 2-22$$

where, d_i corresponds to the degeneracy of the i^{th} mode of vibration. The sum is over all 3N-5 vibrational modes in a polyatomic linear molecule. Equation 2-22 is valid only for the simple harmonic model. One of the consequences of considering anharmonicity is that not only fundamental transitions but their overtones are also possible, i.e., $\Delta v = \pm 1, \pm 2, \pm 3$ are allowed.

Similarly, transition between states corresponding to a combination of two or more vibrational modes is also possible. Thus the final energy level expression for an anharmonic oscillator model of a polyatomic linear molecule would have more than one vibrational quantum number.

$$G(v_1, v_2, \dots) = \sum_1^{3n-5} \tilde{\nu}_i(v_i + \frac{d_i}{2}) + \sum_i \sum_{k \geq i} x_{ik}(v_i + \frac{d_i}{2})(v_k + \frac{d_k}{2}) + \dots \quad 2-23$$

where, x_{ik} is the anharmonicity constant. In a combined vibrational transition, two or more modes of vibration are excited by a single photon simultaneously.

2.4. Rotation-vibration transitions

In infrared spectroscopy molecules vibrate and rotate simultaneously. So the total energy of a molecule undergoing simultaneous rotation and vibration would be the sum of rotational and vibrational energy.

$$T = G(v_1, v_2, \dots) + F(J), \quad 2-24$$

where G represents vibrational energy given by equation 2-23 and F represents the rotational energy expressed by equation 2-12.

2.4.1. Dependence of Rotational Constants on Vibration

The rotational constants (B and D) corresponding to different vibrational levels are slightly different from each other. This is because the values of these constants depend upon the value of the moment of inertia I , as shown in equation 2-9. And for a specific vibrational level the value of I is slightly different than its average value at the equilibrium position. This dependence of rotational constants on the molecular vibrations can be expressed by the following two expressions,

$$B_v = B_e - \sum_i \alpha_i \left(v_i + \frac{d_i}{2} \right), \quad 2-25$$

$$D_v = D_e - \sum_i \beta_i \left(v_i + \frac{d_i}{2} \right), \quad 2-26$$

where $d_i = 1$ represents non-degenerate levels and 2 represents levels with double degeneracy. The values of the constants α_i and β_i are much smaller than the equilibrium values of the rotational constants B_e and D_e , respectively. Therefore, we can rewrite equation 2-12 in terms of the new rotational constants B_e and D_e as,

$$F(J) = B_v J(J+1) - D_v [J(J+1)]^2. \quad 2-27$$

2.4.2. Vibrational angular momentum

Dr. Peter Bernath in his book “*Spectra of atoms and molecules*” gave a comprehensive description of the concept of vibrational angular momentum and its application in molecular spectroscopy [58]. Generally any linear polyatomic molecule would have degenerate modes of vibration arising from its bending motion. For example, the CO₂ molecule has $3 \times 3 - 5 = 4$ fundamental modes of vibration, 2 of them being the symmetric and antisymmetric stretching and the remaining two are doubly degenerate bending modes. Classically, these degenerate vibrations can be pictured as oscillations in the mutually perpendicular directions x and y, which in turn creates an overall rotation of the molecule about the z direction.

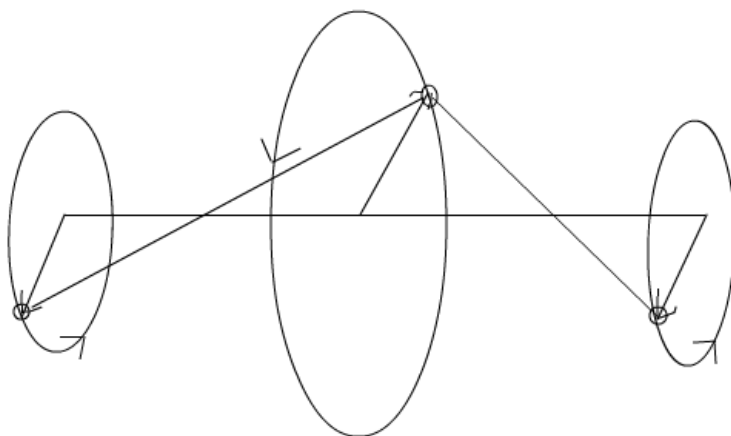


Fig. 2.2. Classical picture of the molecular vibrations and rotation [58].

In quantum mechanics this angular motion is quantized and the possible angular momentum values for this motion is equal to $\pm l\hbar$. l is called the vibrational angular momentum. For a degenerate vibrational level ν the possible values of l are as follows,

$$|l| = \nu, \nu-2, \nu-4 \dots 0 \text{ or } 1. \quad 2-28$$

Therefore, the total angular momentum in a molecule can be given as,

$$\vec{J} = \vec{R} + \vec{l} , \quad 2-29$$

where, R and l are rotational and vibrational angular momentum, respectively.

Taking into account vibrational angular momentum l , the expression 2-27 can be rewritten as,

$$F(J, l) = B_v[J(J+1) - l^2] - D_v[J(J+1) - l^2]^2. \quad 2-30$$

Putting the values of $F(J, l)$ and $G(v_1, v_2, \dots)$ in equation 2-24 the expression for the total energy of a ro-vibrational system can be given as,

$$T = \sum_{i=1}^{3n-5} \omega_i \left(v_i + \frac{d_i}{2} \right) + \omega_i \sum_i \sum_{k \geq i} x_{ik} \left(v_i + \frac{d_i}{2} \right) \left(v_k + \frac{d_k}{2} \right) + \sum_i g_{ii} l_i^2 + B_v J(J+1) - D_v [J(J+1)]^2 , \quad 2-31$$

In this expression, $d_i = 1$ means non-degenerate and $d_i = 2$ means doubly degenerate vibrational level. In case of a non-degenerate level $l_i = 0$ as well as $g_{ik} = 0$. g_{ik} are small constants with the same order of magnitude as x_{ik} . ω_i is the vibrational angular frequency corresponding to the i^{th} energy level.

2.4.3. Parallel and perpendicular bands

Ro-vibrational transitions can be classified into two types, parallel and perpendicular band. During an absorption of a photon, molecules undergo a change in total dipole moment. If the direction of this dipole moment change is parallel to the molecular axis, the transition would belong to a parallel band and if perpendicular, then it would belong to a perpendicular band. A parallel band comprises of 2 types of branches denoted by the letters P and R, whereas the perpendicular band has 3 types of branches: P, Q and R. This branching of ro-vibrational bands can also be explained by the selection rules. In ro-vibrational spectroscopy only the allowed transitions can be observed, i.e. transitions

that abide by the vibrational and rotational selection rules. For $\Delta J = \pm 1$, only P ($\Delta J = -1$) and R ($\Delta J = +1$) branches can be observed, whereas $\Delta J = 0, \pm 1$ gives rise to observable P, Q ($\Delta J = 0$) and R branches in the ro-vibrational band.

From equation 2-31 we can derive expressions for transition frequencies corresponding to P, Q and R branches. For example, the P and R branches would have the following expressions for transitions from v'' to the v' vibrational level.

$$\nu_P(v', J-1 \leftarrow v'', J) = \nu_0 - (B'_v + B''_v)J + (B'_v - B''_v)J^2, \quad 2-32$$

$$\nu_R(v', J+1 \leftarrow v'', J) = \nu_0 + 2B'_v + (3B'_v - B''_v)J + (B'_v - B''_v)J^2, \quad 2-33$$

where, ν_0 is the band origin. The above two expressions can be rewritten in a single form as below,

$$\nu = \nu_0 + (B'_v + B''_v)m + (B'_v - B''_v)m^2, \quad 2-34$$

where, $m = -J$ represents P branch and $m = J+1$ corresponds to R branch transitions.

2.5. Theory of line shapes

Suppose monochromatic light of frequency ν and initial intensity I_0 passes through a temperature- and pressure-stabilized gas cell. The cell is filled up with a homogeneous gas medium.

According to Beer-Lambert law [59, 60, 61], light that comes out of the cell would have a reduced intensity due to absorption by the gas medium. This can be expressed by the following expression,

$$I(\nu) = I_0(\nu)e^{-K(\nu)L}, \quad 2-35$$

where, I is the reduced light intensity and L is the length of the gas cell. $K(\nu)$ represents the spectral absorption coefficient.

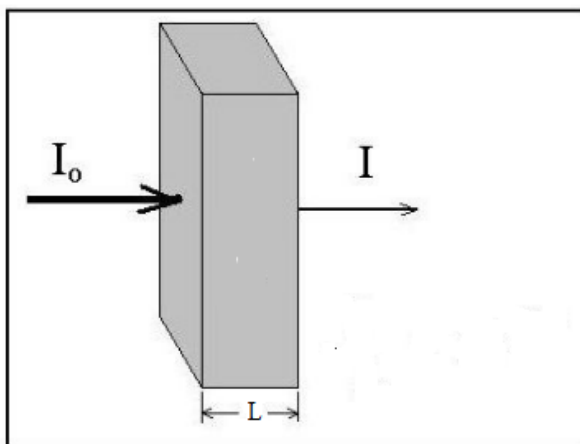


Fig. 2.3. Intensity of the incident light is reduced by the sample molecules.
 [http://www.brighthub.com/]

Equation 2-35 can be rearranged to express $K(\nu)$ as,

$$K(\nu) = \frac{1}{L} \ln \left[\frac{I_0(\nu)}{I(\nu)} \right]. \quad 2-36$$

If the frequency ν is close to the energy difference between any two ro-vibrational states of the molecular species present in the gas medium, then the light will be strongly absorbed. And the molecule will be excited from a lower to a higher energy state. By varying the frequency ν of the incident light, we can record spectra of all the possible ro-vibrational transitions occurring in a region of the electromagnetic spectrum. These transitions are called spectral lines.

The absorption coefficient $K(\nu)$ and the line-shape function $F(\nu)$ corresponding to an isolated line are related by the expression,

$$K(\nu) = AF(\nu - \nu_0), \quad 2-37$$

where ν_0 is the center of the spectral line. $F(\nu - \nu_0)$ is a normalised function with a normalisation factor A .

$$A = \int_{-\infty}^{+\infty} K(\nu) d\nu. \quad 2-38$$

This integral form of absorption corresponds to the number of molecules in a unit volume.

A spectral line is characterized by two line-shape features, namely the half width at half maximum (γ) and the pressure shift of the line from its center (δ). Depending upon the pressure and temperature these two parameters can change noticeably, thus transforming the line shape of the spectral line [56]. This is why it is important to discuss the different line-shape profiles which can be used to reproduce the absorption line accurately. But before starting this discussion, it would be appropriate to define few spectroscopic terms associated with the spectral line intensity.

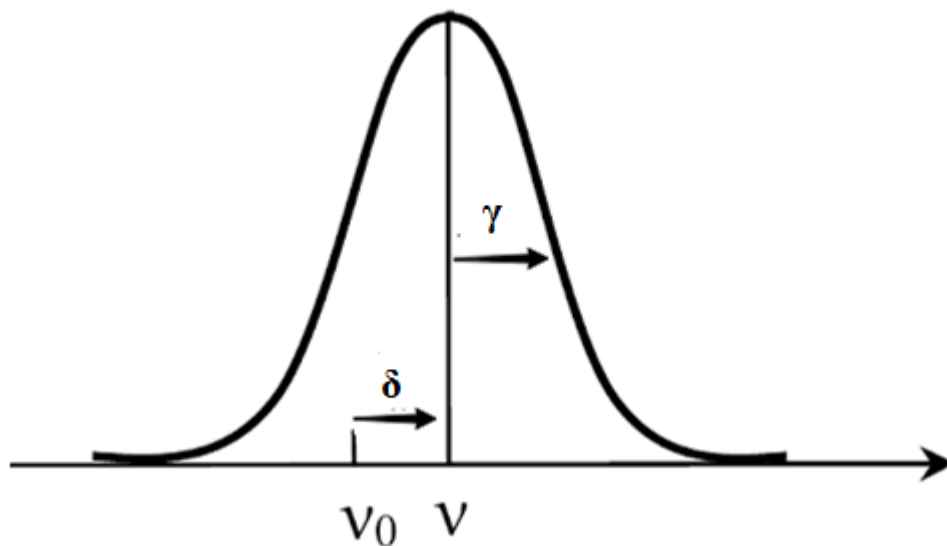


Fig. 2.4. Two main characteristic features of absorption line shapes: the half width at half maximum (γ) and line shift (δ) [56].

2.5.1. Spectral line intensity

Each ro-vibrational transition has an intensity which can be visualised by the area under the curve in fig. 2.4. The most commonly used unit to express intensity is $\text{cm}^{-1}/\text{cm}^2 \cdot \text{molecule}$. The mathematical expression used to calculate line intensity is given as,

$$S_{ij} = I_a \frac{A_{ij}}{8\pi c\nu_{ij}^2} \frac{g' e^{-c_2 E''/T} (1 - e^{-c_2 \nu_{ij}/T})}{Q(T)} \text{ cm}^{-1} / [\text{cm}^{-2} \cdot \text{molecule}], \quad 2-39$$

where, I_a is the natural isotopologue abundance, g' is the upper state statistical weight, E'' is the lower state energy, A_{ij} is the Einstein-A coefficient and $Q(T)$ is the partition function. A complete derivation of equation 2-39 can be found in ref. [62].

The partition function can be expressed as,

$$Q(T) = \sum_k g_k \exp\left(-\frac{c_2 E_k}{T}\right). \quad 2-40$$

Here, g_k and E_k are statistical weight and energy corresponding to the vibrational and rotational contributions in the total energy. c_2 is the second radiation constant.

2.5.2. Einstein-A coefficient

The Einstein-A coefficient is a measure of the transition probability corresponding to a spontaneous emission of photon due to population transfer from an excited state to ground state.

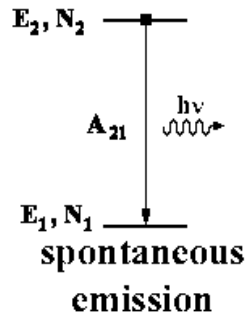


Fig. 2.5. Spontaneous emission of a photon.

If the population of the initial (i) and final (j) energy states in an spontaneous emission (emission of photon without the influence of any external electromagnetic field)

are N_1 and N_2 , respectively, then the rate of change of population of the excited state due to spontaneous emission can be given as,

$$\frac{dN_2}{dt} = -N_2 A_{21} . \quad 2-41$$

The negative sign on the right hand side of equation 2-41 signifies that the population of the excited state will decrease with time. The Einstein-A coefficient can also be expressed in terms of the transition dipole moment R_{ij} [58] as,

$$A_{21} = \frac{64\pi^4}{3h} \nu_{21}^3 \frac{g''}{g'} R_{21} \times 10^{-36} \text{ s}^{-1} . \quad 2-42$$

2.5.3. Transition dipole moment

Transition dipole moment determines the intensity of an absorption line. Light is an electromagnetic wave with electric and magnetic fields oscillating in a mutually perpendicular direction. In order to interact with this oscillating wave (light), the molecule must also have a changing charge distribution, i.e. an oscillating dipole moment. The transition dipole moment is a measure of this changing dipole moment during each transition. This can be expressed as,

$$R_{ij} = \int \Psi_i^* \mu \Psi_j dz \text{ erg} \cdot \text{cm}^3, \quad 2-43$$

where, Ψ_i and Ψ_j are wavefunctions corresponding to the initial and final levels and μ is a dipole moment operator.

2.5.4. Natural broadening of spectral lines

During a photon absorption, a transition occurs from a lower to a higher energy state. From Heisenberg's uncertainty principle, we know that due to the short lifetime of an excited state, the energy of an absorbed photon cannot be determined accurately. This

gives rise to a band of light frequencies getting absorbed in a transition. This frequency spread can be expressed as,

$$\Delta\nu = \frac{1}{2\pi\Delta t}, \quad 2-44$$

where Δt is the lifetime of the excited state. Natural broadening has very little effect on absorption line shapes compared to Doppler or Lorentzian broadening. For example, in a typical rotational transition, the natural line width would be of the order of 10^{-15} cm^{-1} . Therefore, it is often neglected during the fitting of absorption lines.

2.6. Line-shape profiles

2.6.1. Doppler line profile

The Doppler line profile is used to fit absorption lines recorded at very low pressures when the intermolecular collisions can be assumed to have negligible effect on the line shape. At this pressure range the line shape is dominated by the random motion of the molecules at a certain temperature. This random motion of the molecules relative to the direction of light propagation gives rise to the Doppler effect. The result is that the molecule moving toward the light source will absorb light at a slightly lower frequency than the molecule moving away.

Using the Maxwell-Boltzmann distribution for molecular velocities a line-shape profile can be constructed that takes into account the shift in absorbed light frequencies due to the Doppler effect. The Maxwell-Boltzmann velocity distribution function can be written as,

$$f(\bar{u})d\bar{u} = \left(\frac{m_a}{2\pi K_B T}\right)^{3/2} \exp\left(-\frac{m_a \bar{u}^2}{2K_B T}\right) d\bar{u}, \quad 2-45$$

where, u is the molecular velocity and m_a is the mass of the molecule. K_B is the Boltzmann constant and T is the absolute temperature.

The associated line shape profile can be given as

$$F_D(\nu) = \sqrt{\frac{\ln 2}{\pi}} \frac{1}{\gamma_D} \exp\left[-\ln 2 \left(\frac{\nu - \nu_0}{\gamma_D}\right)^2\right] 1/cm^{-1}, \quad 2-46$$

where γ_D is the Doppler half width which is written as,

$$\gamma_D = \sqrt{\frac{2 \ln 2 K_B T}{m_a c^2}} \nu_0. \quad 2-47$$

The Doppler profile is a Gaussian function and the half width of the lines in the Doppler regime is typically of the order of 10^{-3} cm^{-1} wavenumbers.

2.6.2. Lorentz profile

In infrared spectroscopy the spectral lines recorded at pressures higher than 100 Torr can no longer be fitted accurately with the Doppler profile. This is due to the fact that in this pressure regime the intermolecular collisional effects dominate over the Doppler effect. Molecular collisions in this pressure regime can be explained well with the impact approximation, which assumes that the time duration of a collision is negligible compared to the time between two consecutive collisions. Molecular collisions are considered to be elastic. Thus the kinetic energy of the molecules before and after collision is conserved. But due to collisions, the vibrational motion of the molecules undergoes a phase shift which, in the frequency domain, corresponds to a change in frequency distribution or transformation of the line shape of an absorption line. In other words, the molecular collisions result in absorption of light at a slightly different frequency. The distribution of

molecular collisions can be expressed by a Poisson distribution and a new line-shape profile is formed as

$$F_L(\nu) = \frac{1}{\pi} \frac{\gamma_c}{(\nu - \nu_0 - \delta_c)^2 + \gamma_c^2} \quad 1/cm^{-1}, \quad 2-48$$

where, γ_c is the collisional half width and δ_c is the collisional shift. As the pressure increases, the number of intermolecular collisions also increases. Thus more molecules undergo phase shift. This induces a spread out of the frequency distribution corresponding to a spectral line. Thus, at higher pressures, a spectral line gets broadened. This is called collisional broadening or pressure broadening. The width of the spectral lines increases linearly with pressure. Intermolecular collisions also induce a change of the position of the spectral lines from their corresponding line centers. This is referred to as collisional shift and, like broadening, the shift also has a linear relationship with pressure. This linear relation can be explained from the fact that as the pressure increases the number of intermolecular collisions also increases. Due to this collision, the energy levels in a molecule are perturbed. Therefore the energy gap between a ground and an excited state gets shortened, shifting the central position of the absorption line.

2.6.3. Voigt profile:

The Voigt profile is used to fit spectral lines recorded at intermediate pressures when both collisional and Doppler effects are considered to have significant impact on the line shape. The Voigt profile is the convolution of the Lorentz and Doppler profiles. It can be expressed as,

$$F_V(\nu) = \sqrt{\frac{\ln 2}{\pi}} \frac{1}{\gamma_D} \frac{y}{\pi} \int_{-\infty}^{\infty} \frac{\exp(-t^2)}{y^2 + (x-t)^2} dt. \quad 2-49$$

Equation 2-43 can be rewritten in terms of a complex probability function $W(x,y)$ developed by applying different computational algorithms [63, 64].

$$W(x, y) = \frac{i}{\pi} \int_{-\infty}^{+\infty} \frac{\exp(-t^2)}{x + iy - t} dt . \quad 2-50$$

Thus, after considering the line shift ($x \rightarrow x'$), equation 2-49 can be modified as,

$$F_V(x', y) = \frac{y}{\pi} \int_{-\infty}^{+\infty} \frac{\exp(-t^2)}{y^2 + (x' - t)^2} dt = \text{Re } W(x', y) , \quad 2-51$$

where, x and y are dimensionless parameters which can be given as,

$$x = \sqrt{\ln 2} \frac{v - v_0}{\gamma_D} , \quad 2-52$$

$$y = \sqrt{\ln 2} \frac{\gamma_C}{\gamma_D} . \quad 2-53$$

At lower pressures, when ($\gamma_D \gg \gamma_C$) the Doppler part of the Voigt profile becomes dominant and the line shape looks more like a Doppler one whereas the line shape becomes more compatible with a Lorentz profile at higher pressures ($\gamma_D \ll \gamma_C$).

2.6.4. Speed-dependent Models

The Voigt model has been very successful in fitting atmospheric and laboratory spectroscopic data. But in some cases, for spectra recorded with a signal-to-noise ratio above 1000, the Voigt profile also cannot fit the experimental data accurately. It can be noticed that the recorded spectral lines are higher and narrower than the mathematically modeled line from Voigt profile.

2.6.4.1. Speed-Dependent Voigt Line-Shape Model

Earlier, while discussing the Doppler model, we considered that all molecules follow the Maxwell-Boltzmann velocity distribution. In order to fit the experimental data

more accurately, a different line-shape model has been suggested that takes into account the effect of velocity changes in molecules. Berman [65] first gave the expression of the Speed-dependent Voigt profile as,

$$F_{SDV} = \frac{1}{\pi} \text{Re} \left\{ \int \frac{f(\vec{u})}{\Gamma(u) - i(\tilde{\omega} - \Delta(u)) - \vec{k} \cdot \vec{u}} d^3\vec{u} \right\} / \text{cm}^{-1}, \quad 2-54$$

where, $\tilde{\omega}$ is the angular frequency corresponding to the line position. $\tilde{\omega} = 2\pi\nu c$, where ν is the line position in wavenumbers. $f(\vec{u})$ is the Maxwell-Boltzmann velocity distribution function. $\Gamma(u)$ and $\Delta(u)$ are referred to as speed-dependent broadening and shift. \vec{k} is the direction of light propagation. It should be noted that if the $\vec{k} \cdot \vec{u}$ term is taken out, then equation 2-54 becomes a weighted sum of Lorentz profiles.

2.6.4.2. The Soft and Hard Collision Line-Shape Models

At intermediate pressures, (~ 50 Torr) the experimentally recorded spectral lines have been found to be much narrower than the fitted line shape from the Voigt model. This narrowing of spectral lines could be explained by the Dicke effect [66]. This is also called collisional narrowing effect which occurs when the mean free path between molecules become equal or less than the absorbed light wavelength.

The Doppler profile can take into account this narrowing effect by adding a correction term in the expression [56]. First we consider that the molecular collisions are no longer elastic. Therefore, at intermediate pressures, collisions induce the thermal velocity of the molecules to decrease because of diffusion. This results in a changes in the shape of the absorption lines. The first corrected model given by Wittke and Dicke [67] could only fit lines recorded at higher pressures of the Dicke regime. Because at that time, they did not take into consideration the nature of the intermolecular collisions and how they

would change the velocity after each collision. Afterwards, two new models based on two types of collisions were introduced. One was the ‘soft’ collisions model given by Galatry [68] and another was the ‘hard’ collisions model introduced by Rautian and Sobelman [69].

In the soft collision model intermolecular collisions are considered to be soft. It assumes that in order for the velocity of a molecule to change, it has to collide with a large number of neighboring molecules. In this case, the motion of the molecules can be described using the diffusion expression given by Chandrasekhar [70]. The corresponding line-shape model can be given as,

$$F_G(x', y, z) = \frac{1}{\pi} \operatorname{Re} \left(\int_0^{\infty} \exp \left\{ ix't - yt + \frac{1}{2z^2} [1 - zt - \exp(-zt)] \right\} dt \right) / \text{cm}^{-1}. \quad 2-55$$

In this expression, z is a parameter which is related to the narrowing coefficient β as,

$$z = \sqrt{\ln 2} \frac{\beta}{\gamma_D}. \quad 2-56$$

Rautian and Sobelman described the “hard” collision model [69] which assumes that an intermolecular collision changes the velocity of a molecule in such a way that it completely loses its memory of initial velocity before collision. In this case the molecule (radiator) can be treated as comparatively lighter than its perturbing counterparts. The line-shape profile for the Rautian-Sobel’man model can be derived from the kinetic equation as,

$$F_R(x', y, z) = \frac{1}{\sqrt{\pi}} \operatorname{Re} \left[\frac{W(x', y+z)}{1 - \sqrt{\pi} z W(x', y+z)} \right] / \text{cm}^{-1}, \quad 2-57$$

where, $W(x', y+z)$ is a complex probability function given by equation 2-50. If the molecular collisions are elastic, i.e. if $\beta = z = 0$, then equation 2-57 reduces to a Voigt line-shape function.

2.7. Line mixing

The theoretical approaches discussed so far can be applied to fit laboratory and atmospheric spectral data. But all these theoretical models are constructed to reproduce the isolated absorption lines. We already know from the description of ro-vibrational bands that each absorption line has many neighboring lines in a band. If these absorption lines are isolated, then the absorption coefficient can be given as a sum of all the lines as,

$$K(\nu) = P_a \sum_{k=1}^N A_{P_k} F_k(\nu - \nu_k), \quad 2-58$$

where, P_a is referred to as the partial pressure. The intensity of the k^{th} line is A_{P_k} with its line center at ν_k . $F_k(\nu - \nu_k)$ is the line shape of the corresponding line.

In case of overlapping neighboring lines, intensity from one line may transfer to another. This phenomena can be observed in experimental spectra recorded at high pressures. At higher pressures, the width of the lines increases as they get closer to each other. For spectral lines influenced by line mixing, the fitted residuals have been observed to be significantly high and thus result in a wrong estimation of the line-shape parameters such as broadening and shift coefficients. Therefore, in order to improve accuracy of line fitting, the line-shape model should be able to fit not only isolated lines, but also multiple overlapping lines simultaneously.

Line mixing between lines which weakly overlap, can be taken into account by adopting a relaxation matrix formalism developed by Rosenkranz [71]. Using this method, the Lorentz profile can be modified to account for line mixing as,

$$F_k(\nu - \nu_k) = \frac{1}{\pi} \frac{\gamma_k + (\nu - \nu_k)Y_k}{\gamma_k^2 + (\nu - \nu_k + \delta_k)^2} \frac{1}{\text{cm}^{-1}}, \quad 2-59$$

where, Y_k is the line-mixing coefficient associated with the K^{th} line. If Γ_{lk} are the diagonal elements of the relaxation matrix, then Y_k can be given as,

$$Y_k = 2 \sum_{l \neq k} \frac{d_l}{d_k} \frac{\Gamma_{lk}/2\pi c}{(v_k - v_l)}, \quad 2-60$$

where, d_l and d_k are transition dipole moments corresponding to line l and k . During my research work, I calculated line-mixing coefficients for three weak ro-vibrational bands of CO_2 using a theoretical method known as Exponential Power Gap (EPG). A brief description of this method is given.

2.7.1. Exponential Power Gap (EPG) calculations for line mixing

We followed the same approach adopted by Levi *et al.* [72] for this type of calculation. In this approach each band of CO_2 is taken into account as a whole. Two approximations were implemented in our calculations: impact approximation and factorized density matrix formalism [73]. Levi *et al.* considered a relaxation matrix that exhibits itself as an entire band of CO_2 with all the physical parameters associated with it. The diagonal elements of this matrix are the Lorentz broadening (real part) and line-shift coefficients (imaginary) while the off-diagonal elements correspond to line mixing effect. The EPG law enables us to calculate the off-diagonal elements of the relaxation matrix.

Based on the EPG approximation collisional transfer rates of the molecule of interest in going from ground rotational state of k line to a ground rotational state of j line can be expressed as,

$$\kappa_{jk} = a \left[\frac{|\Delta E_{jk}|}{B_0} \right]^{-b} \exp \left(\frac{-c |\Delta E_{jk}|}{k_B T} \right), \quad 2-61$$

where ΔE_{jk} is the energy difference between neighboring rotational lines corresponding to ground vibrational level of j and k lines, B_0 denotes the rotational constant and a, b, c are fitting parameters in a non-linear fitting routine. At a constant temperature, the rate constant in equation 2-61 is related to the population of the rotational levels corresponding to j and k lines by detailed balance equation which can be expressed as,

$$\rho_k K_{jk} = \rho_j K_{kj}, \quad 2-62$$

where, ρ_k is the population of a rotational level corresponding to k line. The collisional transfer rate is related to the diagonal elements of the relaxation matrix by the following equation,

$$W_{kk} = \frac{1}{2} \left[\sum_j K_{jk} \right]_{upper} + \frac{1}{2} \left[\sum_j K_{jk} \right]_{lower}, \quad 2-63$$

where upper and lower correspond to upper and lower vibrational states, respectively. The off-diagonal elements which correspond to the line-mixing effects can be calculated from the following expression,

$$W_{jk} = -\beta k_{jk}, \quad 2-64$$

where β is a constant. In our study $\beta = 0.56$, determined by a sum rule: the sum of the relaxation matrix elements from any column add to zero.

After determining the off-diagonal elements of the relaxation matrix, the line-mixing coefficient can be found from the expression as,

$$Y_{ok}(T) = 2 \sum_{j \neq k} \frac{d_j}{d_k} \frac{W_{jk}}{\nu_k - \nu_j} atm^{-1}, \quad 2-65$$

where, d_j and d_k are dipole matrix elements whereas ν_j and ν_k are the frequencies belonging to the corresponding transitions.

2.7.2. Energy Corrected Sudden (ECS) approximation

The values corresponding to line-mixing parameters from EPG, have been compared with the database (AER database [www.aer.com]). This database stores the line-mixing parameters calculated using Energy Corrected Sudden approximation from different bands of CO₂ [74]. The ECS approach for calculating line-mixing parameters have been proved to be accurate when compared with the laboratory observations in the 10 - 20 μm region [75]. In this approach, a relaxation matrix similar to that described for EPG, is constructed using line parameters from the HITRAN database. The off-diagonal elements of this matrix (associated with line mixing) are calculated using the following expression,

$$\begin{aligned} \left\langle \left\langle J'_i l_i J'_f l_f | W(T) | J_i l_i J_f l_f \right\rangle \right\rangle &= (2J'_i + 1) \sqrt{(2J_f + 1)(2J'_f + 1)} (-1)^{l_i + l_f} \times \\ &\sum_{L \text{ even} \neq 0} \begin{pmatrix} J_i & L & J'_i \\ l_i & 0 & -l_i \end{pmatrix} \begin{pmatrix} J_f & L & J'_f \\ -l_f & 0 & l_f \end{pmatrix} \begin{Bmatrix} J_i & J_f & 1 \\ J'_f & J'_i & L \end{Bmatrix} \\ &\times (2L + 1) \frac{\Omega(J_i, T)}{\Omega(L, T)} Q(L, T) \end{aligned} \quad 2-66$$

where, $J_f \leftarrow J_i$ and $J'_f \leftarrow J'_i$ are two downward ro-vibrational transitions coupled due to line mixing (J is rotational quantum number). l_i and l_f are angular momentum quantum numbers associated with the degenerate vibrational levels ($v_1^f v_2^f l_f v_3^f \leftarrow v_1^i v_2^i l_i v_3^i$). $\Omega(J_i, T)$ and $Q(L, T)$ are correction factors applied to the infinite order sudden approximation [20]. $\Omega(J_i, T)$ is given as,

$$\Omega(J, T) = \left[1 + \frac{1}{24} \left(\frac{\omega_{J, J-2} l_c}{v_r} \right)^2 \right]^{-2}, \quad 2-67$$

and

$$Q(L, T) = A(T, P) [L(L+1)]^{-\lambda(T, P)} \exp \left[-\beta(T, P) \frac{hcE_L}{K_B T} \right]. \quad 2-68$$

In equation 2-67 and 2-68, $\omega_{J,J-2}$ is the spacing between J and $J - 2$ levels, v_r is referred to as mean relative velocity for radiator-perturber collisions and l_c is the scaling length. E_L corresponds to the rotational energy at level L . Temperature-and pressure-dependent terms A , λ , β and l_c are adjustable parameters obtained from fitting the corresponding equations [76].

2.8. Temperature dependence of line parameters

The line shape of any absorption line changes with temperature. These deviations can be modeled by deriving a relationship between the line-shape parameters (i.e. broadening and shift) and temperature. In order to do this we make an assumption that the collisional frequency of the molecules is linearly dependent on the density and average velocity of the molecules. This leads us to the following expression,

$$\frac{\sigma_1}{\sigma_2} = \left(\frac{T_1}{T_2} \right)^{-n}, \quad 2-69$$

where σ_1 and σ_2 are line-shape parameters of interest corresponding to the temperatures T_1 and T_2 respectively. n is called the temperature-dependent exponent. This is a semi-classical method for modeling the temperature dependence of line-shape parameters [www.hitran.org]. But this approach is not valid for very low temperatures.

Chapter 3. Experimental details

A tunable diode laser spectrometer (TDLS) has a laser as light source capable of scanning through a range of frequencies of the electromagnetic spectrum. For diode lasers the frequency is modulated by changing the temperature within the cavity of the active medium or by changing the current supplied to the diode. The emitted light from the laser enters into a chamber or a cell filled with a molecular species of interest. The optical design of this gas container is of great importance in this type of spectroscopy. Materials of high reflectivity are used to design the interior parts of the chamber and the entrance as well as the exit windows are designed to ensure a minimum loss of light that propagates through it. Light that comes out from the chamber then goes directly to an infrared detector, which measures the variation in light intensity as voltages.

TDLS systems are generally used for accurate measurements of gas concentrations as well as for line-shape studies. Absorption lines are recorded by measuring the change in light intensity before and after passing through the gas. The sensitivity of this spectrometer depends mostly on the path length of the gas cell. Different designs of multi-pass gas cells have been developed to increase the detection sensitivity of this type of spectrometer.

3.1. TDLS facility at the University of Lethbridge

The laser-spectrometer facility in our lab at the University of Lethbridge consists of three channels. One is the temperature and pressure (P-T) controlled cell which is used to record spectral lines at different P-T conditions. A gas mixture of C_2H_2 and CO_2 is put inside this chamber as the light absorbing medium. The second channel is a reference cell which is always kept at low pressure (a few Torr) and room temperature. This channel is used to measure line parameters without being perturbed by the changing pressure and

temperature conditions. The third channel records the background signal of the laser before being sent to the first or second chamber. By recording these three sets of data simultaneously, we can study the transformation of line shapes corresponding to each spectral line in a ro-vibrational band.

In order to perform high-resolution spectroscopic studies, the laser light source should have a power output which is sufficiently high. Also the laser width should be narrow compared to the spectral line width and the line shape of the laser light should be stable for a sufficiently long time. Keeping in mind these requirements, we opted to use a New FocusTM Velocity laser (Model - 6300, Serial – 270) source for our recordings. This laser is tunable between 1500 and 1630 nm and produces light of approximately 9 mW as an output. The width of the laser is very narrow (<300 KHz). The tuning speed of this laser could reach up to 20 nm s^{-1} .

I recorded spectra for 22 transitions from the P-branch of the $\nu_1 + \nu_3$ band of acetylene. The lines were recorded at different pressure and temperature conditions with pressures ranging from 50 to 750 Torr and temperatures from 216 to 333 K. Stability of temperature during each recording is crucial for accurate measurement of line-shape parameters in this type of study. I have used a Neslab ULT-80 temperature bath for controlling the channel temperature. Ethanol was used as a cooling component in this thermal bath temperature control system. The whole system is cascaded to provide a quick and efficient refrigeration. The coolant liquid is circulated around the gas chamber using a circulating pump which is connected to the Neslab ULT-80 temperature bath.

The scanning of the laser was done using a LabVIEW program designed to control and monitor each step of the experimental process. First, LabVIEW sends a signal to the laser controller to set its central frequency to the absorption line frequency of interest,

acquired from the HITRAN 2012 database [77]. A schematic diagram of the experimental set-up is shown in the panels of Fig. 3.1.

(A)



(B)

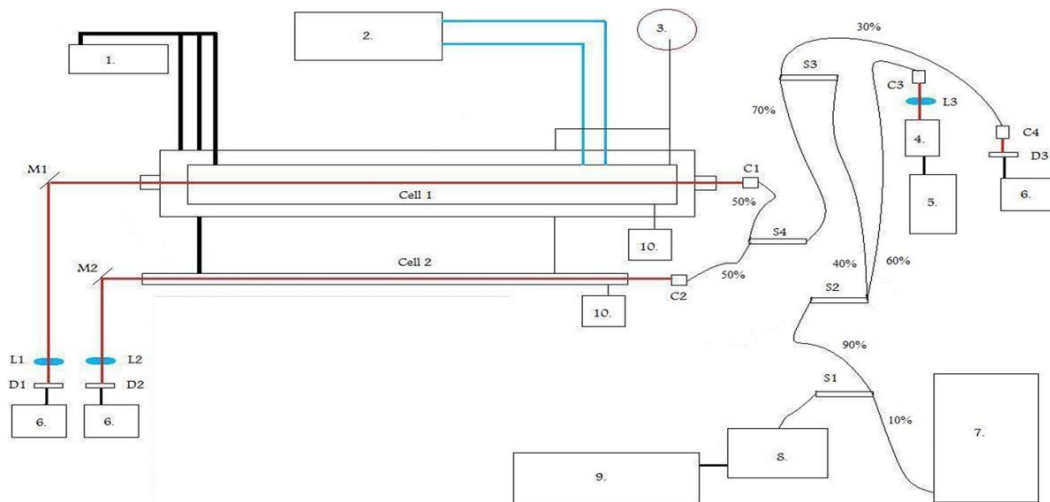


Fig. 3.1. Configuration of 3-channel TDLDS instrument: (A) Photo of the lab set-up, (B) 1. Vacuum pump, 2. Neslab temperature controller, 3. Gas cylinder, 4 & 5. Fabry Perot interferometer and controller, 6. Detector pre-amplifiers and power source, 7. Wavenumber, 8 & 9. Laser head and controller, 10. Pressure gauge. L₁, L₂ and L₃ are lenses for the detectors. M₁ and M₂ are beam guiding mirrors. D₁, D₂ and D₃ are detectors used. C₁, C₂, C₃ and C₄ correspond to the collimators. S₁, S₂, S₃ and S₄ are the beam splitters [51].

Afterwards, a command is sent to the piezoelectric device in the laser controller to vary the voltage from -3 to +2.7 V in increments of .001 V. This results in the tuning of the laser frequency around the absorption line position.

The increments of piezo voltage non-linearly change the wavelength of the laser. Thus, in order to create a more accurate wavenumber scale, we used the ThorLabs SA200-14A Fabry Perot interferometer. This interferometer has a free spectral range of 0.05 cm^{-1} . Details of this technique will be described in section 3.2 of this chapter.

3.1.1. Temperature- and pressure-controlled gas cell

The cell is 1.54 m long with an inner radius of 0.104 m. The cell is kept inside a larger chamber to isolate and control its pressure and temperature conditions. The two ends of the cell are welded with flanges designed to accommodate 5 platinum resistance thermometers. These thermometers have a measurement accuracy up to $\pm 0.001 \text{ K}$. The thermometers were mounted at 3 different lengths of 6", 18", and 30" inside the gas cell.

An MKS pressure gauge (Model: 690A-11098) was used to monitor the change of gas pressure inside the cell. This pressure gauge is capable of measuring gas pressures accurately (.05% accuracy) up to 1000 Torr. Before any gas was let inside the inner gas cell, I evacuated the cell along with the outer chamber by using a turbo molecular pump. A schematic diagram of the inner and outer chamber is shown in fig. 3.2. As the figure shows, the outer chamber has several specifically designed stubs to allow access to different measuring and controlling equipment inside.

The temperature- and pressure-controlled cell was filled with a gas mixture of C_2H_2 and CO_2 (C_2H_2 : $93 \pm 0.05\%$, CO_2 : $7 \pm 0.05\%$). The pressure gauge reading helped me to control and monitor the gas pressure inside the cell.

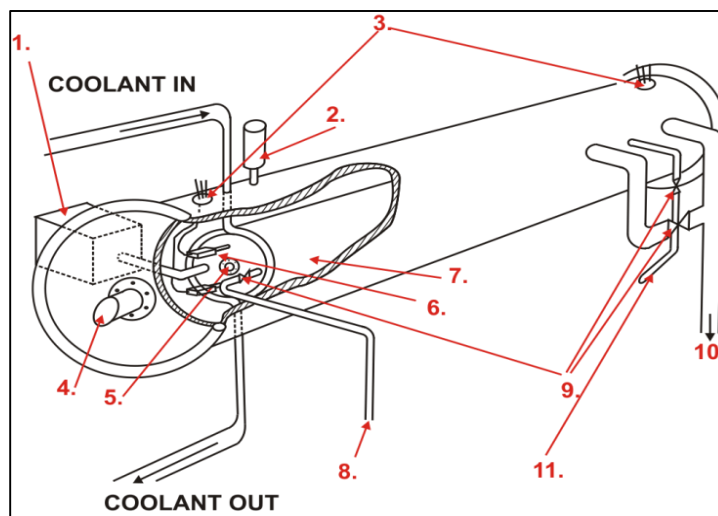


Fig. 3.2. Configuration of the temperature and pressure controlled cell: 1. MKS Pressure gauge, 2. Pirani pressure reader, 3. vacuum points, 4. CaF₂ glass windows for the outer chamber, 5. Windows for the gas cell, 6. Thermometers, 7. Body of the gas cell, 8. gas inlet point, 9. Vacuum valve points, 10. Gas outlet point, 11. Air flow port for the outer chamber [51].

3.1.2. Reference gas cell

The reference cell is of exactly the same size (length of 1.54 m and inner radius of 0.104 m) as the main temperature- and pressure-controlled cell. It is also evacuated before the recording using the vacuum pump. It is filled with only a small amount (6 Torr in our case) of pure C₂H₂. An MKS pressure gauge (Model: 690A11TRA) capable of measuring pressure up to 10 Torr was used to monitor the gas pressure. The C₂H₂ gas pressure was kept at 6 Torr consistently throughout the recording period for the reference cell. There is no temperature-controlling device connected to this cell. The cell was kept at thermal equilibrium by keeping the temperature of the room at 296 K.

3.1.3. Detectors

Three detectors were used to record the intensity of the transmitted light from the three channels (T-P controlled cell, reference cell and the laser background). These are photodiodes made from indium gallium arsenide (InGaAs) purchased from Edmund Optics. They are capable of detecting light in the near-infrared frequency region. The detectors are connected to preamps, power control box and the computer. The detector configuration is very important for getting a high signal-to-noise ratio. Before starting the recording I had to adjust the alignment of the laser beam passing through many optical fibers, the gas cell and finally to the detector.

3.2. Data processing and analysis

For accurate measurement of line-shape parameters, spectral data corresponding to three channels (T-P controlled cell, reference cell and the laser background) were recorded simultaneously. The laser background was recorded and corrected using a polynomial fit. This background information helped me to correct the baseline of the recorded spectral lines corresponding to the $\nu_1+\nu_3$ band of acetylene broadened by CO₂.

A Labview program called “Velocity.vi” written by previous group members [51] was used to control and monitor the data recording. For obtaining better accuracy, each spectral line was recorded four times and at the final step of processing were averaged to create the input file for Labfit (spectroscopic analysis software [78, 79]). Two data files called “Peak” and “Spectra” were generated during each scan of the laser. The “Peak” file contains the peak positions measured by the Fabry-Perot interferometer whereas the “Spectra” file has all the intensity values and corresponding piezo voltages recorded during each scan from the three channels. A set of Labview programs developed by other group

members were used to process these two data files and create a transmission file for each spectrum. Brief descriptions of each program are as follows:

(1) The program “Peak file correction.vi” was used to assign wave numbers to each peak in the “Peak” file. The wavemeter records the line position of the first peak in wave numbers. This program uses the fringe spacing ($.05 \text{ cm}^{-1}$) to set positions in wavenumbers for the rest of the peaks.

(2) The second program “Wave converter.vi” uses these corrected peak positions and Fabry-Perot scanning signals in the “Spectra” file to calculate the number of points between each pair of peaks. The fringe spacing divided by the number of points gave me the spacing between consecutive points in wavenumbers. Thus, I assigned a wavenumber for every signal recorded by the detectors from the three channels. Three new files “Converted CH1”, “Converted CH2” and “Converted BG” corresponding to the main cell, reference cell and laser background were generated. In order to fit the spectra in Labfit (fitting routine) the wavenumbers corresponding to the recorded signals must be evenly spaced. But due to the nonlinear relationship between piezo voltage and corresponding laser frequency, the number of data points between successive peaks is not the same. Thus the wavenumber spacing between points also vary from peak to peak. This is corrected by using a linear interpolating function.

(3) To create transmission files corresponding to the channel 1 and channel 2 spectra, I used a program called “Correctionfit.vi”. Using this program, I calculated the residual between the baseline of each absorption line and the simultaneously recorded laser background. Baseline is the spectra recorded from channel 1 and channel 2 with all the spectral features cut off from the data using the program “Correctionfit.vi”.

$$\text{Residual} = \text{Spectral Baseline} - \text{Laser Background}$$

This residual was then fitted with a Chebyshev polynomial [80] fitting routine to generate a corrected baseline for the spectral lines. Chebyshev polynomials can produce a high order polynomial fit with only a few parameters, therefore does a better job in fitting than conventional polynomials at a much faster computing rate.

$$\text{Baseline} = \text{Fitted Polynomial} + \text{Laser Background}$$

Dividing the raw spectra in the “Converted CH1” and “Converted CH2” files by this corrected baseline resulted in the desired transmission file corresponding to each spectrum recorded. In the final step these transmission files along with their corresponding pressure and temperature information were used to generate input files that could be read by Labfit for performing spectral analysis. Each spectrum recorded at a specific pressure and temperature was added separately to include in the input file. And line parameter values found in HITRAN database corresponding to the $\nu_1+\nu_3$ band of acetylene were used as guess parameters in the fit. A detailed description of Labfit will be given in section 3.4.

3.3. Fourier transform spectrometers

A typical Fourier-transform spectrometer (FTS) consists of a broad frequency light source that covers the frequency range corresponding to the absorption band, a beam splitter, two mirrors (one fixed, another movable) and a detector for recording the signal. The gas sample is placed in front of the detector. Fig. 3.3 shows a typical Michelson interferometer used to measure the spectra of a gas sample.

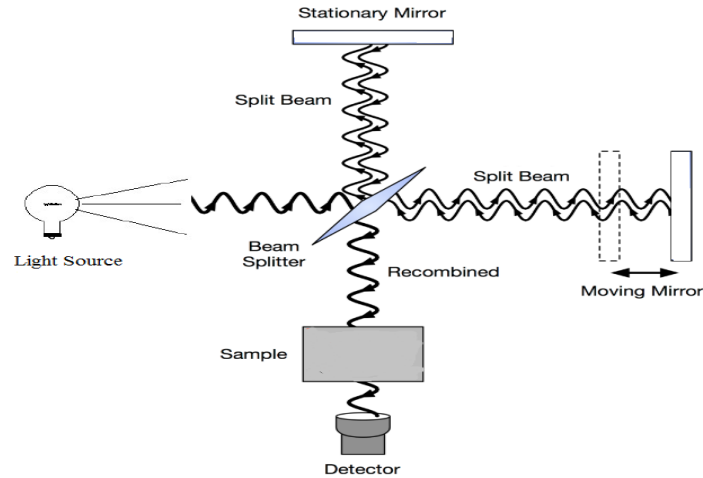


Fig. 3.3. Layout of a Michelson interferometer. [Photo: <http://www.muelaner.com/laser-interferometers/>]

3.3.1. Working Mechanism of a Michelson Interferometer

As the Fig. 3.3 shows, light from the source is incident on the beam splitter where $\frac{1}{2}$ of the beam gets reflected and the other $\frac{1}{2}$ gets transmitted through it. These reflected and transmitted light beams are then reflected by the mirrors and propagate back to the beam splitter. Here again, half of each beam gets reflected and transmitted. The beams that recombine produce an interference pattern that passes through the sample to the detector. When the two reflecting mirrors are at the same distance from the beam splitter, the interference is constructive. In terms of optical path difference δ and wavelength of the light source λ , when $\delta = 0$ or an integer multiple of λ , the detector records maximum intensity. In contrast, when $\delta = \frac{\lambda}{2}$ or $\frac{\lambda}{2} +$ an integer multiple of λ , the interference is destructive, i.e. the detector records minimum intensity. Therefore, the intensity recorded by the detector would be a sinusoidal function of δ . For a monochromatic light source, this can be expressed as,

$$I(\delta) = \frac{I_0}{2} \left[1 + \cos\left(\frac{2\pi}{\lambda} \delta\right) \right], \quad 3-1$$

where, I_0 corresponds to the intensity of the monochromatic light source. A graph of intensity vs. optical path difference (OPD) is referred to as an interferogram. A broad band light source can be considered as made up of a large number of monochromatic waves. Thus the intensity detected by the detector can be expressed as a sum of intensities corresponding to individual wavelength of light.

$$I(\delta) = \int_{-\infty}^{+\infty} d\nu S(\nu) \cos(2\pi\nu\delta), \quad 3-2$$

where, $S(\nu)$ is referred to as the spectra of light source. ν is the frequency of light expressed in wavenumbers ($\nu = \frac{1}{\lambda} \text{ cm}^{-1}$). The interferogram which is a spatial function can be converted to the spectra as a function of wavenumbers by applying a simple inverse Fourier transform, i.e.

$$S(\nu) = \int_{-\infty}^{+\infty} d\delta I(\delta) \cos(2\pi\nu\delta). \quad 3-3$$

The resolution of the FTS spectra depends upon the maximum displacement of the movable mirror from zero path difference position. If the maximum displacement is X cm, then the resolution of the spectra would be $\frac{1}{2X} \text{ cm}^{-1}$. In order to obtain the spectra of the gas sample, usually two interferograms are recorded, one with sample and the other one without the sample placed in the system. A ratio of these two gives us the transmittance spectrum of the sample. A detailed description of the FTS instrument in Canadian Light Source (CLS) is given in the next section.

3.3.2. Fourier transform spectroscopy facility at CLS

The CO₂ spectra corresponding to three weak bands (12201-03301, 11101-10002 and 12201-11102) were recorded (by Dr. Adriana Predoi-Cross and Dr. Brant Billingham) in May, 2008 at the Canadian Light Source using a Bruker IFS 125 Fourier transform spectrometer. A total of 41 spectra of CO₂ (pure CO₂ and CO₂ + air mixture) were recorded at room temperature and pressures ranging from few Torr to 140 Torr. 32 of those spectra were recorded with a Synchrotron source whereas 9 spectra were obtained using a Globar source. Measurement of highly accurate line parameters require a high signal-to-noise ratio as well as comparatively small instrumental line shape. These requirements for obtaining high-resolution spectra were fulfilled by putting the gas sample inside a multi-pass cell of 2 m length and optical pass length of 72.15 m. The entrance and exit windows of this cell were made of KBr. A helium cooled Ge:Cu detector was used to record the interferograms. The temperature inside the cell was monitored using a thermocouple (0.5% accuracy). The pressure was recorded by a MKS Baratron pressure gauge (Model: 690A-11098; Range: 0-1000 Torr). Different parts of the experimental set-up are shown in Fig. 3.4.

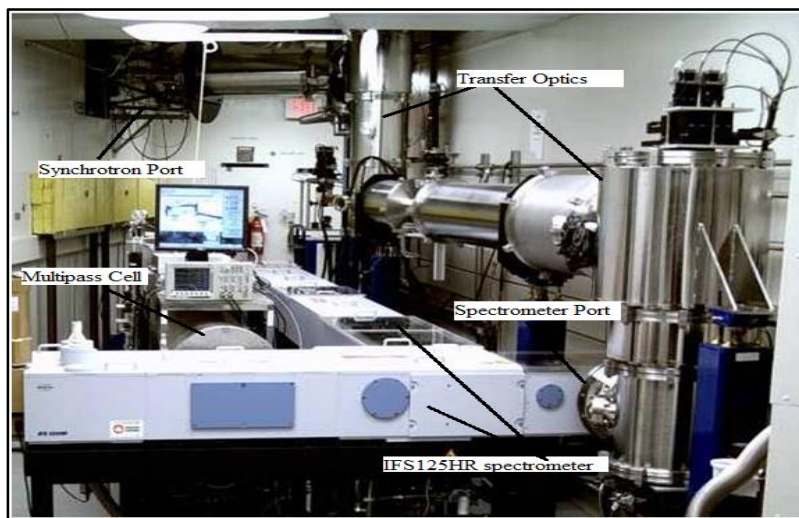


Fig. 3.4. Photo of the high-resolution spectrometer located at the far-infrared beamline at CLS.

For my thesis work I have analyzed the 6 spectra (2-140 Torr) recorded for only pure CO₂ gas. The experimental details of these spectra and the spectrometer are presented below.

Table 3.1. Details of the experimental set-up.

Cell Length	2 m	Detector	Ge:Cu (300-1850 cm ⁻¹)
Path Length	72 m	Beam Splitter	Ge/KBr (400-4800 cm ⁻¹)
Aperture size	1.5 mm	Sampling rate	40 KHz
Window Material	KBr (400-5000 cm ⁻¹)	Detector Filter	F5 (490-1190 cm ⁻¹)
Spectral range	490-1190 cm ⁻¹	Resolution limit	0.002 cm ⁻¹

Table 3.2. Experimental details of the recorded spectra for pure CO₂ recorded at the CLS using the globar source and a 72.15 m path length. The standard deviation of the recorded temperature was 0.16. The accuracy of the pressure readings was up to 0.05%.

Range (cm ⁻¹)	P(Torr)	Temp.(°C)
490-1190	0.50	23.42
490-1190	0.26	23.44
490-1190	1.99	23.71
490-1100	16.34	23.58
490-1105	94.80	23.71
490-1105	75.74	23.58
490-1105	50.44	23.51
490-1190	140.00	23.95
490-1100	29.99	23.60

All the lines recorded were fitted with a multi-spectrum non-linear least-squares fitting software developed by the research group of Chris Benner [78, 79].

3.4. Brief description of the Labfit software

In spectroscopic studies accurate measurements of line-shape parameters corresponding to molecular absorption of light is of great importance. Different algorithms

based on non-linear least squares fitting principles have been developed by research groups all around the globe to retrieve the line parameters of absorption lines. The multi-spectrum fitting routine developed by Chris Benner is based upon Levenberg-Marquardt algorithm [81, 82]. It minimizes the differences between the observed and modelled spectra by fitting the spectral lines to a set of line-shape parameters. This software allows to choose which parameters are fitted and which parameters are fixed, allowing flexibility in the fitting strategies. The whole process of fitting is done in two steps: creating single monochromatic absorption lines and taking into account systematic errors in the line shape arising from the instability of the spectrometer. For example Labfit can take into account channeling effects in the recorded spectra due to external vibrations. In case of pure CO₂ spectra no channeling effect was observed.

The generation of fitted lines require precise calculation of the derivatives of each point in the spectra with respect to each parameter considered. One reliable technique for determining these derivatives is to repeatedly recalculate the spectra by taking into account small changes to the fitting parameters. Labfit employs a weighted multi-spectrum fitting technique because it allows users to take into account the number of sampling points in the spectral lines. Thus a spectrum with greater number of points would in turn have a greater value for its weight in the solution, simply because it would require fitting for more sampling points than the rest of the spectra.

In most cases, for low-pressure spectra, the Voigt line-shape model which takes into account parameters such as line position, line width and line shift is adequate for generating the best fit. But in cases where adjacent lines overlap at high pressure, the Voigt model sometimes cannot predict the transformation of line shapes within experimental uncertainty limit. Because the degree of correlation between different fitting parameters become more

significant for such cases. One method of solving this problem is to carry out a constrained fitting of the spectra and taking into account line-mixing effects [83]. The method of constraint analysis is described in more details in the next chapter.

3.4.1. Implementing Rozenkranz line mixing in Labfit

Line mixing is a phenomenon that transforms the shape of the absorption lines at higher pressures. The pressure regime where line mixing can be observed depends upon the distance or difference in wavenumbers between neighboring lines in an absorption band. Line-mixing effects are considered strong if the neighboring lines are very close, more specifically if the separation between two neighboring lines is comparable with the Lorentz half-width of the individual lines. But if the neighboring lines are far from each other then, weak line mixing is observed. Labfit uses Rozenkranz [71] method to take into account weak line-mixing effects occurring between absorption lines.

Due to molecular collision the initial and final energy levels corresponding to a ro-vibrational transition are perturbed. If two neighboring absorption lines (transition) are close enough (small difference between transition frequencies) then, due to perturbation, their corresponding initial and final energy states can mix. This gives rise to the probability of absorption of a same energy photon in two different transitions. Therefore, in a recorded spectrum we would observe the overlap between two neighboring lines. For n number of lines in a band, Rozenkranz uses n-1 parameters to describe line mixing between them.

Mathematically, the transformation of Lorentzian line shape due to line-mixing effects has been expressed by equation 2-59, where the term Y_k is the Rozenkranz parameter expressed as,

$$Y_k = P \sum_{i=1}^n \chi_i Y_{0_i}, \quad 3-4$$

where, P is the gas pressure (atm), χ is the unitless gas mixing ratio and Y_0 is the coefficient of line mixing given by Labfit in atm^{-1} . n denotes the number of gases in the gas mixture and i represents each individual gas.

Chapter 4. Line-shape study of Q branches of three weak bands of CO₂

The following project is part of a manuscript submitted to the Journal of Molecular Spectroscopy.

A Bruker IFS 125 FTS system was used to record pure CO₂ spectra corresponding to the Q branches of the three weak bands 12201-03301, 11101-10002 and 12201-11102. Description of the experimental set up for is provided in section 3.3.2. in chapter 3.

The CO₂ ro-vibrational bands are represented as $v_1^f v_2^f l_f v_3^f r^f - v_1^i v_2^i l_i v_3^i r^i$, where, v_1 , v_2 and v_3 are fundamental vibrational modes. l is a angular momentum corresponding to the v_2 degenerate bending mode. r represents the Fermi resonant level (v_1) in the band [84, 85]. Fermi resonance is the resonance between a fundamental vibrational mode and an overtone (located very close to each other) which splits the energy levels farther apart, therefore, shifting corresponding line positions as well as changing their intensities. For example, the v_1 fundamental vibrational mode of CO₂ (1388 cm⁻¹) is perturbed by the overtone band of v_2 fundamental mode (1334 cm⁻¹) due to Fermi resonance. r can have any value between 1 and $v_1 + 1$. f refers to final or upper vibrational level whereas i represents the lower level.

4.1. Data retrieval for CO₂ spectra:

The accuracy of retrieved line-shape parameters depends upon the model or the fitting routine used. In this study a non-linear least squares fitting routine (Labfit) was used. The details of this software could be found in Chapter 3. Line-mixing effects significantly change the line shapes for the Q branch transitions of CO₂ bands located in the 700-850 cm⁻¹ region [53]. In order to take into account the asymmetries from collisional effects (line

mixing) in the line shapes of the absorption lines, the non-linear fitting routine utilizes the off-diagonal relaxation matrix formalism.

As described in section 3.4. and for example, in Ref. [86], when the pressure widths of the adjacent lines become comparable to the energy difference between individual transitions in a band, line mixing causes transfer of intensity from weaker to stronger neighboring lines. The degree of line mixing between two adjacent lines can be computed using the Rosenkranz method, implemented in Labfit. Fitting the spectra by taking into account line mixing significantly reduces the residual of the fit.

A modification to the fitting software was implemented to find the ro-vibrational constants (G, B, D, H) as well as the transition moment constants (vibrational band strength S_v , and the Herman-Wallis type coefficients a_1, a_2, a_3 , and a_4) corresponding to each band [78]. The equations used for this constraint analysis are as follows:

$$\begin{aligned} \nu_i = & G' - G'' + (B'J'[J' + 1] - D'\{J'[J' + 1]\}^2 + H'\{J'[J' + 1]\}^3) \\ & - (B''J''[J'' + 1] - D''\{J''[J'' + 1]\}^2 + H''\{J''[J'' + 1]\}^3) \end{aligned} \quad 4-1$$

The equation used for band intensity parameters is expressed as,

$$S_i = \frac{S_{sb} \nu_i \text{iso} L_i F}{Q_r \nu_0} \exp\left(\frac{-C_2 E''}{T_0}\right) \left[1 - \exp\left(\frac{-C_2 \nu_i}{T_0}\right)\right], \quad 4-2$$

where,

$$F = (1 + a_1 m + a_2 m^2 + a_3 m^3 + a_4 J(J + 1))^2, \quad 4-3$$

where, ν_i corresponds to the line position of each transition, whereas the upper and lower vibrational states are denoted by prime and double prime, respectively. In the following

equation L_i and C_2 are Hönl-London factors [86] and the second radiation constant. ν_0 is the band center and Q_r corresponds to the rotational partition function. P, Q and R branches are represented by index m . $m = -J''$ is the P branch whereas $m = 0$ and $m = J''+1$ are Q and R branches, respectively.

In the constraint analysis method the measured line parameters such as line positions and intensities are constrained to fit to the above mathematical expressions [86]. A Voigt model has been used to fit the pure CO₂ spectra. Using constrained parameters in the fit efficiently reduces the correlations between different spectral features of absorption lines (correlation between intensity and Lorentz half width, zero-pressure line position and pressure shifts). In this study, I have reported the ro-vibrational constants belonging to the three bands (12201-03301), (11101-10002) and (12201-11102).

Table 4.1. Ro-vibrational and band intensity parameters of the 12201-03301 band of CO₂. The error in bracket is one standard deviation.

12201←03301 Band (Rotational Constants)		12201←03301 Band (Intensity parameters)	
Parameter	Value	Parameter	Value
$G' - G''$	757.478965(8)	S_{sb}	$0.627(2) \times 10^{-22}$
B_e'	0.3915628(1)	a_1	0.0 Fixed
D_e'	$1.419(1) \times 10^{-7}$	a_2	0.0 Fixed
H_e'	$-0.61(2) \times 10^{-12}$	a_3	0.0 Fixed
B_f'	0.3915669(1)	a_4	$3.6(9) \times 10^{-6}$
D_f'	$1.2872(6) \times 10^{-7}$		
H_f'	$0.21(2) \times 10^{-12}$		
B_e'' (Fixed)	0.392398537		
D_e'' (Fixed)	0.140969×10^{-6}		
H_e'' (Fixed)	0		
B_f'' (Fixed)	0.392394358		
D_f'' (Fixed)	0.140893×10^{-6}		
H_f'' (Fixed)	0		

Table 4.2. Ro-vibrational and band intensity parameters of the 11101-10002 band of CO₂.

11101←10002 Band (Rotational Constants)		11101←10002 Band (Intensity parameters)	
Parameter	Value	Parameter	Value
$G' - G''$	791.447585(4)	S_{sb}	$3.69(1) \times 10^{-22}$
B_e' (Fixed)	0.39040968	a_1	0.0 Fixed
D_e' (Fixed)	1.25861×10^{-7}	a_2	0.0 Fixed
H_e' (Fixed)	9.31792×10^{-14}	a_3	0.0 Fixed
B_f'	0.39133407(2)	a_4	$-0.31(1) \times 10^{-4}$
D_f'	$0.12125(2) \times 10^{-6}$		
H_f'	$0.7(1) \times 10^{-13}$		
B'' (Fixed)	0.390482283		
D'' (Fixed)	0.157203×10^{-6}		
H'' (Fixed)	2.41827×10^{-13}		

Table 4.3. Ro-vibrational and band intensity parameters of the 12201-11102 band of CO₂.

12201←11102 Band (Rotational Constants)		12201←11102 Band (Intensity parameters)	
Parameter	Value	Parameter	Value
$G' - G''$	828.25462(4)	S_{sb}	$0.484(4) \times 10^{-23}$
B_e'	0.3915490(2)	a_1	0.0 Fixed
D_e'	$1.447(1) \times 10^{-7}$	a_2	0.0 Fixed
H_e' (Fixed)	7.13899×10^{-13}	a_3	0.0 Fixed
B_f'	0.3915477(2)	a_4	$-4.5(9) \times 10^{-5}$
D_f'	$1.283(1) \times 10^{-7}$		
H_f' (Fixed)	0.90038×10^{-13}		
B_e'' (Fixed)	0.390745013		
D_e'' (Fixed)	0.149498×10^{-6}		
H_e'' (Fixed)	0.1118×10^{-12}		
B_f'' (Fixed)	0.391690235		
D_f'' (Fixed)	0.156290×10^{-6}		
H_f'' (Fixed)	0.1008×10^{-12}		

Non-linear least squares fitting of the spectra corresponding to the 12201-03301, 11101-10002 and 12201-11102 band is shown in fig. 4.1. (A) – (C). Among the three bands, the smallest residual was observed for the (B) 11101-10002 band with an overall standard deviation of 0.819 %. The highest residual was observed for the weakest band, (C) 12201-11102. It had a standard deviation of 1.068 %. (A) 12201-03301 band transitions were fitted with 1.020 % standard deviation.

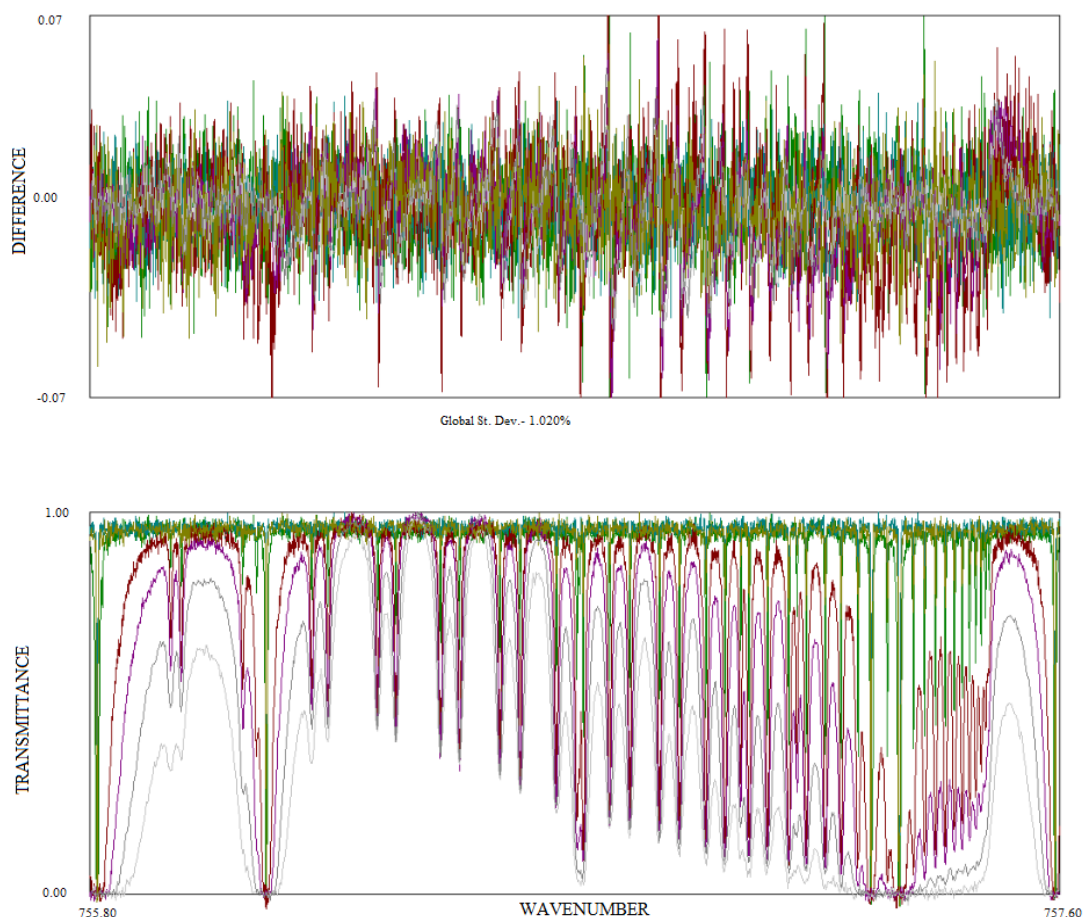


Fig. 4.1. (A). Non-linear least squares fit of spectra from 12201-03301 band. The narrowest line represents spectrum recorded at 0.26 Torr pressure and room temperature (296 K). The gradually broadened lines were recorded at increasing pressures up to 140 Torr.

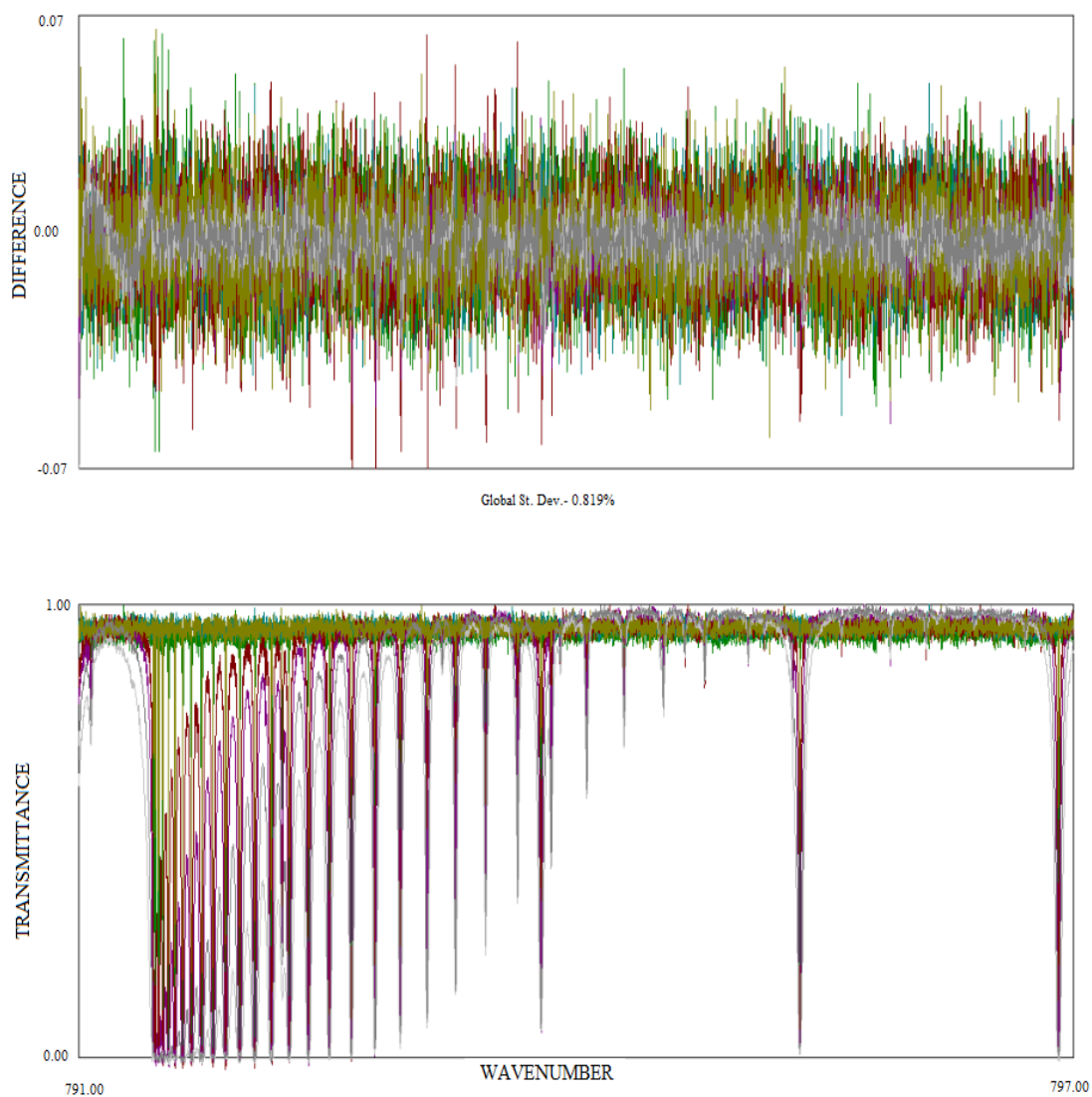


Fig. 4.1. (B). Non-linear least square fit of spectra from 11101-10002 band. The narrowest line represents spectrum recorded at 0.26 Torr pressure and room temperature (296 K). The gradually broadened lines were recorded at increasing pressures up to 140 Torr.

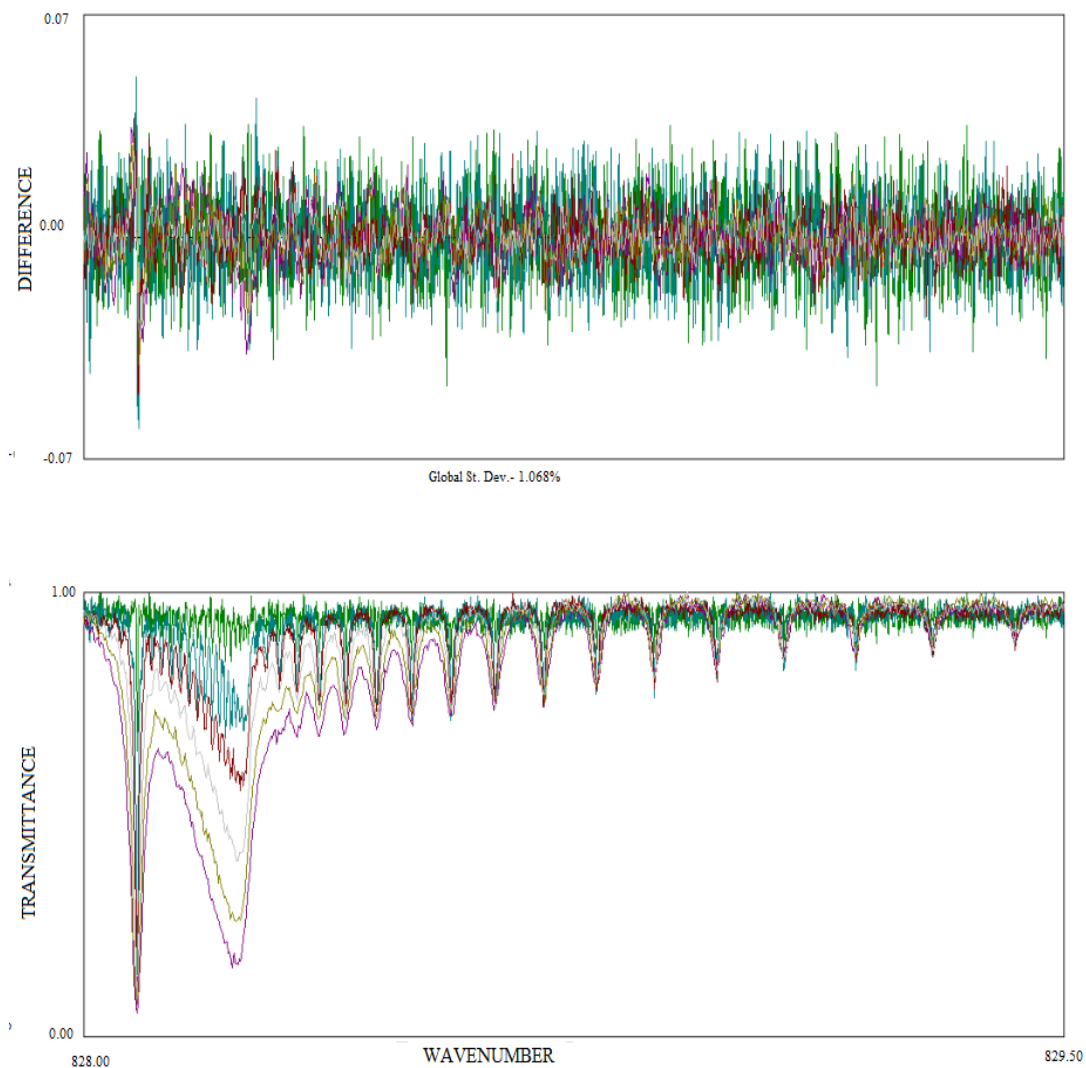


Fig. 4.1. (C). Non-linear least square fit of spectra from 12201-11102 band. The narrowest line represents spectrum recorded at 0.26 Torr pressure and room temperature (296 K). The gradually broadened lines were recorded at increasing pressures up to 140 Torr.

4.2. Retrieved line parameters

The non-linear least squares fitting software (Labfit) designed to perform a line-shape analysis of spectroscopic data sets has been used for the infrared spectra of pure CO₂ recorded in the laboratory. This is a weighted multi-spectrum fitting routine that takes into

account the asymmetries arising in Lorentzian line shapes due to collision-induced line-mixing effects at high pressure.

The fitting procedure has been described in references [78] and [79]. Different line-shape parameters were found from the fit (position, intensity, broadening and line-mixing coefficient). The Lorentzian half width and shifted positions of the individual absorption lines at pressure p and temperature T were found by implementing the following equations:

$$\gamma(p, T) = p \times \left[\gamma_{self}^0(p_0, T_0) \times \left[\frac{T_0}{T} \right]^n \right], \quad 4-4$$

$$\nu(p, T) = \nu_0 + p \times [\delta_{self}^0(T)], \quad 4-5$$

where γ^0 and δ^0 are pressure broadening and shift coefficients ($\text{cm}^{-1} \text{atm}^{-1}$). γ and ν are the Lorentz halfwidth (in cm^{-1}) and line position at pressure p and temperature T . n in equation 4-4 is the temperature-dependence exponent corresponding to the broadening coefficient. In case of room-temperature spectra, the value of n is taken as 1.

The retrieved line positions, intensities and broadening coefficients from the three bands have been reported in Table 4.4. (a) to (c). In this present study it was observed that the absorption lines from the three bands shifted very little due to pressure. So, the value for shift coefficients have been taken to be constants, $-0.003 \text{ cm}^{-1}\text{atm}^{-1}$ for 12201-03301 band and $-0.002 \text{ cm}^{-1}\text{atm}^{-1}$ for 11101-10002 and 12201-11102 bands.

It is evident from the tables 4.4. (a) – (c) that the uncertainties are the highest for 12201-11102 band and lowest for 11101-10002 band transitions. This is to be expected since 12201-11102 band is the weakest among the three bands of interest and therefore

exhibits comparatively higher measurement uncertainties arising from the relatively lower quality of fitting of this band.

In contrast to the line positions, the highest uncertainty has been observed for line intensities from 11101-10002 band (Table 4.4. (b)). The uncertainty is much lower for 12201-03301 band and the lowest for 12201-11102 band transitions.

Table 4.4. (a). Line parameters retrieved using Labfit for Q branch lines from 12201-03301 band of CO₂.

Line label ¹	m	Line Positions cm ⁻¹	Line intensities × 10 ⁻²⁴ cm ⁻¹ / (cm ⁻¹ ² ·molecule)	Self-broadening coefficient cm ⁻¹ atm ⁻¹
Q 3e	3	757.4690(8)	0.814(2)	0.135(5)
Q 4f	4	757.4623(7)	1.444(4)	0.135(4)
Q 5e	5	757.4540(7)	1.979(5)	0.131(3)
Q 6f	6	757.4440(7)	2.450(6)	0.124(3)
Q 7e	7	757.4324(6)	2.867(7)	0.122(2)
Q 8f	8	757.4191(6)	3.237(8)	0.120(2)
Q 9e	9	757.4042(6)	3.560(9)	0.122(2)
Q 10f	10	757.3875(6)	3.837(9)	0.117(2)
Q 11e	11	757.3694(5)	4.070(10)	0.118(2)
Q 12f	12	757.3492(6)	4.258(10)	0.116(3)
Q 13e	13	757.3280(5)	4.403(10)	0.115(4)
Q 14f	14	757.3043(6)	4.506(10)	0.097(27)
Q 15e	15	757.2801(6)	4.567(10)	0.123(5)
Q 16f	16	757.2527(6)	4.590(9)	0.098(10)
Q 17e	17	757.2256(6)	4.576(9)	0.108(3)
Q 18f	18	757.1944(7)	4.528(9)	0.106 (2)
Q 19e	19	757.1647(7)	4.450(8)	0.105(2)
Q 20f	20	757.1295(8)	4.343(8)	0.107(2)
Q 21e	21	757.0974(7)	4.213(8)	0.103(2)
Q 22f	22	757.0578(8)	4.061(7)	0.107(2)
Q 23e	23	757.0237(8)	3.892(7)	0.104(2)
Q 24f	24	756.9795(8)	3.708(7)	0.098(2)
Q 25e	25	756.9436(8)	3.514(6)	0.098(2)
Q 26f	26	756.8945(8)	3.312(6)	0.099(2)
Q 27e	27	756.8573(8)	3.105(6)	0.099(2)
Q 28f	28	756.8027(8)	2.896(6)	0.102(2)
Q 29e	29	756.7649(9)	2.687(6)	0.094(2)
Q 30f	30	756.7042(9)	2.481(6)	0.098(2)
Q 31e	31	756.6662(10)	2.280(6)	0.097(2)
Q 32f	32	756.5990(11)	2.085(5)	0.092(2)
Q 33e	33	756.5616(12)	1.897(5)	0.092(2)
Q 34f	34	756.4869(13)	1.718(5)	0.088(2)
Q 35e	35	756.4510(14)	1.549(5)	0.087(2)

¹ Each transition in a band is characterized by 3 characters. First character is a letter which represents the branch where the transition occurred. 2nd character is a number representing the m index described in section 2.4.3. of chapter 2. The 3rd character is a letter (e or f) which represents a pair of transitions occurring between degenerate vibrational levels.

Q 36f	36	756.3681(16)	1.391(5)	0.088(2)
Q 37e	37	756.3345(17)	1.242(5)	0.084(2)
Q 38f	38	756.2423(18)	1.105(4)	0.083(2)
Q 39e	39	756.2122(20)	0.978(4)	0.084(2)
Q 40f	40	756.1098(21)	0.862(4)	0.090(4)
Q 41e	41	756.0843(23)	0.757(4)	0.080(3)
Q 42f	42	755.9702(23)	0.661(3)	0.076(2)
Q 43e	43	755.9508(26)	0.575(3)	0.086(3)

Table 4.4. (b). Line parameters retrieved for Q branch lines from 11101-10002 band of CO₂.

Line label	m	Line Positions cm ⁻¹	Line intensities ×10 ⁻²³ cm ⁻¹ / (cm ⁻² molecule)	Self-broadening coefficient cm ⁻¹ atm ⁻¹
Q 2e	2	791.452697(4)	0.691(23)	0.1249(32)
Q 4e	4	791.464635(4)	1.210(40)	0.1283(35)
Q 6e	6	791.483423(4)	1.675(55)	0.1286(23)
Q 8e	8	791.5091(3)	2.065(67)	0.1193(15)
Q10e	10	791.541716(3)	2.368(76)	0.1113(12)
Q12e	12	791.581338(3)	2.576(81)	0.1108(10)
Q14e	14	791.628044(2)	2.688(83)	0.1097(9)
Q16e	16	791.681928(2)	2.709(81)	0.1074(8)
Q18e	18	791.743095(2)	2.648(77)	0.1058(8)
Q20e	20	791.811665(3)	2.519(71)	0.1024(8)
Q22e	22	791.887773(3)	2.336(64)	0.1029(8)
Q24e	24	791.971564(3)	2.116(56)	0.1012(8)
Q26e	26	792.063200(3)	1.874(48)	0.0967(7)
Q28e	28	792.162852(3)	1.625(41)	0.0949(8)
Q30e	30	792.270708(3)	1.380(34)	0.0927(8)
Q32e	32	792.386968(3)	1.149(29)	0.0887(8)
Q34e	34	792.511843(3)	0.938(24)	0.0894(9)
Q36e	36	792.645558(4)	0.751(19)	0.0855(9)
Q38e	38	792.788352(4)	0.591(16)	0.0871(11)
Q40e	40	792.940475(5)	0.456(13)	0.0868(12)
Q42e	42	793.102190(5)	0.346(11)	0.0809(12)
Q44e	44	793.273771(6)	0.257(9)	0.0806(13)
Q46e	46	793.455505(7)	0.188(7)	0.0735(13)
Q48e	48	793.647691(8)	0.135(6)	0.0740(15)
Q50e	50	793.850641(10)	0.096(4)	0.0759(18)
Q52e	52	794.064675(14)	0.066(3)	0.0735(21)
Q54e	54	794.290128(20)	0.045(2)	0.0734(28)

Table 4.4. (c). Line parameters retrieved for Q branch lines from 12201-11102 band of CO₂.

Line label	m	Line Positions cm ⁻¹	Line intensities ×10 ⁻²⁵ cm ⁻¹ / (cm ⁻² molecule)	Self-broadening coefficient cm ⁻¹ atm ⁻¹
Q 2f	2	828.25378(4)	0.606(1)	0.094(13)
Q 3e	3	828.26426(4)	1.049(2)	0.108(4)
Q 4f	4	828.25181(4)	1.433(2)	0.112(9)
Q 5e	5	828.27872(4)	1.781(3)	0.110(2)
Q 6f	6	828.24871(4)	2.096(3)	0.096(4)
Q 7e	7	828.29964(4)	2.382(3)	0.115(2)
Q 8f	8	828.24452(4)	2.635(4)	0.091(2)
Q 9e	9	828.32703(3)	2.859(4)	0.113(1)
Q10f	10	828.23923(3)	3.047(4)	0.091(2)
Q11e	11	828.36094(3)	3.205(4)	0.112(1)
Q12f	12	828.23288(3)	3.326(4)	0.087(1)
Q13e	13	828.40141(3)	3.420(4)	0.111(1)
Q14f	14	828.22549(3)	3.475(4)	0.084(1)
Q15e	15	828.44848(3)	3.508(4)	0.106(1)
Q16f	16	828.21709(3)	3.501(4)	0.083(1)
Q17e	17	828.50222(3)	3.478(4)	0.108(1)
Q18f	18	828.20771(3)	3.418(3)	0.083(1)
Q19e	19	828.56270(3)	3.348(4)	0.106(1)
Q20f	20	828.19741(3)	3.244(4)	0.082(1)
Q21e	21	828.62998(3)	3.137(4)	0.103(1)
Q22f	22	828.18622(3)	3.000(4)	0.081(1)
Q23e	23	828.70416(3)	2.868(4)	0.103(1)
Q24f	24	828.17421(3)	2.708(4)	0.081(1)
Q25e	25	828.78532(4)	2.561(4)	0.099(1)
Q26f	26	828.16142(4)	2.390(4)	0.083(1)
Q27e	27	828.87356(4)	2.236(5)	0.098(1)
Q28f	28	828.14794(4)	2.063(5)	0.082(1)
Q29e	29	828.96899(4)	1.911(5)	0.096(1)
Q30f	30	828.13382(4)	1.744(5)	0.083(1)
Q31e	31	829.07174(4)	1.600(5)	0.091(1)
Q32f	32	828.11916(5)	1.444(5)	0.080(2)
Q33e	33	829.18191(5)	1.313(4)	0.090(1)
Q34f	34	828.10404(5)	1.173(4)	0.076(2)
Q35e	35	828.25378(4)	1.056(4)	0.094(13)

A comparison between line positions from the present study and from well-known data base sources (HITRAN 2012 & GEISA 2015) is shown in fig. 4.2. (A) - (C). The 12201-03301 band in fig. 4.2. (A). shows good agreement with HITRAN for up to $J = 28$. The best agreement was found for 11101-10002 band (fig. 4.2. (B)) with HITRAN for J up to 45. The 12201-11102 band is the weakest among the three bands of interest. And as expected, the observed line positions from this band show least agreement with HITRAN in comparison to the other two bands. The residuals from this band deviate randomly from zero as shown in fig. 4.2 (C).

In case of comparisons with GEISA database, the second band 11101-10002 (fig. 4.2. (B)) shows the best agreement for the observed results whereas the first and the third band residuals (fig. 4.3. (A) and (C) respectively) are consistently high in magnitude even for lower J lines, which indicates a difference in calibration standards between two databases. As described in ref. [87], usually the line parameters of HITRAN and GEISA databases are extracted from different separate laboratory spectra recorded using different spectrometers. Very often, the frequency scaling used in these spectrometers for recording is not the same, which in turn induces systematic errors in the retrieved line parameters.

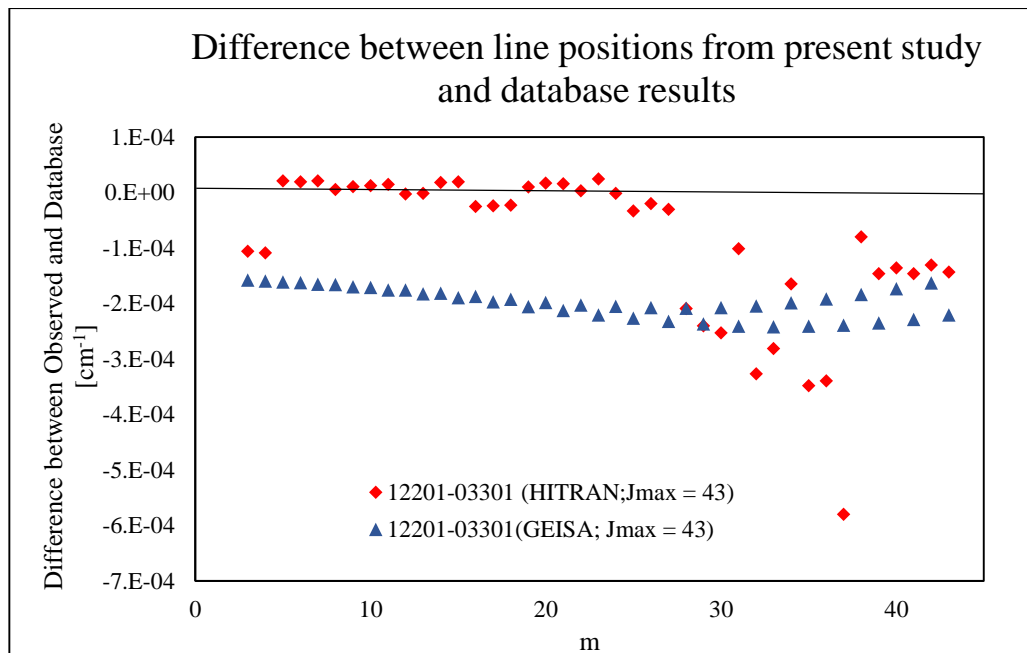


Fig. 4.2. (A). Difference between line positions from 12201-03301 band and the HITRAN 2012 [77] and GEISA 2015 [88] dataset plotted against m ($m = J$ for Q branch transitions).

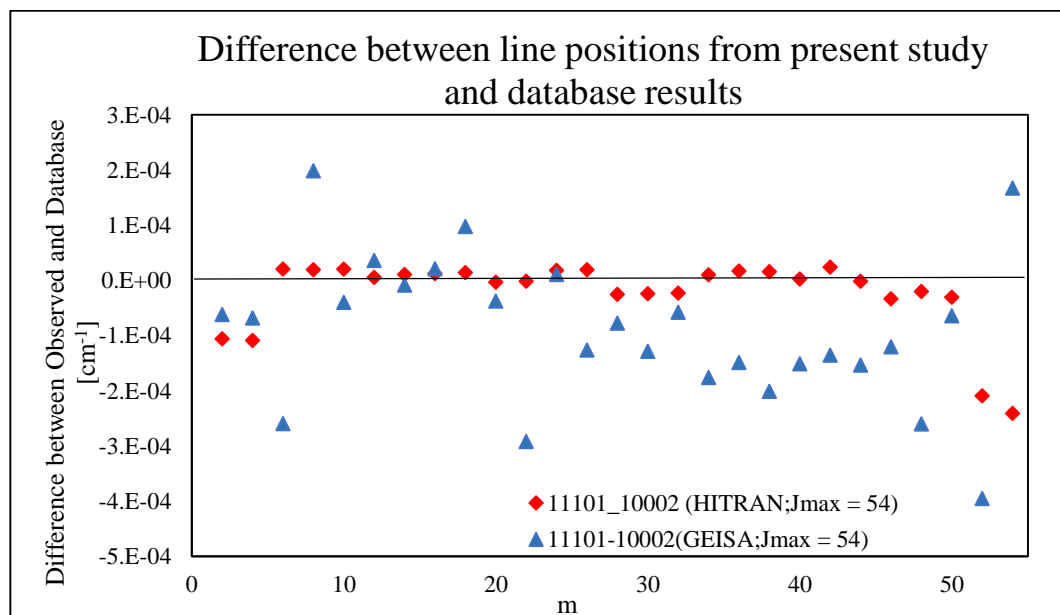


Fig. 4.2. (B). Difference between line positions from 11101-10002 band and the HITRAN 2012 [77] and GEISA 2015 [88] dataset plotted against m ($m = J$ for Q branch transitions).

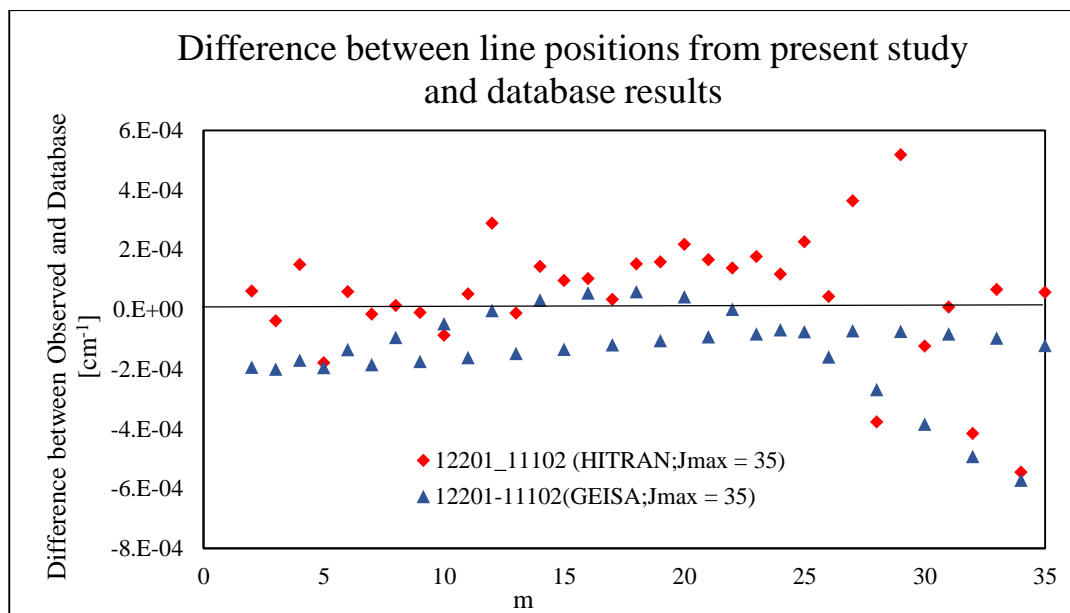


Fig. 4.2. (C). Difference between line positions from 12201-11102 band and the HITRAN 2012 [77] and GEISA 2015 [88] dataset plotted against m (m = J for Q branch transitions).

Line intensities from the three bands (12201-03301, 11101-10002 and 12201-11102) have been plotted in fig. 4.3. (A) – (C). As the figures show, 11101-10002 band intensities are much higher than the other two bands, which indicates that the change in dipole moment due to the absorption transitions is higher for this band.

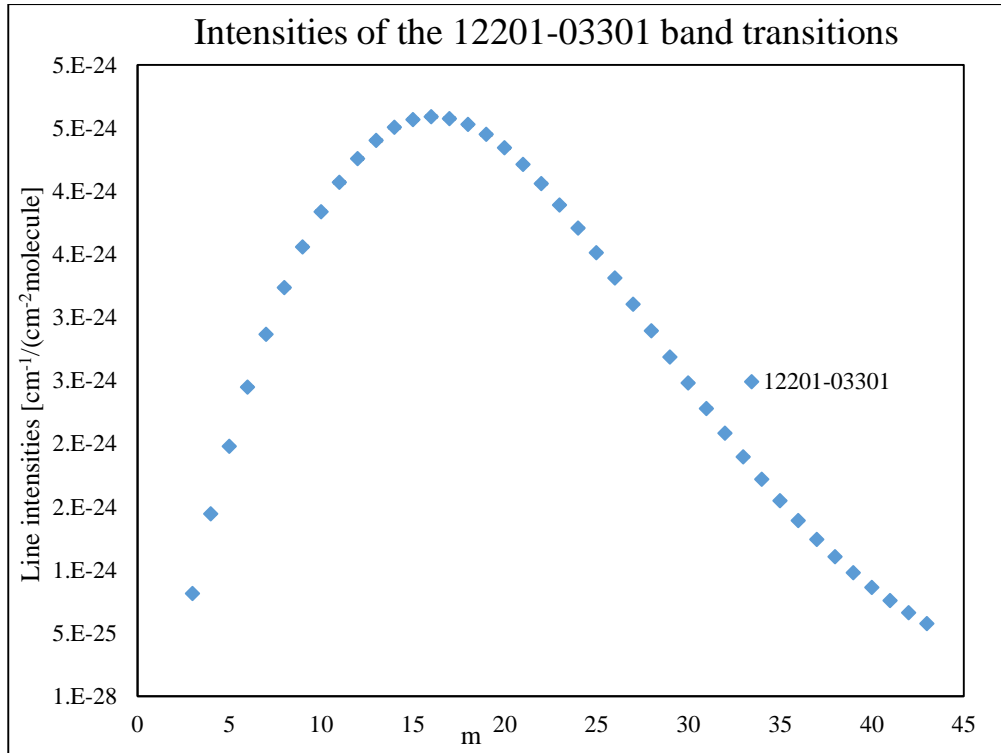


Fig. 4.3. (A). Line intensities from 12201- 03301 band of CO₂. The uncertainties shown as error bars are smaller than the size of the symbols.

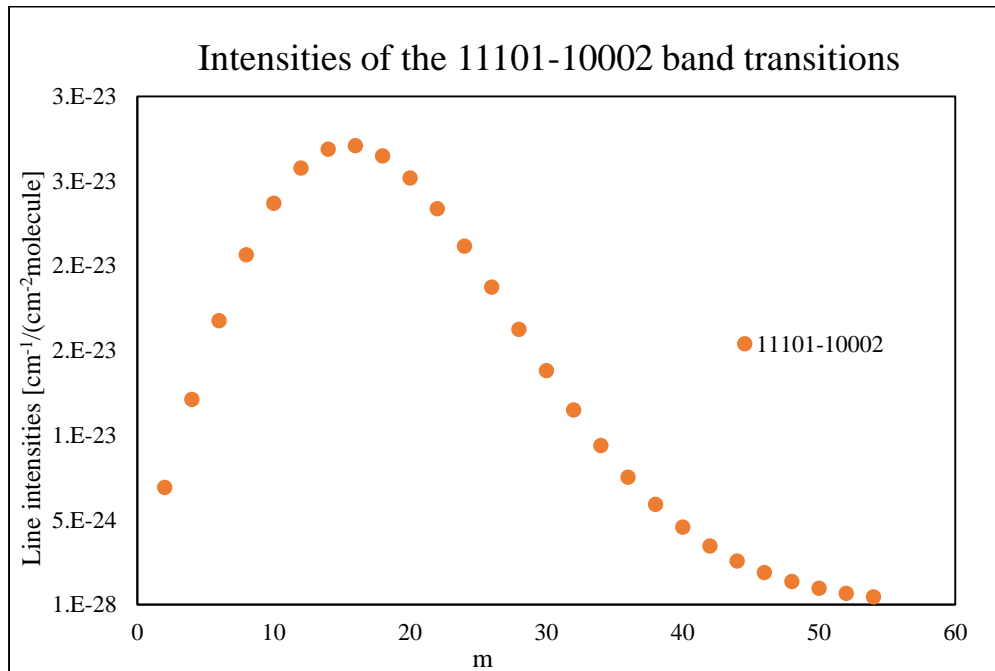


Fig. 4.3. (B). Line intensities from the 11101-10002 band of CO₂. The uncertainties shown as error bars are much larger than the symbols used.

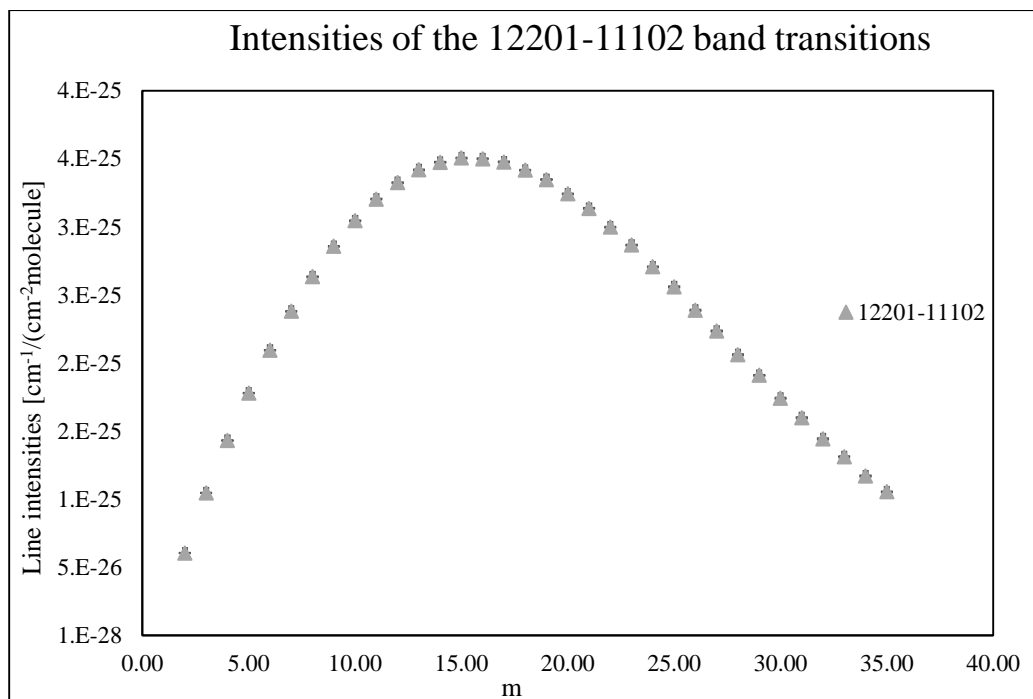


Fig. 4.3. (C). Line intensities from the 12201-11102 band of CO₂. The uncertainties shown as error bars are much larger than the symbols used.

In order to verify the line intensities of the corresponding lines listed in Table 4.4. (a)-(c), we have determined the ratio of intensities between our experimentally observed values and HITRAN 2012 and GEISA 2015 datasets for the three bands of interest. As can be seen from Fig. 4.4. the best agreement between observed and both database - HITRAN and GEISA values are found for 11101-10002 band whereas the agreement is least for 12201-11102 band transitions. Intensity values for observed and HITRAN are in better agreement for first two bands (12201-03301, 11101-10002) compared to values from GEISA database. But interestingly for 12201-11102 band, the observed values show better agreement with GEISA dataset. I found out that the line intensity values for this band has been updated recently in the GEISA database. The previously mentioned line intensity values for this band does not agree well with my observed values.

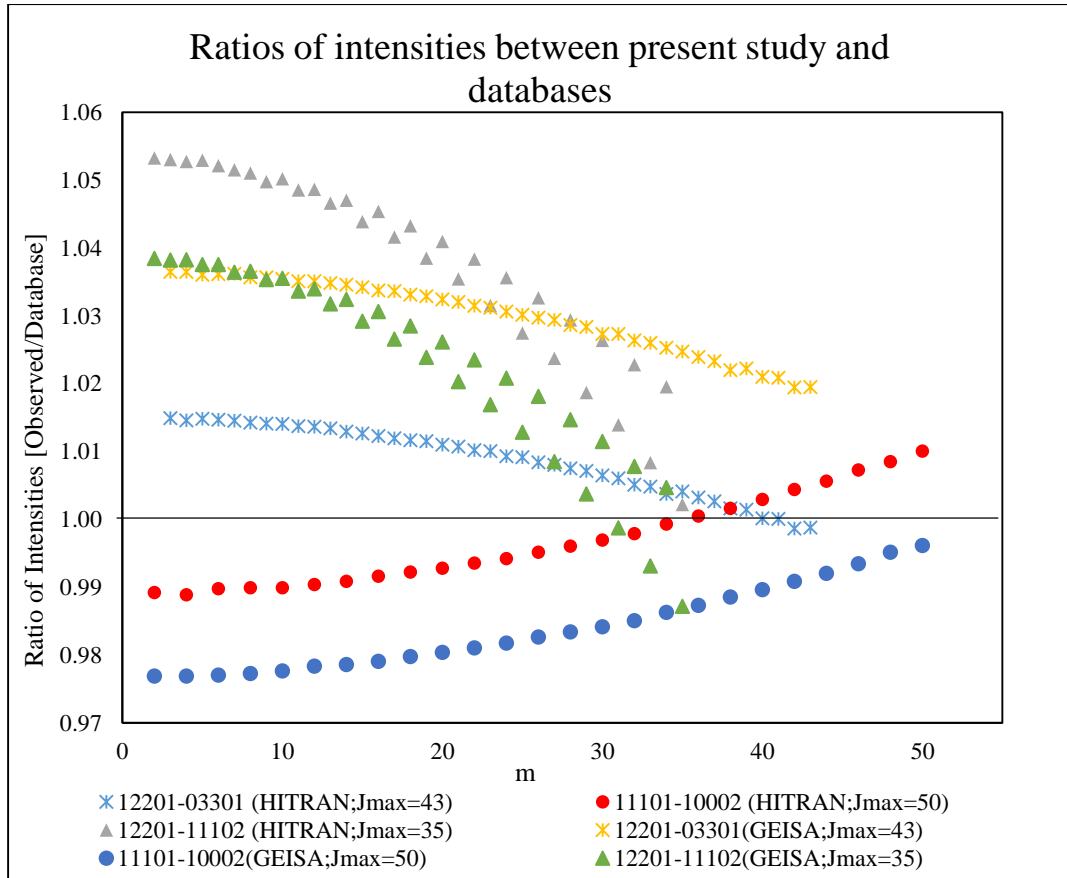


Fig. 4.4. Ratio of measured line intensities and the (HITRAN & GEISA) dataset for the three bands.

The broadening coefficients from the three band transitions have been plotted against index m in fig. 4.5. As can be seen from the figure, the broadening parameters from 12201-03301 and 11101-10002 band have similar values with a gradually descending trend for increasing J . But 12201-11102 band transitions have two distinguishable trends for broadening coefficients associated with the e (even J) and f (odd J) type transitions. The f type transitions show very much similar trend as the other two bands whereas the e type transitions have comparatively lower broadening coefficients.

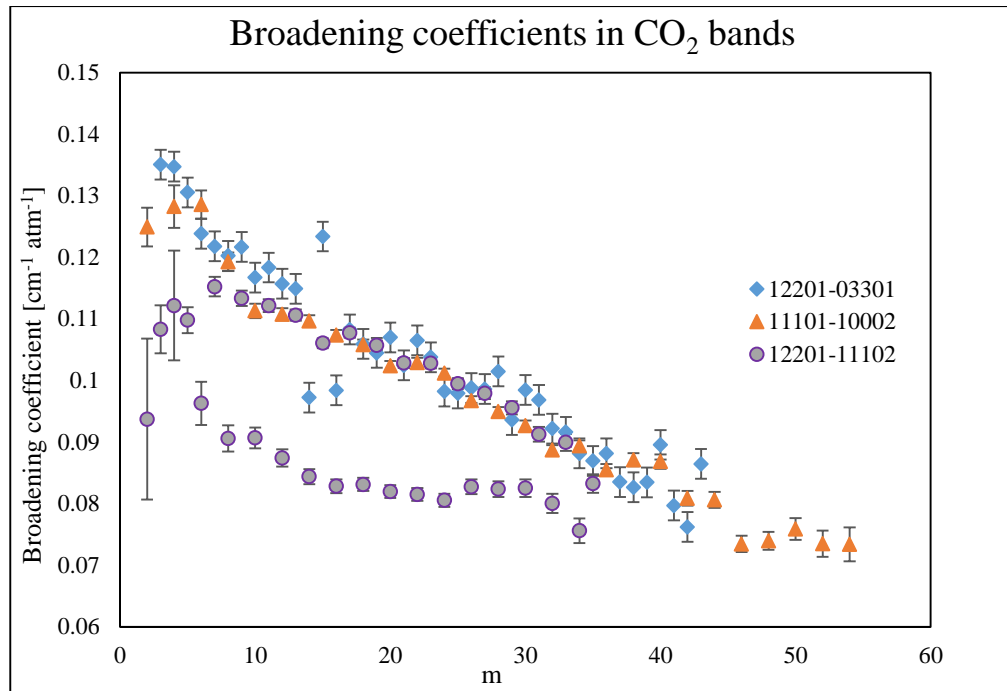


Fig. 4.5. Broadening coefficients from the three bands of CO₂ with the associated uncertainties shown as error bars.

A comparison between experimentally observed and calculated values (EPG) for broadening coefficients along with HITRAN and GIESA databases for the three CO₂ bands have been shown in fig. 4.6. (A) - (C). As the graphs suggest, all the three sets of values agree well, 93.5% for 12201-03301 band and 97.5% for 11101-10002 band except for the 12201-11102 band where the agreement is about 88.6 %. The measured broadening coefficients corresponding to the 12201-03301 band (fig. 4.6. (A)) show some scatter but an overall steady decreasing trend. The scatter in the broadening coefficient values may be due to the low line intensities in this band as well as the correlation between broadening and line mixing parameters. Also the broadening coefficients were not fitted with constrained values, thus increasing the measuring uncertainty in the fit. In Fig. 4.6. (B), the observed broadening coefficients corresponding to the strongest of the three bands (11101-10002), show very good agreement with the calculated and database values. Fig 4.6. (C)

shows broadening parameters corresponding to e and f type transitions of 12201-11102 band. It can be noticed that the odd lines, i.e. the f type transitions, have comparatively higher values for broadening coefficients than the even, e type, transitions. These results do not agree with the calculated values (EPG) as well as the HITRAN or GIESA database.

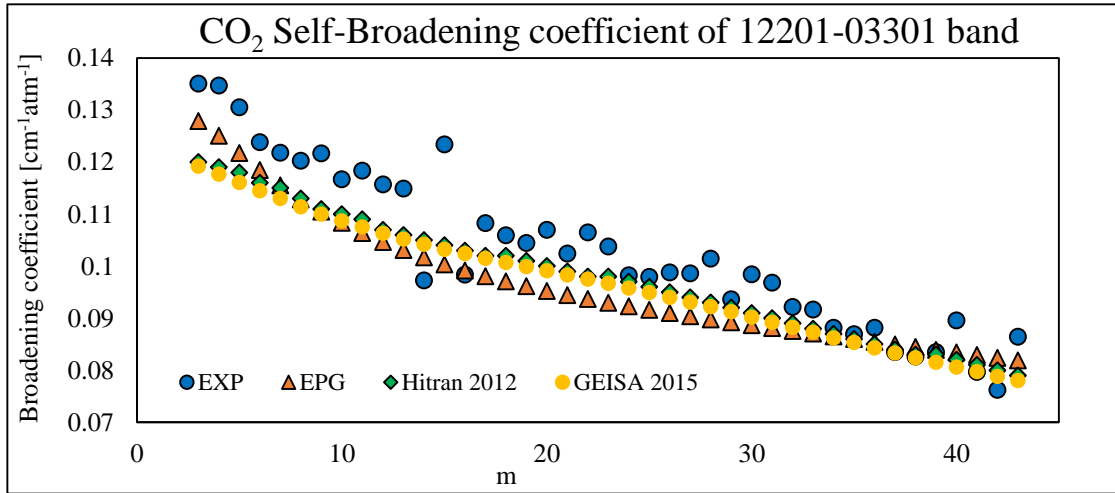


Fig. 4.6. (A). Comparison of self-broadening coefficients between observed, HITRAN 2012, GEISA 2015 and calculated (EPG) values from 12201-03301 band.

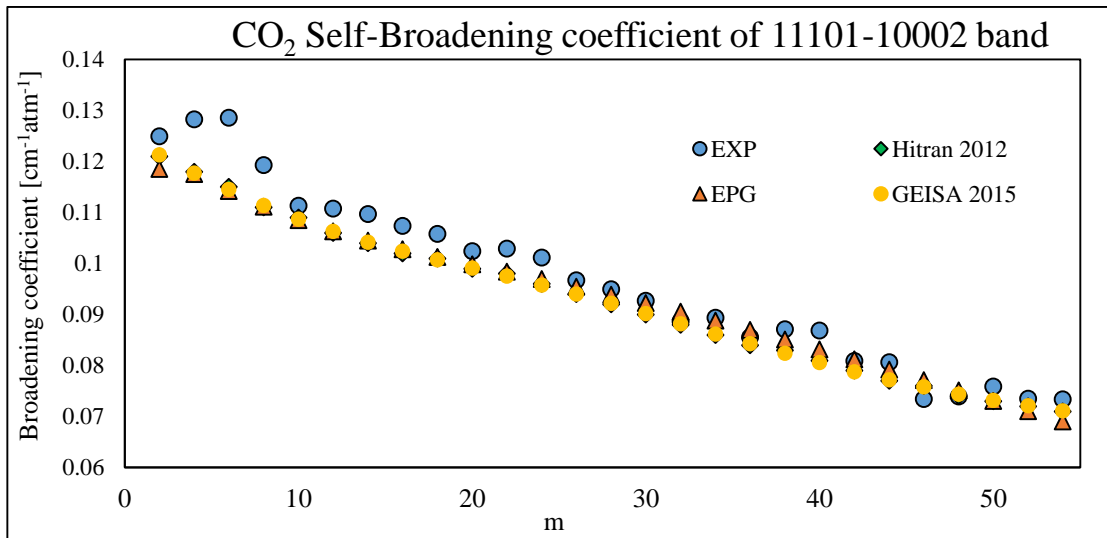


Fig. 4.6. (B). Comparison of self-broadening coefficients between observed, HITRAN 2012, GEISA 2015 and calculated (EPG) values from 11101-10002 band.

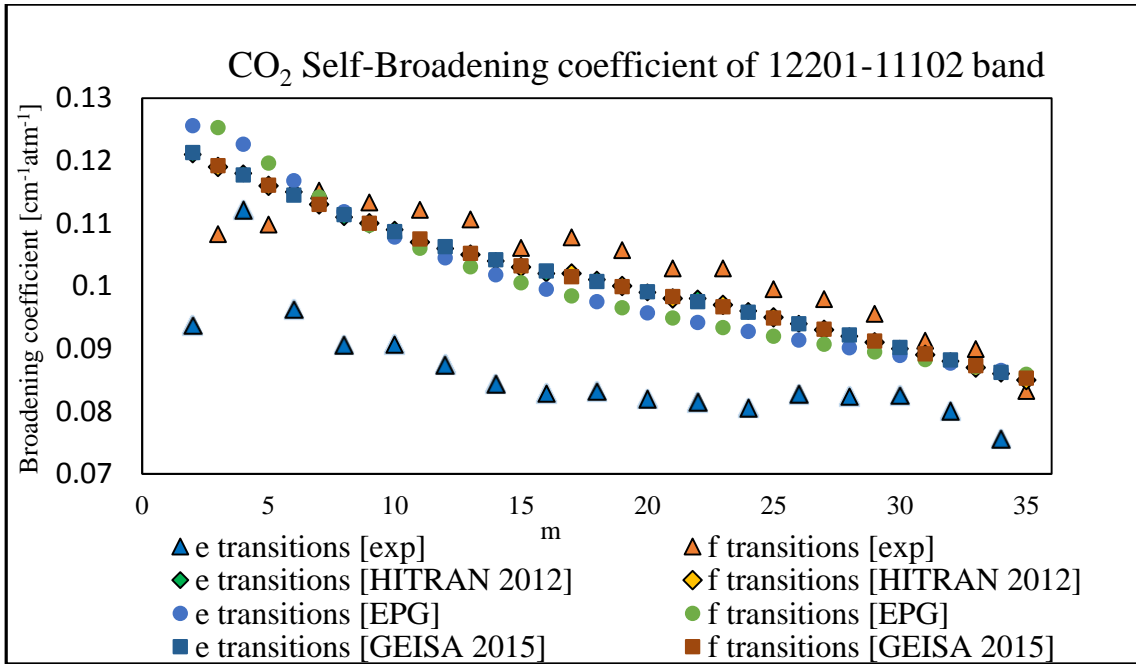


Fig. 4.6. (C). Comparison of self-broadening coefficients between observed, HITRAN 2012, GEISA 2015 and calculated (EPG) values from 12201-11102 band.

Table 4.5. Measured and calculated (EPG) line-mixing coefficients of the three bands.
This parameter has a unit atm^{-1} .

12201-03301			11101-10002			12201-11102	
m	Observed (atm^{-1})	Calculated (EPG) (atm^{-1})	m	Observed (atm^{-1})	Calculated (EPG) (atm^{-1})	m	Calculated (EPG) (atm^{-1})
3	-6.8(13)	-7.243	2	3.10(32)	3.839	2	-19.8742
4	-2.3(9)	-2.746	4	0.03(24)	0.642	3	-5.82653
5	-1.3(12)	-1.241	6	0.38(17)	0.101	4	-4.65810
6	0.2(1)	-0.600	8	0.41(11)	-0.060	5	-3.04814
7	-0.8(4)	-0.239	10	0.27(7)	-0.129	6	5.539519
8	-0.2(3)	-0.077	12	0.10(6)	-0.159	7	-1.87140
9	0.3(3)	0.072	14	-0.02(6)	-0.173	8	2.19391
10	0.2(3)	0.102	16	0.02(5)	-0.176	9	-1.26044
11	-0.3(3)	0.198	18	-0.12(5)	-0.174	10	1.97099
12	1.0(3)	0.171	20	-0.05(5)	-0.170	11	-0.92139
13	1.7(5)	0.257	22	0.22(5)	-0.164	12	1.32838
14	-0.1(16)	0.195	24	-0.04(5)	-0.157	13	-0.70737
15	-1.9(8)	0.287	26	-0.12(5)	-0.149	14	1.38318
16	Fixed	0.198	28		-0.141	15	-0.57009
17	-0.8(5)	0.305	30		-0.134	16	1.26788
18	0.3(3)	0.190	32		-0.127	17	-0.47037
19	0.5(3)	0.316	34		-0.120	18	1.14738
20	-0.1(3)	0.175	36		-0.113	19	-0.39998
21	0.1(3)	0.323	38		-0.106	20	1.04600
22	0.8(3)	0.157	40		-0.100	21	-0.34506
23	-0.2(3)	0.330	42		-0.095	22	1.00182
24	-0.1(3)	0.136	44		-0.089	23	-0.30229
25	0.6(3)	0.337	46		-0.084	24	0.93329
26	0.6(3)	0.113	48		-0.079	25	-0.26811
27	-0.2(3)	0.345	50		-0.075	26	0.872424
28	-0.4(3)	0.088	52		-0.070	27	-0.24040
29	0.5(3)	0.355	54		-0.066	28	0.89565
30	-0.2(5)	0.061	56		-0.063	29	-0.21764
31		0.368	58		-0.059	30	0.78527
32		0.031	60		-0.056	31	-0.19625
33		0.383	62		-0.053	32	0.79189
34		-0.003	64		-0.050	33	-0.17984
35		0.405	66		-0.047	34	0.76334
36		-0.044	68		-0.045	35	-0.16509
37		0.435	70		-0.043	36	0.74437
38		-0.099				37	-0.15222
39		0.482				38	0.71639
40		-0.183				39	-0.14083
						40	0.69790

The line-mixing coefficients (measured and calculated values) corresponding to 12201-03301, 11101-10002 and 12201-11102 band are listed in Table 4.5. Due to low intensity of the observed lines, it was only possible to measure line-mixing parameters for 12201-03301 band up to $J = 30$ and for 11101-10002 band up to $J = 26$. For lines above the highest J , the values for line-mixing parameter were assumed to be zero while performing the non-linear least squares fit. It was not possible to measure line-mixing coefficients for 12201-11102 band transitions because of their very weak line strength. However, calculated values for line mixing coefficients for this band were obtained by adopting EPG approximation and are listed in Table 4.5.

In Fig. 4.7. (A) and 4.7. (B), the observed line-mixing coefficients corresponding to 12201-03301 and 11101-10002 band have been compared with the calculated values from EPG law and the values found using Energy Corrected Sudden approximation (ECS) listed in AER (Atmospheric and Environmental Research) database. This database enlists all the line parameter information from HITRAN. But it also included the calculated line-mixing coefficient values for numerous bands of CO_2 . A detailed description of the format of ECS method could be found in section 2.7.2 in chapter 2 as well as in ref. [71]. In fig. 4.7. (A), the experimental values show good agreement with the calculated results (EPG and ECS) for 12201-03301 band. But for 11101-10002 band the observed line-mixing parameters are comparatively higher than the calculated values as shown in fig. 4.7. (B). The calculated values of line-mixing coefficients for 12201-11102 band have been shown in fig. 4.7. (C). The figure shows two distinguishable patterns for e and f type transitions of this band. As mentioned before a similar behavior has been noticed for the broadening coefficients of this band.

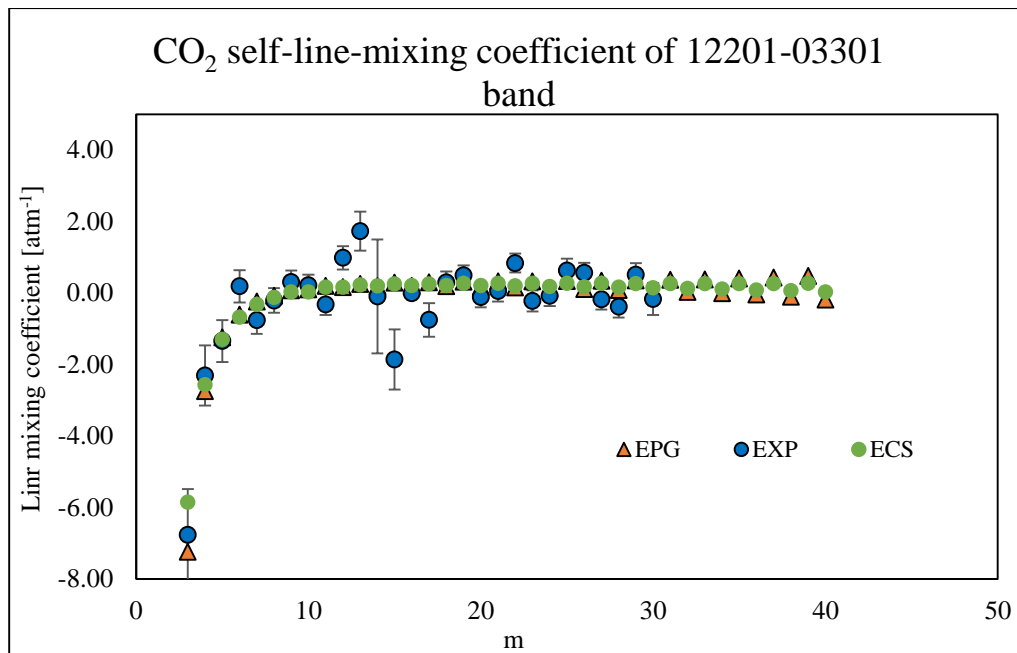


Fig. 4.7. (A). Calculated (EPG, ECS) self-line mixing coefficients from 12201-03301 band. Uncertainties associated with the observed self-line-mixing values are shown as error bars.

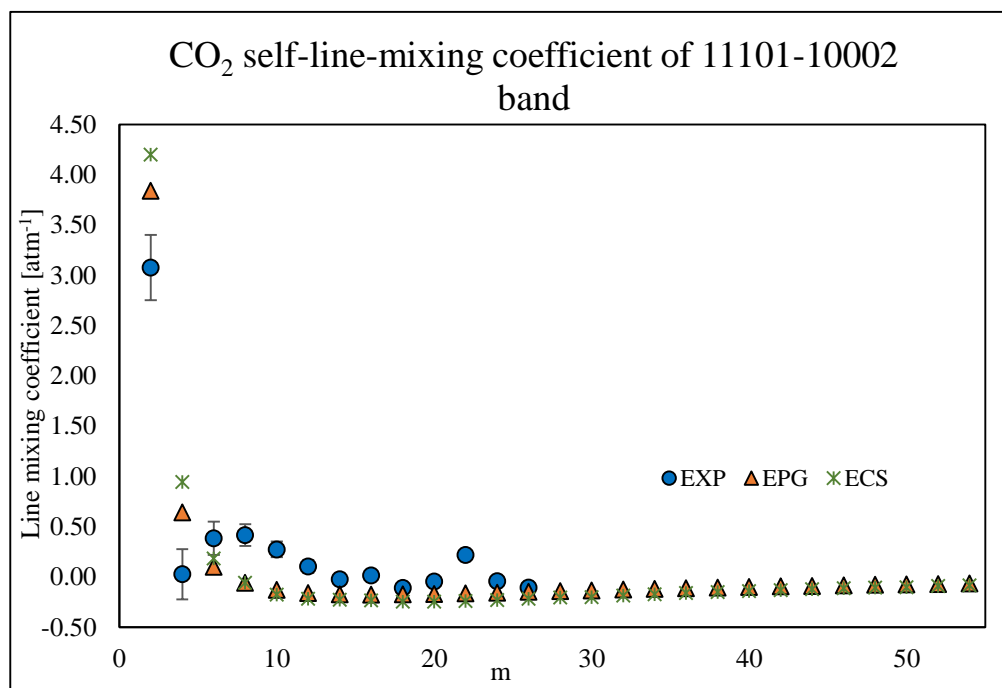


Fig. 4.7. (B). Observed and calculated (EPG, ECS) self-line-mixing coefficients from 11101-10002 band. Uncertainties associated with the observed self-line mixing values are shown as error bars.

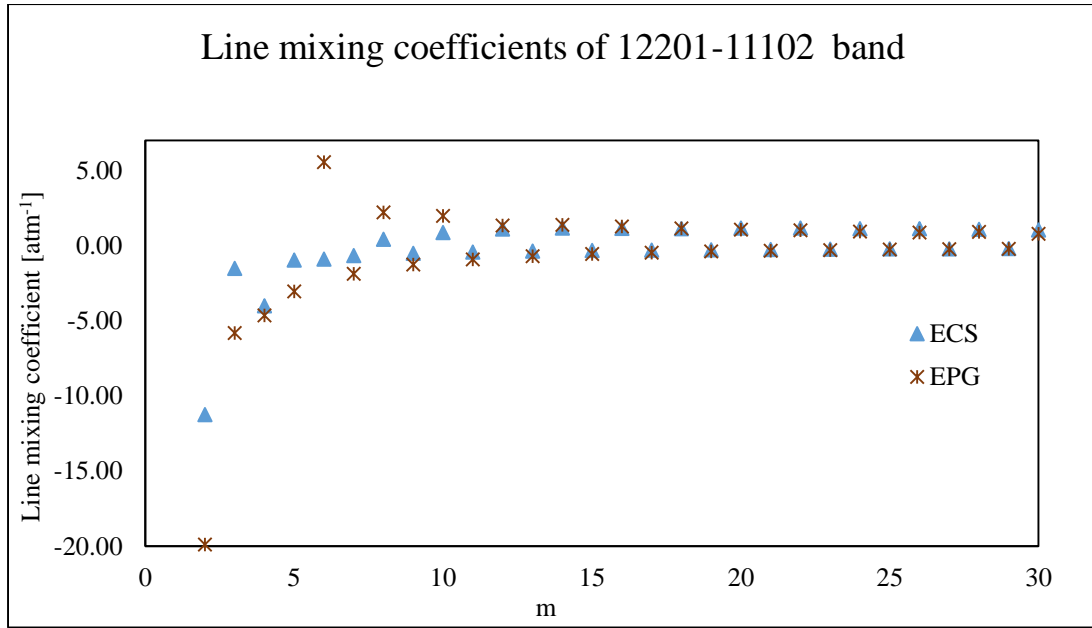


Fig. 4.7. (C). Calculated (EPG, ECS) self-line-mixing coefficients from 12201-11102 band.

The following table 4.6. lists the average values of the uncertainties associated with the line-shape parameters corresponding to the three band transitions. In case of line positions, the average uncertainty is the highest for 12201-11102 and lowest for 11101-10002 band. In contrast, for intensity measurements, the average uncertainty associated with 12201-11102 band is the lowest and highest for the strongest 11101-10002 band. This is because a small asymmetry in residuals for a fitted high intensity line produces a much larger uncertainty in line-shape parameters compared to a similar asymmetry in low intensity line. For the very same reason the uncertainty in broadening parameters is higher for 12201-03301 band than the weaker 12201-11102 band. In case of line mixing, both 12201-03301 and 11101-10002 band show high degree of uncertainty, which may be associated with the fact that in constraint analysis the line positions and intensities are restricted by the theoretically computed band centers and band intensities (equation 4-1 and

4-2). This may result in a slightly higher degree of uncertainty in the overall fit due to small asymmetries not taken into account. Although parameters like broadening and shift are not much affected in this method, but those small asymmetries induce a much higher level of uncertainty in retrieving accurate values for line mixing parameter.

Table 4.6. Average values of uncertainties associated with the line-shape parameters corresponding to the three band transitions.

Average Uncertainty				
Bands	Line position cm⁻¹	Intensity cm⁻¹/(cm⁻²·molecule)	Broadening coefficient cm⁻¹atm⁻¹	Line mixing coefficient atm⁻¹
12201-03301	1.02×10^{-05}	6.44×10^{-27}	3.16×10^{-3}	0.37
11101-10002	4.92×10^{-06}	3.85×10^{-26}	1.35×10^{-3}	0.10
12201-11102	3.71×10^{-05}	3.66×10^{-28}	1.96×10^{-3}	Not measured

Overall my retrieved line-shape parameters show good agreement with the database results as well as with the calculated values from EPG and ECS approximations. Also all the three bands were recorded with very high resolution (limit 0.0020067 cm⁻¹) to ensure accurate retrieval of spectral information.

Chapter 5. Line-shape study of the $\nu_1+\nu_3$ band of acetylene broadened by CO_2

In this work 19 spectral lines corresponding to the P-branch of the $\nu_1+\nu_3$ band of acetylene were recorded at different pressures (50 – 750 Torr) and 6 different temperatures from 216 to 333 K using a tunable diode laser spectrometer. Experimental details of this set-up have been discussed in section 3.1. of chapter 3.

$\nu_1 + \nu_3$ is a combination of two fundamental bands ν_1 and ν_3 . This combination of two bands can also be represented as 10100-00000, where 10100 is the upper vibrational level and 00000 is the ground or lower vibrational level.

The raw spectra were processed using the Labview software and prepared for a line shape analysis using the Labfit program [74, 75]. In the final processing step all the “bad” spectra were removed, for example spectra that were found to be saturated. The room-temperature values for line intensities were found using equation 4-2. The line position, broadening and shift coefficients as well as their temperature-dependence exponents were calculated by implementing equations 4-4 and 4-5 in Labfit.

It can be noticed from the Table 5.1. that the uncertainties associated with line positions are much higher for lines corresponding to high J , i.e. for lines with low intensities (fig. 5.5). This is expected since the weaker lines in a band have lower number of sampling points, therefore increasing the uncertainties associated with the retrieved parameters from non-linear least squares fit.

In comparison to the line positions, it is more difficult to interpret the uncertainty pattern associated with the line intensities. In contrast to line positions, the measurement uncertainties for line intensities are much higher for lower J lines (Table 5.1.). This is because the higher J lines are much weaker (smaller in intensity) than the lower J lines. And a small asymmetry in a fitted residual of a high-intensity line is usually much higher

in magnitude than the asymmetries observed in the residuals of a line with comparatively lower intensity.

Table 5.1. Line parameters obtained from the P branch of $\nu_1+\nu_3$ band of acetylene. The errors quoted in parentheses are one standard deviation.

Line label	m	Line positions (cm ⁻¹)	Line intensities $\times 10^{-21}$ cm ⁻¹ /(cm ⁻² · molecule)	Broadening coefficients (cm ⁻¹ atm ⁻¹)	Shift coefficients (cm ⁻¹ atm ⁻¹)
P2e	2	6551.7327(3)	1.6137(17)	0.1516(15)	-0.00298(2)
P4e	4	6546.8978(1)	2.4994(10)	0.1473(15)	-0.00366(1)
P6e	6	6541.9606(2)	3.2103(17)	0.1363(14)	-0.00394(1)
P8e	8	6536.9214(2)	3.6618(16)	0.1307(13)	-0.00452(1)
P10e	10	6531.7804(2)	3.7225(18)	0.1232(12)	-0.00471(1)
P12e	12	6526.5386(2)	3.3973(18)	0.1098(11)	-0.00579(1)
P14e	14	6521.1953(2)	2.9401(11)	0.1027(10)	-0.00659(1)
P16e	16	6515.7516(2)	2.3908(9)	0.0955(10)	-0.00668(1)
P20e	20	6504.5640(1)	1.2789(6)	0.0817(8)	-0.01010(1)
P21e	21	6501.7050(3)	3.6801(39)	0.0778(8)	-0.01264(2)
P22e	22	6498.8208(2)	0.8471(4)	0.0746(7)	-0.01161(1)
P23e	23	6495.9116(4)	2.3478(20)	0.0708(7)	-0.00928(2)
P24e	24	6492.9786(3)	0.5339(3)	0.0706(7)	-0.01397(1)
P25e	25	6490.0203(2)	1.3206(5)	0.0736(7)	-0.01232(1)
P26e	26	6487.0375(2)	0.3269(3)	0.0677(7)	-0.01368(1)
P27e	27	6484.0300(4)	0.9079(15)	0.0647(7)	-0.01274(2)
P28e	28	6480.9987(5)	0.1933(3)	0.0669(6)	-0.01805(2)
P29e	29	6477.9427(4)	0.4931(14)	0.0589(7)	-0.01376(2)
P30e	30	6474.8613(6)	0.0911(2)	0.0560(6)	-0.01677(3)

Table 5.2. Temperature-dependence exponents for broadening and shift coefficients. The errors quoted in parentheses are one standard deviation.

Line label	Temperature-dependence exponents for broadening	Temperature-dependence exponents for shift
P2e	0.838(1)	0.0000430(6)
P4e	0.888(1)	0.0000296(5)
P6e	0.837(1)	0.0000158(5)
P8e	0.829(1)	0.0000094(3)
P10e	0.595(2)	0.0000121(6)
P12e	0.688(1)	0.0000032(3)
P14e	0.678(1)	0.0000102(2)
P16e	0.660(1)	0.0000181(4)
P20e	0.761(2)	0.0000363(4)
P21e	0.732(3)	0.0000430(5)
P22e	0.786(1)	0.0000371(2)
P23e	0.780(2)	0.0000407(3)
P24e	0.816(1)	0.0000384(3)
P25e	0.805(1)	0.0000417(3)
P26e	0.820(2)	0.0000396(5)
P27e	0.883(1)	0.0000492(3)
P28e	0.886(4)	0.0000568(9)
P29e	0.882(2)	0.0000679(5)

Fig. 5.1 shows the fitting of the P 14 line using a multi-spectrum fitting software (Labfit) used in my present study. After each trial of fitting, the software calculates the RMS for every fitted spectrum as well as the standard deviation for the whole spectra. This information is very helpful for obtaining a very good fit of the recorded spectra.

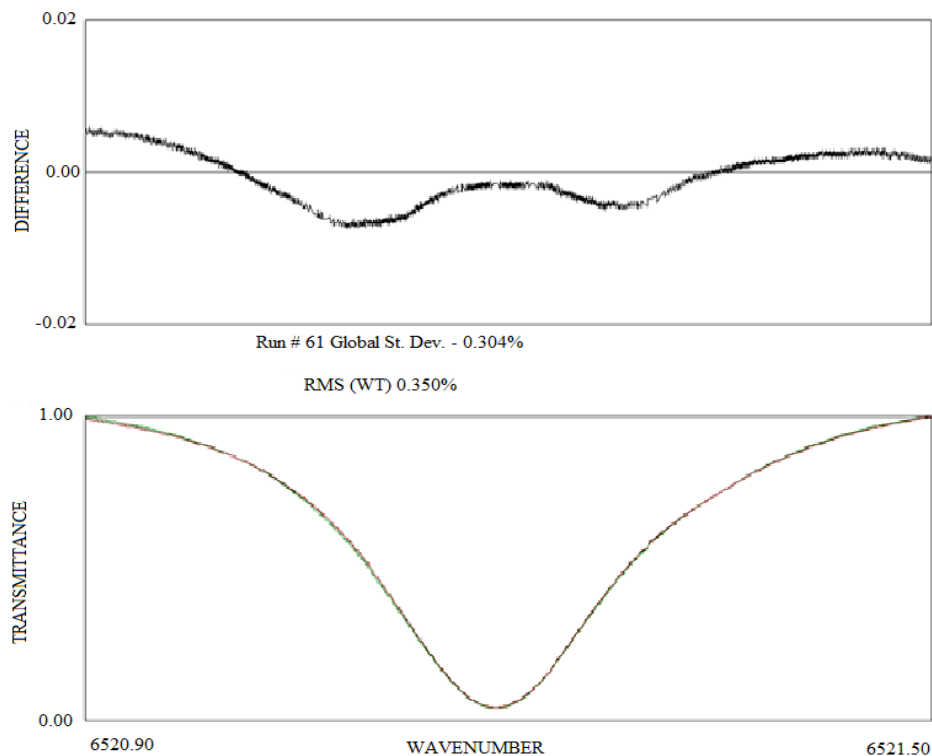


Fig. 5.1. Photo of on-linear fit of P14 line done by applying the Voigt profile in Labfit [78, 79].

Fig. 5.2. shows 46 spectra of the same P14 line recorded at different temperatures and pressures. In this figure each band of fitted lines represents spectra recorded at the same pressure but different temperatures. For example, the narrowest band of lines represent lines corresponding to 50 Torr pressure and temperatures ranging from 216 K to 333 K. Therefore it is evident from the figure that the broadening of spectral lines due to pressure is much higher than the temperature.

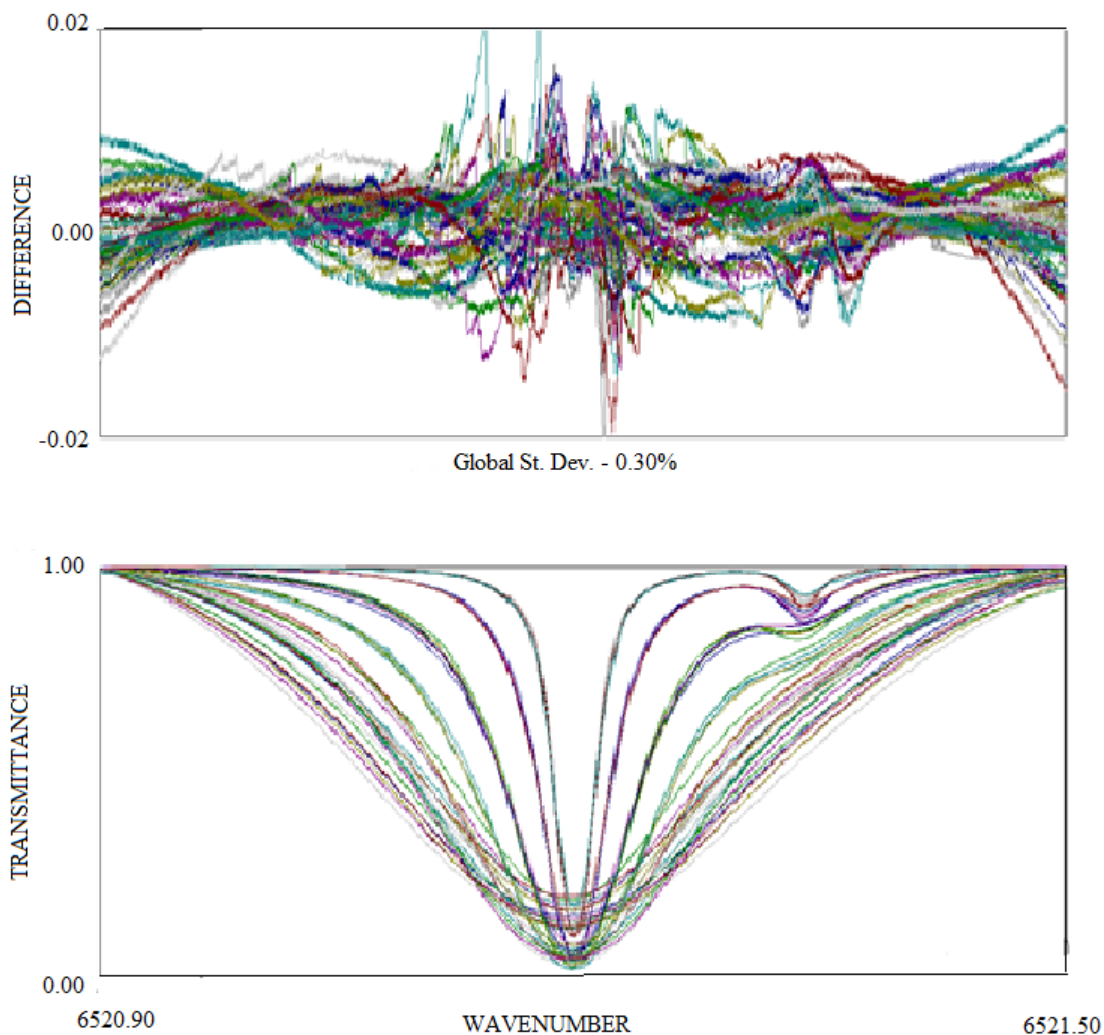


Fig. 5.2. Photo of 46 overlaid spectra of P14 line with an overall standard deviation of 0.30. The narrowest band of lines represents spectrum recorded at 50 Torr pressure and different temperatures (216-333 K). The gradually broadened lines were recorded at increasing pressures up to 750 Torr.

The line positions along with the associated uncertainties are shown in fig. 5.3. The very small uncertainties associated with the retrieved positions indicates high accuracy of the measurements. The line spacing information from this figure can be utilized to calculate different rotational constants (B_0 , D_0 etc.).

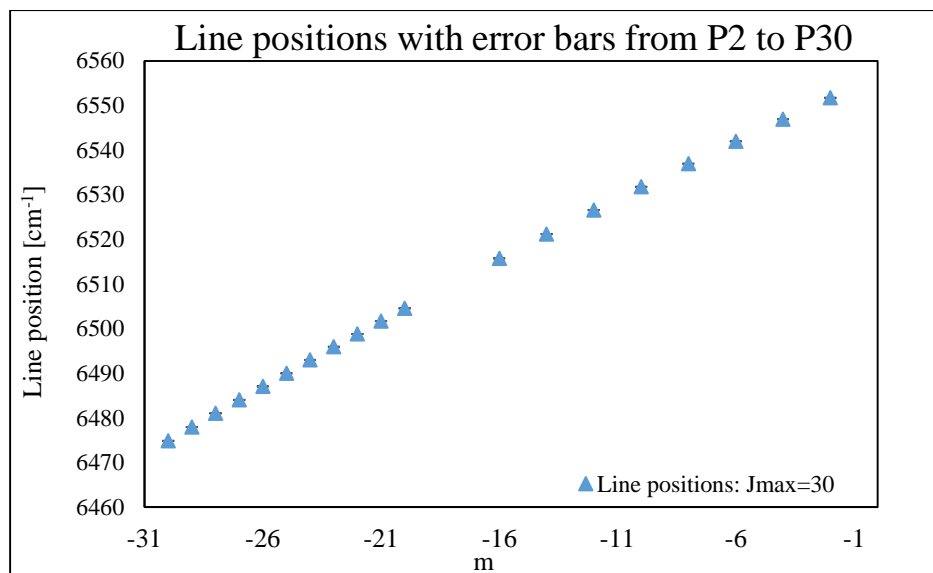


Fig. 5.3. Line position of transitions corresponding to the $\nu_1+\nu_3$ band of acetylene broadened by CO_2 plotted against index m ($m = -J$ for P branch lines, where J is a rotational quantum number). The uncertainties shown as error bars are much smaller than the size of the symbols.

Fig. 5.4. shows the difference in line positions between the present study and the databases of HITRAN 2012 [73] and GEISA 2015 [83]. It can be noticed from the figure that the residuals found from observed and GEISA 2015 values are consistently smaller than the (observed – HITRAN 2012) values. Also the residuals corresponding to the higher J lines are much larger than the lower J lines. This can be explained by the weak line strength of the higher J lines, which makes it difficult for the fitting routine to extract accurate positions corresponding to the individual line. Also, the collected line positions from HITRAN are slightly different than the GEISA values, which is evident from the shown residuals in the figure. This difference in line positions is explained in the previous chapter as well as in ref. [82].

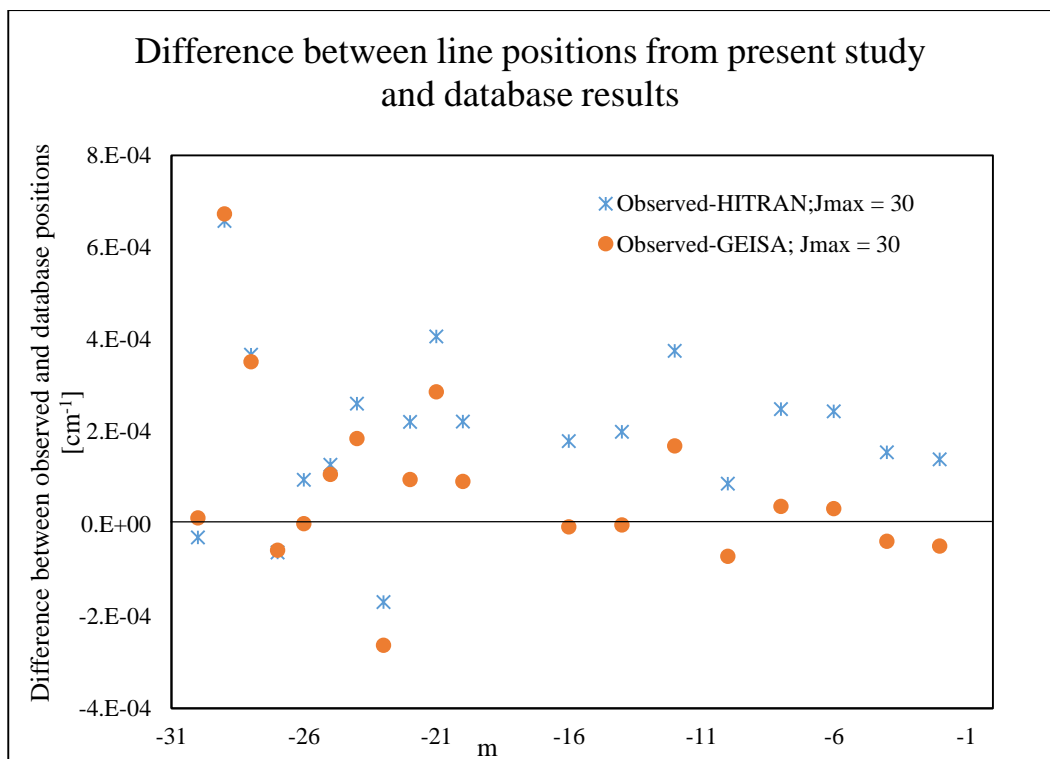


Fig. 5.4. Residuals of measured line positions and database results for the P branch of $\nu_1+\nu_3$ band of acetylene plotted against m ($m = -J$ for P branch lines, where J is a rotational quantum number [See section 2.4.3]).

Fig. 5.5. shows line intensities obtained from the present study and databases like HITRAN 2012 and GEISA 2015. It is evident from the figure that the lines corresponding to the even J values have a different intensity pattern than the odd J lines. Also only 22 lines of $\nu_1 + \nu_3$ band were recorded, among which 19 lines are reported in this thesis. The odd J lines up to $J = 20$ have high intensities therefore, are very close to being saturated.

The lines corresponding to $J = 1$ and $J = 18$ were recorded but not included in the fit, because they overlapped with neighboring lines from different bands (unknown) generating a bad fit. Among the even J lines, P10 has the highest line strength.

It can also be noticed from the figure that the experimentally found line strengths corresponding to the even J lines are consistently lower than the database results.

Conversely, the recorded intensity values corresponding to the odd J lines show an opposite trend having higher intensities than the database results. This deviation in line intensity may be associated with the line-mixing effect which in this case is transferring intensity from odd J lines to even J lines [56].

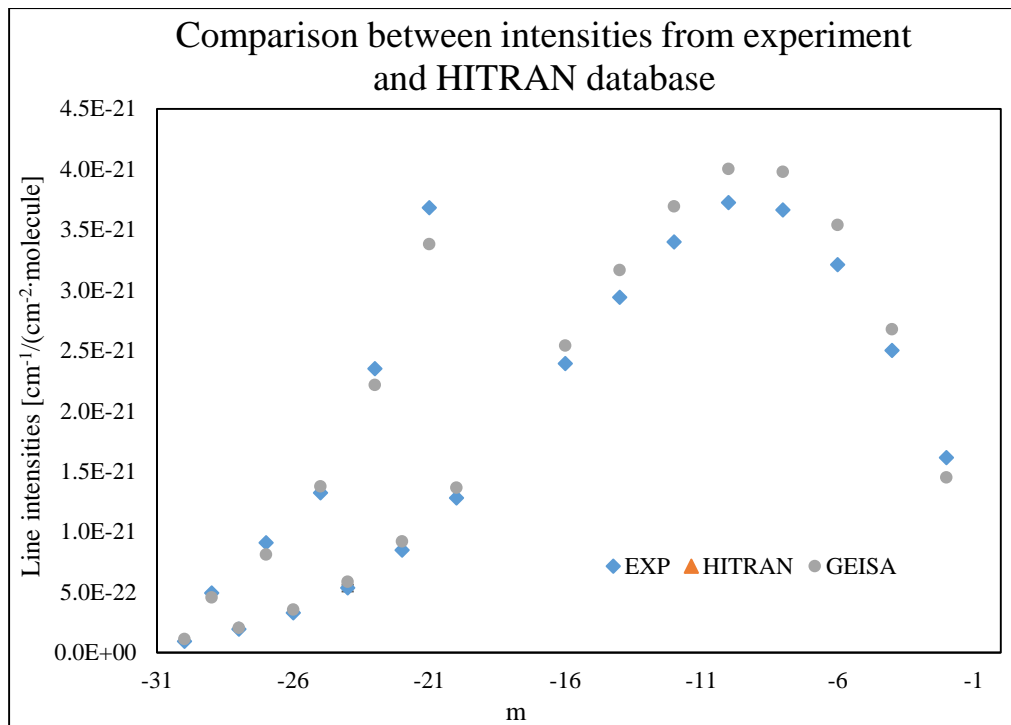


Fig. 5.5. Comparison of line intensities between experimentally observed and collected values from HITRAN 2012 and GEISA 2015 database. Uncertainties shown as error bars are much smaller than the size of the symbols.

The observed broadening coefficients associated with the $\nu_1+\nu_3$ band transitions are shown in fig. 5.6. The measurement uncertainties associated with this line-shape parameter exhibit about the same order of magnitude for all the absorption lines in this band.

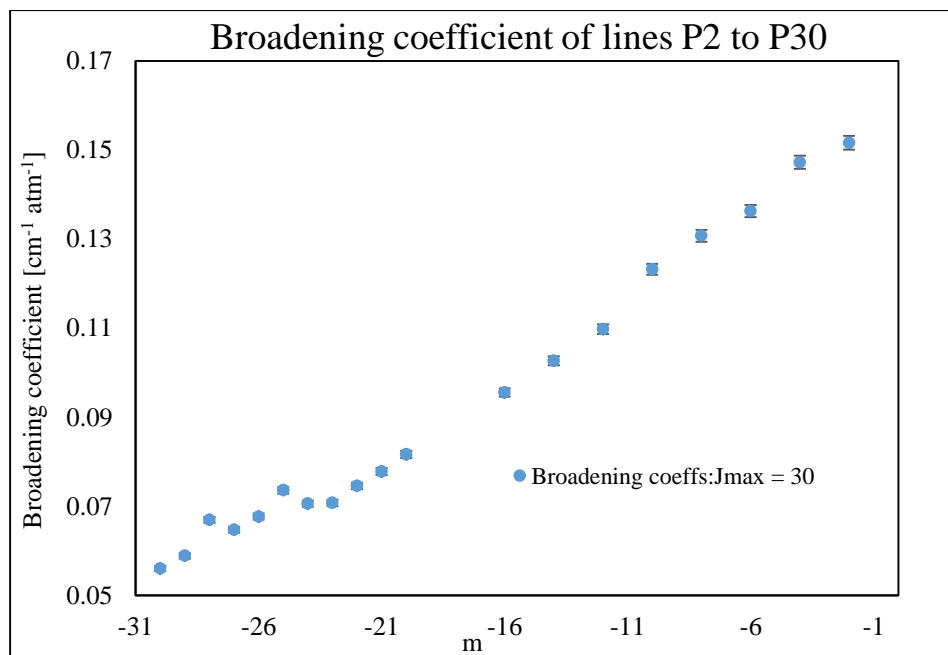


Fig. 5.6. Broadening coefficients of absorption lines from $\nu_1+\nu_3$ band of acetylene broadened by CO_2 . Error bars show uncertainties associated with the retrieved broadening parameters from non-linear least squares fit.

Broadening coefficients found from the $\nu_1+\nu_3$ band transitions of acetylene using different perturber gases have been shown in Fig. 5.7. As can be noticed from the figure that the broadening coefficients found from the present study of acetylene broadened by CO_2 are comparatively lower than the values found from other studies using N_2 [49], Air [42], Xe [42] and H_2 [42] as perturbing gases. The only exception is He, where the broadening coefficients up to $J = 16$ line are comparative lower than the CO_2 study. This is to be expected since the theoretically calculated pressure-broadening coefficients for $\text{C}_2\text{H}_2 - \text{He}$ system (by Thibault [89]) agrees well with the experimentally found results (by Arteaga *et al.* [42]). They confirmed that the $\text{C}_2\text{H}_2 - \text{He}$ system shows negligible rotational or J dependence, which is evident from the fig. 5.7. It can be noticed from this figure that $\text{C}_2\text{H}_2 - \text{H}_2$ system also shows small J dependence. For small molecules like H_2 and He, the

interaction area between neighboring (self and foreign) molecules is also comparatively small. Therefore, the rate of intermolecular collisions is different for different (radiator-perturber) system. Small molecules like H₂ or He cannot perturb the initial and final rovibrational states very easily. Therefore, collision induced line parameters corresponding to this system show negligible change as we go to higher J transitions.

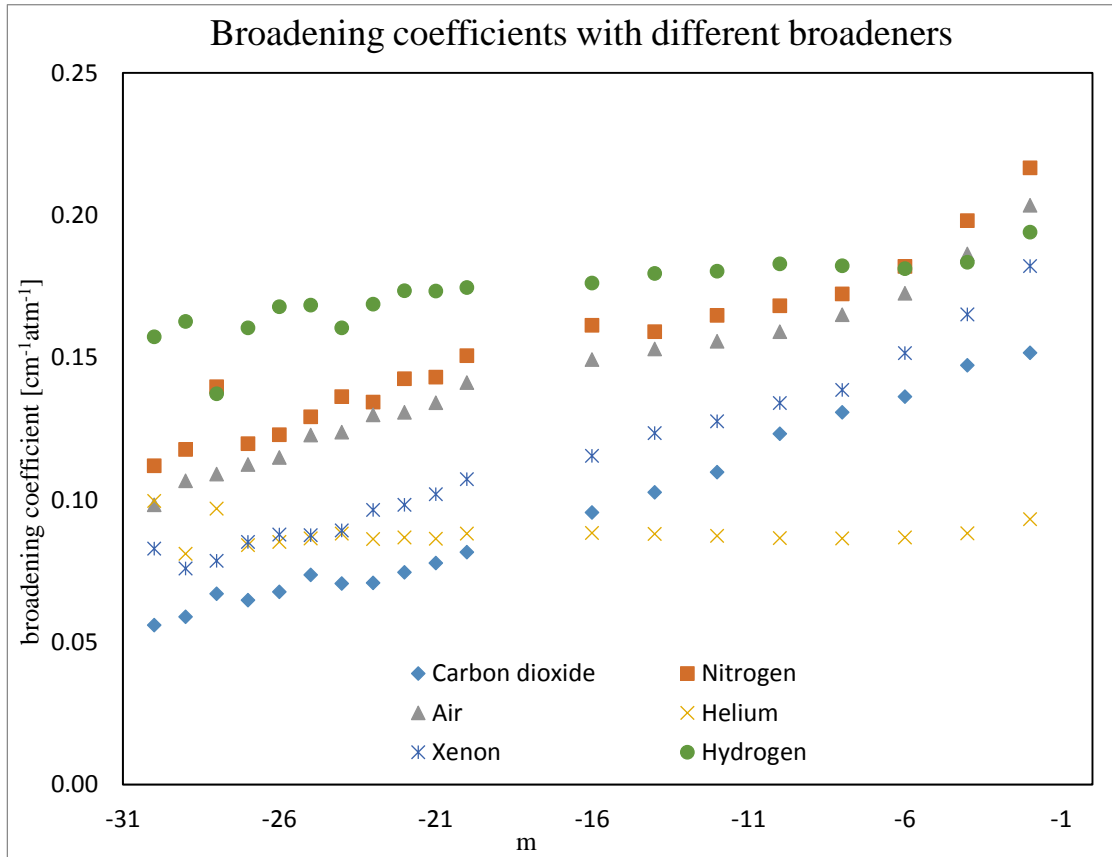


Fig. 5.7. Comparison between broadening coefficients from acetylene broadened by CO₂ study and other studies using different perturbing gases.

The retrieved shift-coefficient parameters and their associated uncertainties have been plotted in fig. 5.8. Similar to the broadening coefficients, the uncertainties associated with the shift coefficients have also about the same order of magnitude for each line in the

$\nu_1+\nu_3$ band. Also it is evident from the figure that the shift coefficient values show a steady decrease up to $J = 20$ line. Afterwards the values show asymmetry from this steady descending trend with even and odd J lines exhibiting distinguishable patterns. This is explained with details in the later section.

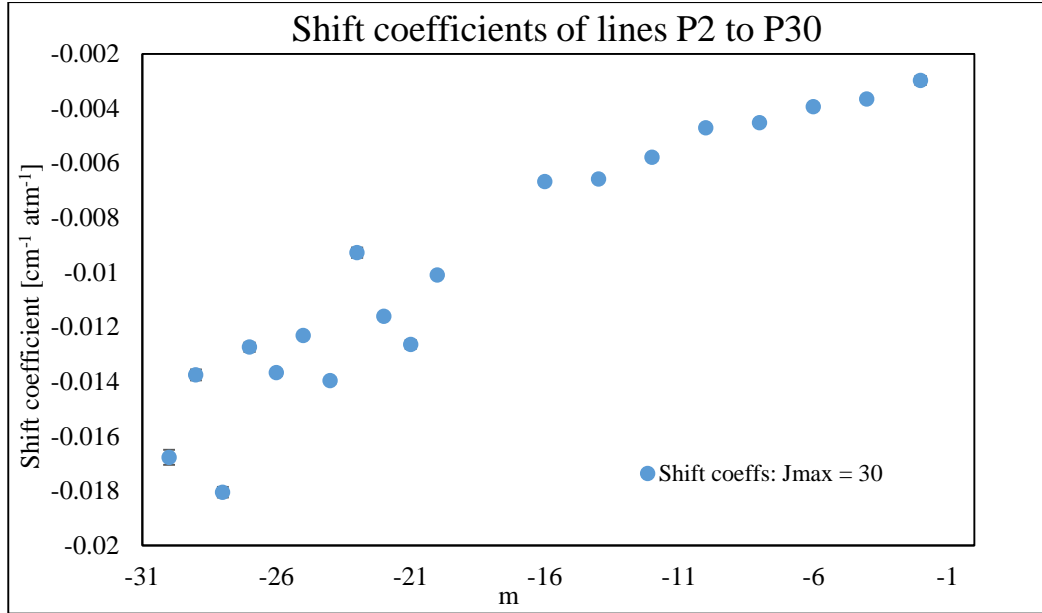


Fig. 5.8. Shift coefficients of absorption lines from $\nu_1+\nu_3$ band of acetylene broadened by CO_2 . Uncertainties shown by error bars are much smaller than the symbols used.

Fig. 5.9. shows shift coefficients from my study and different other studies using different perturbing gases. The shift coefficients found using CO_2 perturber (present study) are comparatively lower than other studies (N_2 [49], air [42] and H_2 [42]) up to $J = 16$, but gradually decreases afterwards. Another noticeable feature is that the shift coefficients corresponding to CO_2 -broadened acetylene are much higher than the He broadened acetylene study [42], but are lower than the values found from Xe broadened acetylene [42]. A similar trend has been noticed for the broadening parameters and can be explained similarly [42].

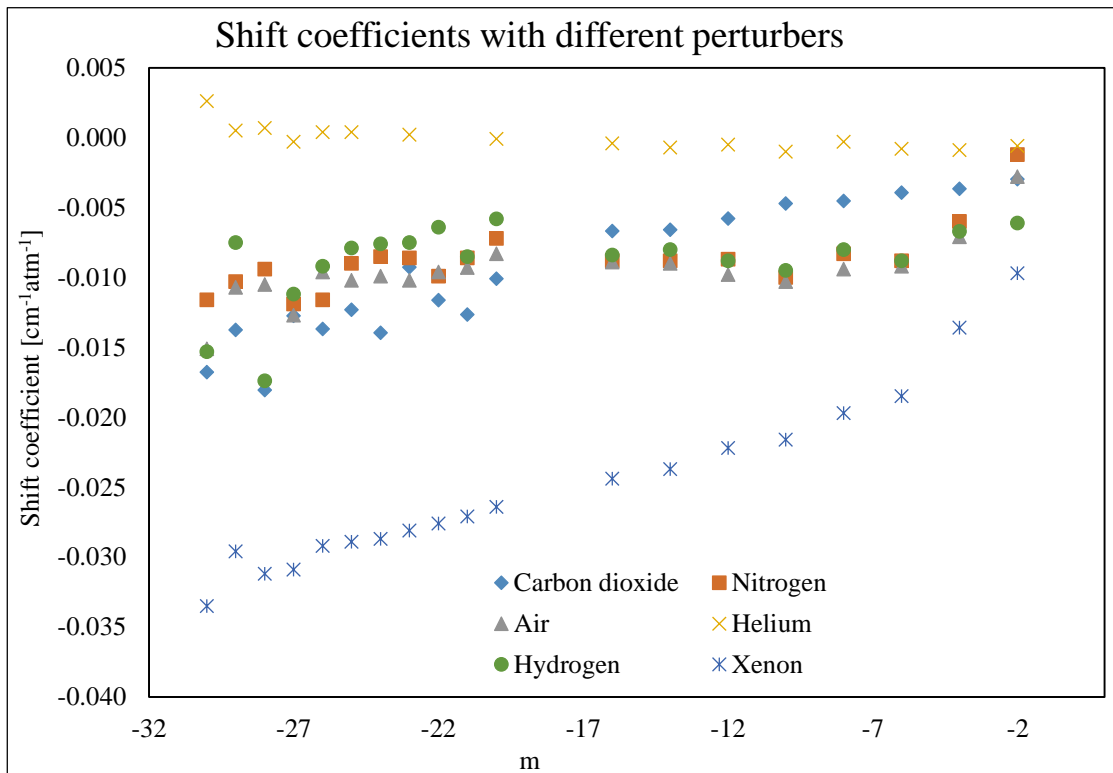


Fig. 5.9. Comparison between pressure-induced shift coefficients from acetylene broadened by CO₂ study and other studies using different perturbing gases.

Fig. 5.10. and 5.11. show the temperature-dependence exponents for broadening and shift for CO₂- and N₂-broadened acetylene. Acetylene broadened by CO₂ shows a gradually decreasing temperature dependence for broadening and shift up to $J = 10$ and $J = 12$ line, respectively. Both these exponents show steady increase afterwards. Also the uncertainties associated with both these parameters are fairly small compared to each measured value.

No previous studies have been done to measure the temperature dependence for acetylene bands broadened by CO₂. However, Hoimonti *et al.* [49] measured the temperature dependence for $\nu_1+\nu_3$ band transitions of acetylene broadened by N₂ gas. N₂-broadened acetylene transitions (for broadening) show comparatively higher temperature

dependence than the CO₂ broadened transitions as shown in fig. 5.10. For shift coefficients perturbed by N₂ (fig. 5.8), dependence on temperature gradually decreases for lines above $J = 10$, whereas the CO₂ study show a steady increase in temperature dependence for higher J lines. Fig. 5.10. also shows the variation of temperature-dependence exponents (for broadening) in comparison to the air-broadened acetylene transitions (calculated) collected from HITRAN database.

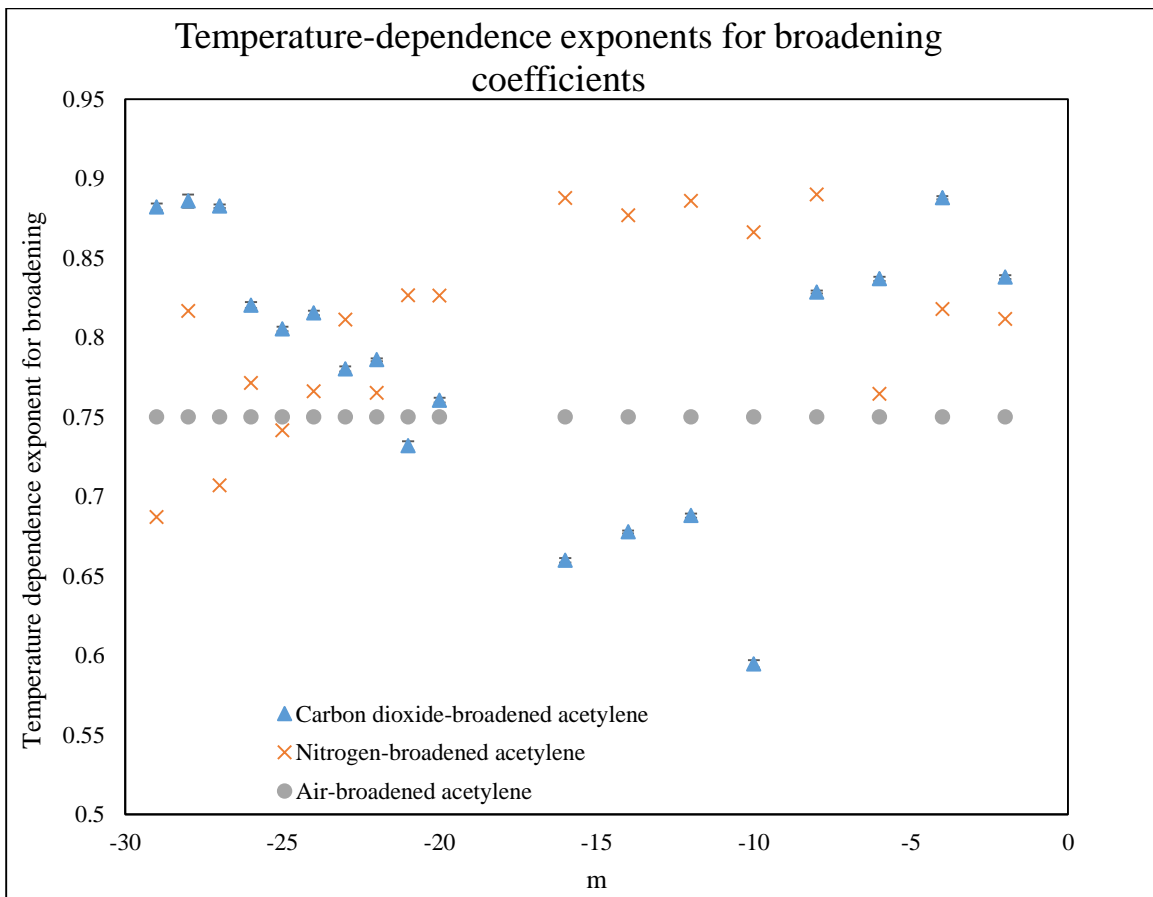


Fig. 5.10. Temperature-dependence exponents from CO₂ (present study) and N₂ [48] broadened Acetylene study, and HITRAN values for air-broadened acetylene (calculated). The observed values are shown with error bars representing uncertainties associated with the non-linear least squares fit.

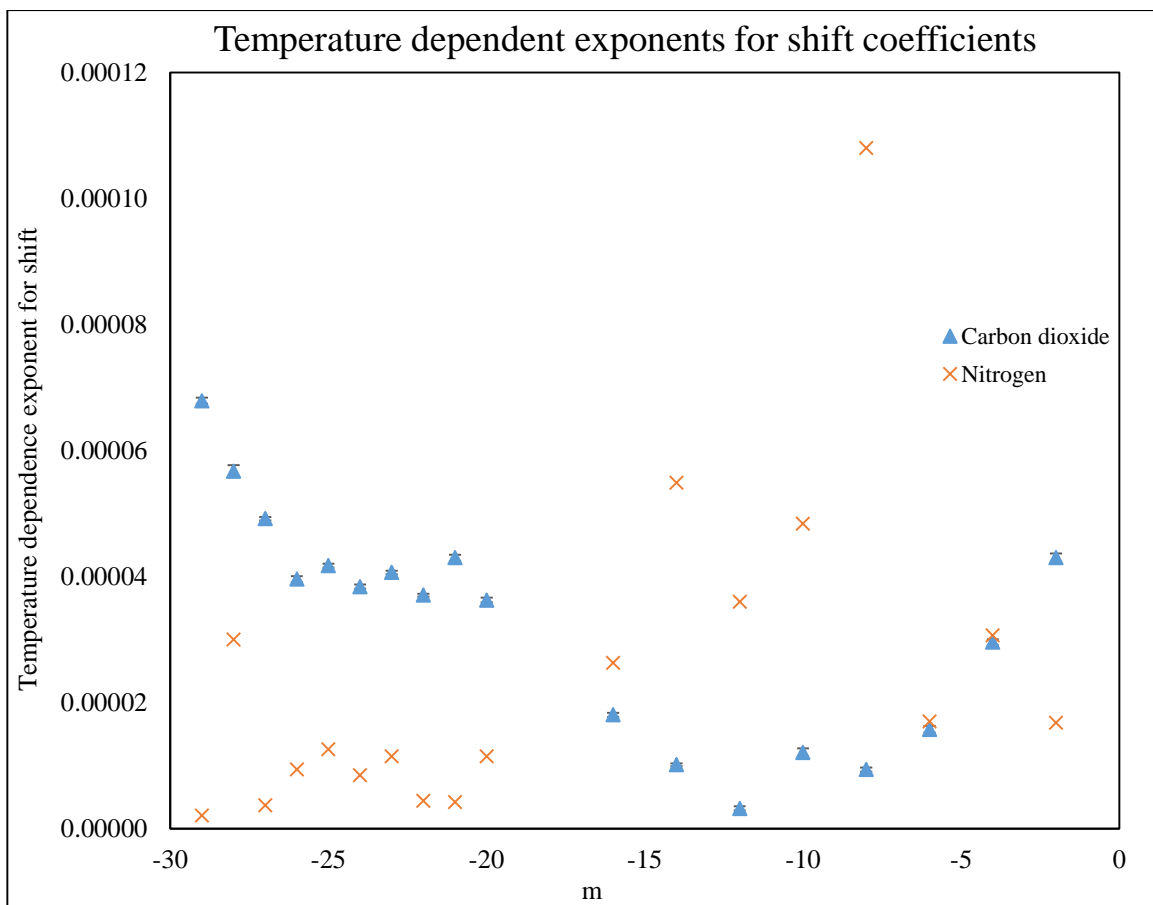


Fig. 5.11. Temperature-dependence exponent of shift coefficients for CO₂ and N₂ perturber. The observed values from the present CO₂ study are shown with error bars.

5.1. Asymmetry in line-shape parameters

It can be noticed from fig. 5.5 that the intensities corresponding to the odd J lines are higher than the even J lines. This alteration in line intensity occurs due to the symmetry properties associated with the acetylene molecule. For molecules like acetylene ($D_{\infty h}$ point group), the even and odd rotational levels have different statistical weights [62, 90], therefore, having different transition probabilities as well as different intensity values for alternate transitions. This may explain the asymmetry in broadening and shift-coefficient values observed for higher J lines ($J > 20$) in fig 5.6 and 5.8. Similarly, the observed temperature-dependent exponents (for broadening and shift coefficients) in fig. 5.10. and

5.11. have abruptly changing values for lines above $J = 20$. In both these figures the odd J lines ($J = 21, 23, 25\dots$) show higher temperature dependence than the neighboring even J lines ($J = 20, 22, 24\dots$). Therefore, it can be concluded that the pressure- and temperature-induced changes in line shapes of absorption lines in acetylene are characterized by the change in line intensities.

5.2. Discussion on measurement accuracy

All the retrieved line parameters and temperature-dependence exponents for broadening and shift have been listed in Table 5.1 and 5.2, respectively. The units used for these parameters are consistent with the HITRAN and GEISA database. A Voigt model has been used to fit for all the recorded spectra. The accuracy of the fitting routine in reproducing the spectra is very important for obtaining precise values for each parameter. The average uncertainty associated with each of these parameters are listed in the following table.

Table 5.3. Average values of uncertainties for each retrieved line-shape parameter.

Line-shape parameters	Average uncertainty
Line position	$2.78 \times 10^{-5} \text{ cm}^{-1}$
Intensity	$1.21 \times 10^{-24} \text{ cm}^{-1}/(\text{cm}^{-2} \cdot \text{molecule})$
Broadening coefficient	$1.21 \times 10^{-4} \text{ cm}^{-1} \text{ atm}^{-1}$
Shift coefficient	$1.35 \times 10^{-4} \text{ cm}^{-1} \text{ atm}^{-1}$
Temperature-dependence exponent for broadening	1.62×10^{-3}
Temperature-dependence exponent for shift	4.25×10^7

The average uncertainty values for all the parameters show very high accuracy which confirms the high efficiency of the fitting routine as well as the fitting profile in reproducing

the recorded spectra. The accuracy of spectroscopic measurements can be tested by making comparisons with database results. The obtained line positions and intensity values in my present study show good agreement with HITRAN and GEISA databases. Also great care was taken during the recording of spectroscopic data to ensure the stability of temperature and pressure inside the gas cell. The average change in temperature and pressure over 4-5 hour period during the scanning of the spectral lines was 0.006 K and 0.108 Torr. This indicates a high stability of gas temperature and pressure maintained during my recordings. Instrumental accuracy is also very important for obtaining accurate results. The wavemeter used for my recording was accurate up to 0.001cm^{-1} and the Fabry-Perot cavity had an accuracy of 0.001 cm^{-1} .

Fig. 5.12. shows simulated intensities of all the acetylene transitions occurring between 6471.75 and 6554.11 cm^{-1} . It can be noticed from the figure that apart from the strong $\nu_1+\nu_3$ transitions, some less intense bands are also located in this region. Therefore, in order to accurately fit for the strong lines of the $\nu_1+\nu_3$ band, we have to take into account the underlying low intensity lines. This was done by identifying all the bands present in this spectral region (belonging to C_2H_2 and its isotopologues $\text{H}^{12}\text{C}^{13}\text{CH}$ and $\text{H}^{12}\text{C}^{12}\text{CD}$) using the HITRAN database and taking those bands into consideration during fitting the spectra. But often, the line-parameter information on the low-intensity bands found in HITRAN are calculated values, therefore not experimentally verified. This may induce some degree ($<10\%$) of uncertainty in my retrieved parameters.

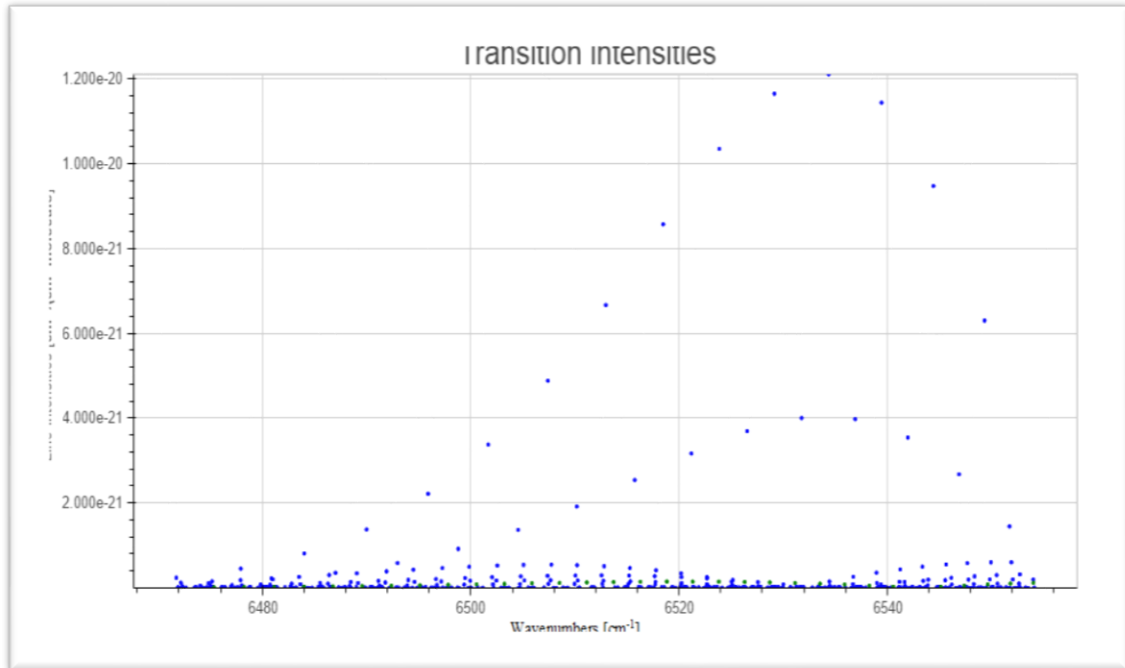


Fig. 5.12. Intensities of all the absorption lines in the spectral region (6471.75 - 6554.11 cm^{-1}) of P branch of $\nu_1+\nu_3$ band of acetylene. [Photo: www.hitran.org]

Overall my retrieved results have good potential to be used as a reference in theoretical modeling of acetylene spectra and will play a significant role in the interpretation of planetary atmospheric spectra in the 1.5 μm spectral region. Specially, the retrieved temperature dependent exponents associated with shift coefficients would be crucial in assigning and identifying spectral signatures of different molecular species at varying temperatures of planetary atmospheres.

5.3. Error budget

In order to measure the precision of retrieved line-shape parameters, it is important to identify and quantify different sources of error which might influence the final results. In case of the TDLS set-up used for the acetylene study, the main sources of uncertainty come from measurement of pressure, temperature and non-linear least squares fit of the

transmission spectra. Using equation 4-4 and 4-5, the Lorentz halfwidth and line position of P14 line at 50 Torr pressure and 276 K temperature can be calculated. The value of halfwidth is 0.007 cm^{-1} . Uncertainty associated with this value can be obtained from using the following formula.

$$\Delta\gamma = \gamma \sqrt{\left(\frac{\Delta p}{p}\right)^2 + 2\left(n \frac{\Delta T}{T}\right)^2 + \left(\frac{\Delta\gamma^0}{\gamma^0}\right)^2}, \quad 5-1$$

where, Δp , ΔT and $\Delta\gamma^0$ are uncertainties associated with pressure, temperature and broadening coefficient (296K). n is the temperature dependent exponent for broadening coefficient. The calculated uncertainty is 6.91×10^{-5} , which is very small.

The pure CO_2 study was carried out at room temperature for different pressures.

Therefore, equation 4-4 can be reduced to

$$\gamma(p) = p \times \gamma^0. \quad 5.2$$

For 12201-03301 band, the HWHM of line Q17 at 50 Torr pressure is 0.007 cm^{-1} . The uncertainty associated with this value can be calculated from the expression,

$$\Delta\gamma = \gamma \sqrt{\left(\frac{\Delta p}{p}\right)^2 + \left(\frac{\Delta\gamma^0}{\gamma^0}\right)^2}. \quad 5.3$$

The calculated uncertainty is 0.0002 cm^{-1} , which is an indicative of highly precious results for the measured line-shape parameters.

Chapter 6. Conclusion

6.1. Summary

The purpose of my research was to study selected ro-vibrational bands of C₂H₂ and CO₂ gas by applying high-resolution spectroscopic techniques (tunable diode laser spectroscopy and Fourier transform spectroscopy). My results contribute to a better understanding of microscopic properties of molecules observable under different temperature and pressure conditions.

In my thesis, line-shape parameters (position, intensity, broadening and line mixing) of Q branch transitions corresponding to three ro-vibrational bands (12201-03301, 11101-10002 and 12201-11102) of pure CO₂ have been reported. The retrieved parameters of position, intensity and broadening have demonstrated good agreement with HITRAN and GEISA databases. Line-mixing parameters have been compared with calculated results obtained using EPG and ECS approximations (fig. 4.7). In this case, the agreement was much worse than other parameters, which may be associated with the weak line strengths of the three bands being studied. Also, the current semi-empirical approaches (Exponential Power Gap law and Energy Corrected Sudden law) for calculating line-mixing coefficients use a relaxation matrix whose diagonal elements are the broadening (real part) and shift coefficients (imaginary part). For obtaining a solution from this matrix formalism, the shift coefficients are ignored in calculation. This may give rise to deference in agreement between experimentally observed and theoretically computed values.

In a second study the line-shape parameters (position, intensity, broadening and shift) of $\nu_1+\nu_3$ band transitions of acetylene (mixed with CO₂) were retrieved using a non-linear least squares fitting software [74, 75]. The obtained parameters of line positions and intensities have shown good agreement with the HITRAN and GEISA databases. In case

of line intensities, the experimentally observed values show systematic deviation from the databases, which may be associated with the line-mixing effects occurring between absorption lines in the $\nu_1+\nu_3$ band. However, no similar studies have been found in literature to make comparisons with the broadening and shift coefficients obtained from my study. Therefore, I made a comparison between my results and results obtained by Arteaga *et al.* [41] and Hoimonti *et al.* [48] using different perturbing species such as N₂, Air, Xe, H₂, He and Xe (fig. 5.7 and 5.9). The temperature-dependence exponents for broadening and shift coefficients have also been reported in this thesis. This is the very first study to report temperature dependence of CO₂-broadened line-shape parameters corresponding to the P branch lines of this band of acetylene.

CO₂ is considered as a greenhouse gas responsible for global warming. Its presence in different planetary atmospheres makes it an important molecular species for spectroscopic studies. The line-shape parameters of CO₂ reported in my thesis would help spectroscopic community in modeling spectroscopic data obtained from terrestrial and planetary atmospheres.

Acetylene is also considered as a pollutant gas in the Earth's atmosphere. Automobile exhaustion is a major source of acetylene. The total amount of pollution caused by the automobile exhaustion can be measured by finding the ratio of the total hydrocarbons to acetylene in the atmosphere. Therefore, in order to accurately measure the concentration of acetylene in air, we need spectroscopic information corresponding to different acetylene bands. The line-shape study of $\nu_1+\nu_3$ band of acetylene reported in this thesis could play a significant role in this regard.

6.2. Future directions

Although I have reported line-mixing coefficients of CO₂ transitions obtained at room temperature, in order to accurately predict the transformation of line shapes at different temperatures, we need to investigate the temperature dependence of line-mixing coefficients.

In order to improve the semi-classical approximations for predicting the impact of line mixing on line shapes, we need to carry out a quantitative investigation by recording a strong band of CO₂ using high resolution spectroscopic technique.

I have used only the Voigt profile to fit for my recorded spectra. Although the fitted residuals were very small, in order to investigate the effects of velocity changing collisions on the spectral lines, speed-dependent line-shape models can be implemented for future studies.

In order to study the atmosphere of a planet, we need accurate information of the concentration of different constituent gases. This can be achieved by creating a gas cell which mimics the atmosphere of the planet of interest. By studying the transformation of absorption line shapes due to changes in the pressure, temperature and concentration of those gases, valuable information can be extracted regarding that atmosphere.

References

- [1] I. Newton, *A Letter of Mr. Isaac Newton, Professor of the Mathematicks in the University of Cambridge; Containing His New Theory about Light and Colors: Sent by the Author to the Publisher from Cambridge, Febr. 6. 1671/72; In Order to be Communicated to the R. Society*, Philosophical Transactions, 1671. **6**: p. 3075-3087.
- [2] G Kirchhoff, R Bunsen, *XLII. Chemical analysis by spectrum observations. — Second memoir*, Philosophical Magazine and Journal of Science 4, 1861. **22**: p. 148.
- [3] J. J. Balmer, *Note on the Spectral Lines of Hydrogen*, Annalen der Physik und Chemie, 1885. **25**: p. 80-85.
- [4] J.M. Hollas, *Modern Spectroscopy*, 4th Edition. 2004.
- [5] R. A. Shaw, H. H. Mantsch, *Vibrational Spectroscopy Applications in Clinical Chemistry: Handbook of Vibrational Spectroscopy 5*. J. M. Chalmers and P. R. Griffiths (Eds), Wiley, Chichester, 2002.
- [6] R. A. Shaw, H. H. Mantsch, *Infrared Spectroscopy in Clinical and Diagnostic Analysis: Encyclopedia of Analytical Chemistry 1*. R. A. Meyers (Ed.), Wiley, Chichester, 2000.
- [7] M. Blanco, J. Coello, H. Iturriaga, S. Maspoch, C. de la Pezuela, *Analyst*. 1998, 135R–150R.
- [8] N. Broad, P. Graham, P. Hailey, A. Hardy, S. Holland, S. Hughes, D. Lee, K. Prebbe, N. Salton, P. Warren, *Guidelines for the Development and Validation of Near-Infrared Spectroscopic Methods in the Pharmaceutical Industry: Handbook of Vibrational Spectroscopy 5*. J. M. Chalmers and P. R. Griffiths (Eds), Wiley, Chichester, 2002.
- [9] B. Stuart, *Infrared Spectroscopy: Fundamentals and Applications*. John Wiley and Sons, Ltd, 2004.
- [10] B. G. Osborne, T. Fearn, *Near-Infrared Spectroscopy in Food Analysis*. Wiley, New York. 1988.
- [11] W. F. McClure, D. L. Stanfield, *Near-infrared Spectroscopy of Biomaterials: Handbook of Vibrational Spectroscopy 1*. J. M. Chalmers and P. R. Griffiths (Eds), Wiley, Chichester, 2002.
- [12] P. Williams, *Near-infrared Spectroscopy of Cereals: Handbook of Vibrational Spectroscopy 5*. J. M. Chalmers and P. R. Griffiths (Eds), Wiley, Chichester, 2002.
- [13] T. Visser, *Infrared Spectroscopy in Environmental Analysis: Encyclopedia of Analytical Chemistry 1*. R. A. Meyers (Ed.), Wiley, Chichester, 2002.

- [14] D. W. T. Griffith, I. M. Jamie, *Fourier-Transform Infrared Spectrometry in Atmospheric and Trace Gas Analysis: Encyclopedia of Analytical Chemistry* 3. R. A. Meyers (Ed.), Wiley, Chichester, 2000.
- [15] R. N. Hall, G. E. Fenner, J. D. Kingsley, T. J. Soltys, R. O. Carlson, *Coherent Light Emission From GaAs Junctions*, Physical Review Letters, 1962. **9** (9): p. 366–369.
- [16] A. Michelson, *The Relative Motion of the Earth and the Luminiferous Ether*, American Journal of Science, 1881. **22**: p. 120–129.
- [17] A. Michelson; E. Morley, *On the Relative Motion of the Earth and the Luminiferous Ether*, **1887**. American Journal of Science. **34** (203): p. 333–345.
- [18] P. Fellgett, *On the Theory of Infra-Red Sensitivities and Its Application to Investigations of Stellar Radiation in the Near Infra-Red*, Thesis, University of Cambridge, 1951.
- [19] J. W. Cooley, J. W. Tukey, *An algorithm for the machine calculation of complex Fourier series*. Mathematics of Computation, 1965. **19**: p. 297-301.
- [20] P. B. Fellgett, *On the ultimate sensitivity and practical performance of radiation detectors*, Journal of Optical Society of America, 1949. **39** (11): 970–976.
- [21] P. Jacquinot, C. J. Dufour, *Optical conditions in the use of photo-electric cells in spectrographs and interferometers*, The National Center for Scientific Research, 1948. **6**: p. 91-103.
- [22] S. Wartewig, *IR and Raman spectroscopy : fundamental processing*, Spectroscopic techniques. 2003, Weinheim, Wiley-VCH: p. 37-40.
- [23] G. G. Abad, N. D. C. Allen, P. F. Bernath, C. D. Boone, S. D. McLeod, G. L. Manney, G. C. Toon, C. Carouge, Y. Wang, S. Wu, M. P. Barkley, P. I. Palmer, Y. Xiao, and T. M. Fu, *Ethane, ethyne and carbon monoxide concentrations in the upper troposphere and lower stratosphere from ACE and GEOS-Chem: a comparison study*, Atmospheric Chemistry and Physics, 2011. **11**: p. 9927–9941.
- [24] E. Davy, *Notice of a new gaseous bicarburet of hydrogen*, Report of the Sixth Meeting of the British Association for the Advancement of Science, **1836**. **5**: p. 62-63.
- [25] Y. L. Yung, W. B. DeMore, *Photochemistry of Planetary Atmospheres*, New York, Oxford University Press 1999.
- [26] J. Li, L. Joly, J. Cousin, B. Parvitte, B. Bonno, V. Zeninari, and G. Durry, *Diode laser spectroscopy of two acetylene isotopologues ($^{12}\text{C}_2\text{H}_2$, $^{13}\text{C}^{12}\text{CH}_2$) in the 1.533 μm region for the PHOBOS-Grunt space mission*, Spectrochimica Acta Part A: Molecular and Biomolecular Spectroscopy, 2009. **74**: p. 1204-1208.

- [27] R. A. Harley, G. R. Cass, *Modeling the atmospheric concentrations of individual volatile organic compounds*, Atmospheric Environment, 1995. **29**: p. 905–22.
- [28] A. M. M. Rao, G. G. Pandit, P. Sain, S. Sharma, T. M. Krishnamoorthy, K. S. V. Nambi. *Non methane hydrocarbons in industrial locations of Bombay*, Atmospheric Environment, 1997. **31**: p. 1077–1085.
- [29] R. A. Whitby and E. R. Altwicker, *Acetylene in the Atmosphere: Sources, Representative Ambient Concentrations and Ratios to Other Hydrocarbons*, Atmospheric Environment, 1978. **12**: p. 1289-1296.
- [30] H. Bovensmann, M. Buchwitz, J. P. Burrows, M. Reuter, T. Krings, K. Gerilowski, O. Schneising, J. Heymann, A. Tretner, and J. Erzinger, *A remote sensing technique for global monitoring of power plant CO₂ emissions from space and related applications*, Atmospheric Measurement Techniques, 2010. **3**: p. 781–811.
- [31] C. Böhringer, *The Kyoto Protocol: A Review and Perspectives*, Oxford Review of Economic Policy Limited, 2003. **19** (3): p. 451-466.
- [32] S. Franck, A. Block, W. von Bloh, C. Bounama, H. J. Schellnhuber, Y. Svirezhev, *Habitable zone for Earth-like planets in the solar system*, Planetary and Space Science, 2000. **48**: p. 1099–1105.
- [33] J. V. Auwera, D. Hurtmans, M. Carleer, M. Herman, *The v_3 fundamental in C₂H₂*, Journal of Molecular Spectroscopy, 1993. **157**: p. 337–357.
- [34] C. P. Rinsland, A. Baldacci, K. N. Rao, *Acetylene bands observed in carbon stars: a laboratory study and an illustrative example of its application to IRC + 10216*, The Astrophysical Journal Supplement Series, 1982. **49**: p. 487–513.
- [35] D. Lambot, A. Olivier, G. Blanquet, J. Walrand, J.P. Bouanich, *Diode-Laser Measurements of Collisional Line Broadening in the Upsilon-5 Band of C₂H₂*. Journal of Quantitative Spectroscopy & Radiative Transfer, 1991. **45**: p. 145-155.
- [36] D. Lambot, J.C. Populaire, J. Walrand, G. Blanquet, J.P. Bouanich, *Diode-Laser Measurements of Self-Broadening Coefficients in the Upsilon (5) Band of C₂H₂ at Low-Temperature*, Journal of Molecular Spectroscopy, 1994. **165**: p. 1-11.
- [37] P. Varanasi, *Intensity and linewidth measurements in the 13.7 μ m fundamental bands of ¹²C₂H₂ and ¹²C¹³CH₂ at planetary atmospheric temperatures*, Journal of Quantitative Spectroscopy and Radiative Transfer, 1992. **47**: p. 263-274.
- [38] D. H. Rank, D. P. Eastman, W. B. Birtley, and T. A. Wiggins, *Shapes and Breadths of Some Molecular Rotation-Vibration Band Lines Perturbed by Rare Gases*. Journal of Chemical Physics, 1960. **33**(2): p. 327-328.

- [39] P. Varanasi, and B. R. P. Bangaru, *Intensity and Half-Width Measurements in the 1.525 μm Band of Acetylene*. Journal of Quantitative Spectroscopy and Radiative Transfer, 1975. **15**(3): p. 267-273.
- [40] P. C. Minutolo, F. D'Amato, and M. De Rosa, *Self- and Foreign-Broadening and Shift Coefficients for C_2H_2 lines at 1.54 μm* . European Physical Journal D, 2001. **17**(2): p. 175-179.
- [41] J. S. Li, G. Durry, J. Cousin, L. Joly, B. Parvitte, V. Zeninari, *Self-broadening coefficients and positions of acetylene around 1.533 μm studied by high-resolution diode laser absorption spectrometry*, Journal of Quantitative Spectroscopy & Radiative Transfer, 2010. **111**: p. 2332-2340.
- [42] S. W. Arteaga, C.M. Bejger, J. L. Gerecke, J. L. Hardwick, Z. T. Martin, J. Mayo, E. A. McIlhattan, J. M. F. Moreau, M. J. Pilkenton, M. J. Polston, B. T. Robertson, and E. N. Wolf, *Line Broadening and Shift Coefficients of Acetylene at 1550 nm*, Journal of Molecular Spectroscopy, 2007. **243** (2): p. 253-266.
- [43] A. S. Pine, *Self-Broadening, N_2 -Broadening and Ar-Broadening and Line Mixing in HCN and C_2H_2* . Journal of Quantitative Spectroscopy & Radiative Transfer, 1993. **50**: p. 149- 166.
- [44] A. Lucchesini, M. De Rosa, D. Pelliccia, A. Ciucci, C. Gabbanini, S. Gozzini, *Diode laser spectroscopy of overtone bands of acetylene*, Applied Physics B-Lasers and Optics, 1996. **63**: p. 277-282.
- [45] B. Martin, J. Walrand, G. Blanquet, J.P. Bouanich, M. Lepere, *CO_2 -broadening coefficients in the $\nu_4 + \nu_5$ band of acetylene*, Journal of Molecular Spectroscopy, 2006. **236** (1): p. 52–57.
- [46] D. Biswas, B. Ray, S. Dutta, P.N. Ghosh, *Diode laser spectroscopic measurement of line shape of $(\nu(1)+3 \nu(3))$ band transitions of acetylene*. Applied Physics B-Lasers and Optics, 1999. **68**, 1125-1130.
- [47] F. Herregodts, D. Hurtmans, J. Vander Auwera, M. Herman, *Laser spectroscopy of the $\nu(1)+3 \nu(3)$ absorption band in $(\text{C}_2\text{H}_2)\text{-C-12}$. I. Pressure broadening and absolute line intensity measurements*, Journal of Chemical Physics, 1999. **111**: p. 7954-7960.
- [48] C. Yelleswarapu, A. Sharma, *Pressure-induced self-broadening and frequency shift measurements of absorption lines of acetylene using tunable diode laser absorption spectroscopy*, Journal of Quantitative Spectroscopy & Radiative Transfer, 2001. **69**: p. 151-158.
- [49] H. Rozario, J. Garber, C. Povey, D. Hurtmans, J. Buldyreva, and A. Predoi-Cross, *Experimental and theoretical study of N_2 -broadened acetylene line parameters in the $\nu_1+\nu_3$ band over a range of temperatures*, Molecular Physics, 2012. **110** (21–22): p. 2645–2663.

- [50] N. T. Campbell, J. D. Cook, B. A. Coombs, E. P. Fuller, J. L. Hardwick, S. M. Hurley, L. K. Ho, P. A. Kovac, E. J. Robertson, E. N. Senning, J. K. Utterback, and R. S. Wisler, *Temperature Dependence of Pressure Broadening and Shifts of Acetylene at 1550 nm by N₂*, *Molecular Physics*, 2011. **109**(17-18): p. 2199-2208.
- [51] C. Povey, A. Predoi-Cross, D. R. Hurtmans, *Line shape study of acetylene transitions in the nu(1) + nu(2) + nu(4) + nu(5) band over a range of temperatures*, *Journal of Molecular Spectroscopy*, 2011. **268**: p. 177-188.
- [52] L. L. Strow and B. M. Gentry, *Rotational collisional narrowing in an infrared CO₂ Q branch studied with a tunable-diode laser*, *The Journal of Chemical Physics*, 1986. **84**: p. 1149-1156.
- [53] B. Gentry and L. L. Strow, *Line mixing in a N₂-broadened CO₂ Q branch observed with a tunable diode laser*, *The Journal of Chemical Physics*, 1987. **86**: p. 5722-5730.
- [54] M. V. Tonkov, J. Boissoles, R. Le Doucen, B. Khalil, F. Thibault, *Q-BRANCH SHAPES OF CO₂ SPECTRUM IN 15 μm REGION: EXPERIMENT*, *Journal of Quantitative Spectroscopy and Radiative Transfer*, 1996. **55**: p. 321-334.
- [55] A. Predoi-Cross, A. D. May, A. Vitcu, and J. R. Drummond, J.-M. Hartmann and C. Boulet, *Broadening and line mixing in the 2000←0110, 1110←0000 and 1220←0110 Q branches of carbon dioxide: Experimental results and energy-corrected sudden modeling*, *Journal of Chemical Physics*, 2004. **120** (22): p. 10520-10529.
- [56] J. Buldyreva, N. Lavrentieva, V. Starikov, *Collisional Line Broadening and Shifting of Atmospheric Gases 2011*, Imperial College Press.
- [57] M. Mueller, *Fundamentals of Quantum Chemistry* 2001, Plenum Publishers, New York.
- [58] P. F. Bernath, *Spectra of Atoms and Molecules* 1995, New York: Oxford University Press, 400.
- [59] P. Bouguer, *Essai d'optique sur la gradation de la lumière*, Paris, France: Claude Jombert, 1729. p. 16–22.
- [60] J. H. Lambert, *Photometria sive de mensura et gradibus luminis, colorum et umbrae*, Germany: Eberhardt Klett, 1760. p. 391.
- [61] Beer, *Determination of the absorption of red light in colored liquids*, *Annalen der Physik und Chemie*, 1852. **86**: p. 78–88.
- [62] M. Simeckova, D. Jacquemart, L. S. Rothman, R. R. Gamache, A. Goldman, *Einstein A-coefficients and statistical weights for molecular absorption transitions in the HITRAN database*, *Journal of Quantitative Spectroscopy & Radiative Transfer*, 2006. **98**: p. 130–155.

- [63] J. Humblíček, *Optimized computation of the Voigt and complex probability functions*. Journal of Quantitative Spectroscopy & Radiative Transfer, 1982. **27**: p. 437-441.
- [64] M. Kuntz, *A New Implementation of the Humblíček Algorithm for the calculation of Voigt Profile Function*. Journal of Quantitative Spectroscopy & Radiative Transfer, 1997. **57**: p. 819-824.
- [65] P. R. Berman, *Speed-Dependent Collisional Width and Shift Parameters in Spectral Profiles*. Journal of Quantitative Spectroscopy & Radiative Transfer, 1972. **12**: p. 1331.
- [66] R. H. Dicke, *The Effect Of Collisions Upon The Doppler Width Of Spectral Lines*. Physical Review, 1953. **89**: p. 472-473.
- [67] J. P. Wittke & R. H. Dicke, *Redetermination of Hyperfine Splitting in the Ground State of Atomic Hydrogen*. Physical Review, 1956. **103**: p. 620-631.
- [68] L. Galatry, *Simultaneous Effect of Doppler and Foreign Gas Broadening on Spectral Lines*. Physical Review, 1961. **122**: p. 1218.
- [69] S. G. Rautian, I. I. Sobelman, *Influence of Collisions on Doppler's width of Spectral Lines*. Soviet Physics Uspekhi-Ussr, 1966. **9**: p. 701.
- [70] S. Chandrasekhar, *Stochastic Problems in Physics and Astronomy*. Review of Modern Physics, 1943. **15**: p. 1-89.
- [71] P. W. Rosenkranz, *Shape of the 5mm Oxygen Band in Atmosphere*. IEEE Transactions on Antennas and Propagation, 1975. **23**: p. 498-506.
- [72] A. Levy, N. Lacome, C. Chackerian Jr., K. Narahari Rao, *Spectroscopy of the Earth's Atmosphere and of the Interstellar Medium*, A. Weber (Eds.) 1992, Academic Press, New York, p. 261-337.
- [73] A. Predoi-Cross, A.V. Unni, W. Liu, I. Schofield, C. Holladay, A. R. W. McKellar, D. Hurtmans, *Line shape parameters measurement and computations for self-broadened carbon dioxide transitions in the 30012← 00001 and 30013← 00001 bands, line mixing, and speed dependence*. Journal of Molecular Spectroscopy, 2007. **245**: p. 34-51.
- [74] F. Niro, K. Jucks, J. -M. Hartmann, *Spectral calculations in central and wing regions of CO₂ IR bands. IV: Software and database for the computation of atmospheric spectra*, Journal of Quantitative Spectroscopy and Radiative Transfer, 2005. **95**: p. 469-481.
- [75] F. Niro, C. Boulet, J. M. Hartmann. *Spectra calculations in central and wing regions of CO₂ IR bands between 10 and 20 mm: I: model and laboratory measurements*, Journal of Quantitative Spectroscopy and Radiative Transfer, 2005. **88**: p. 483-498.

- [76] R. Rodrigues, K. W. Jucks, N. Lacome, Gh. Blanquet, J. Walrand, W. A. Traub, B. Khalile, R. Le Doucenc, A. Valentin, C. Camy-Peyret-, L. Bonamy and J.-M. Hartmann, *Model, Software, And Database For Computation Of Line-Mixing Effects In Infrared Q Branches Of Atmospheric Co₂—I. Symmetric Isotopomers*, *Journal of Quantitative Spectroscopy and Radiative Transfer*, 1999. **61**(2): p. 153-184.
- [77] L. S. Rothman, I. E. Gordon, Y. Babikov *et al.*, *The HITRAN2012 molecular spectroscopic database*, *Journal of Quantitative Spectroscopy and Radiative Transfer*, 2013. **130**: p. 4-50.
- [78] D. C. Benner, C. P. Rinsland, V. M. Devi, D. Atkins, *A Multispectrum Nonlinear Least Squares Fitting Technique*. *Journal of Quantitative Spectroscopy and Radiative Transfer*, 1995. **53** (6): p. 705-721.
- [79] L. R. Brown, D. C. Benner, V. M. Devi, M. A. H. Smith, R. A. Toth, *Line Mixing in Self and Foreign-Broadened Water Vapor at 6 μ m*, *Journal of Molecular Structure*, 2005. **742** (1–3): p. 111-122.
- [80] P. L. Chebyshev, *Théorie des mécanismes connus sous le nom de parallélogrammes*, Mémoires des Savants étrangers présentés à l'Académie de Saint-Pétersbourg, 1854. **7**: p. 539–586.
- [81] K. Levenberg, *A Method for the Solution of Certain Problems in Least-squares*, *The Quarterly of Applied Mathematics*, 1944, **2**: p. 164-168.
- [82] D. W. Marquardt, *An Algorithm for Least-Squares Estimation of Nonlinear Parameters*, *Journal of the Society for Industrial and Applied Mathematics*, 1963. **11** (2): p. 431-441.
- [83] V. M. Devi, D. C. Benner, L. R. Brown, C. E. Miller, R. A. Toth, *Line Mixing and Speed Dependence in CO₂ at 6348 cm⁻¹: Positions, Intensities, and Air- and Self-Broadening Derived With Constrained Multispectrum Analysis*, *Journal of Molecular Spectroscopy*, 2007. **242**: p. 90-117.
- [84] R. A. McClatchey, W. S. Benedict, S. A. Clough, D. E. Burch, R. F. Calfee, K. Fox, L. S. Rothman, J. S. Garing, *AFCRL Atmospheric Absorption Line Parameters Compilation*, Environmental Research Papers No. **434**, 1973.
- [85] L. S. Rothman, L. D. G. Young, *Infrared Intensities Energy Levels And Of Carbon Dioxide-II*, *Journal of Quantitative Spectroscopy and Radiative Transfer*, 1981. **25**: p. 505-524.
- [86] B. J. Drouin, D. Chris Benner, L. R. Brown, M. J. Cich, T. J. Crawford, V. M. Devi, A. Guillaume, J. T. Hodges, E. J. Mlawer, D. J. Robichaud, F. Oyafuso, V. H. Payne, K. Sung, E. H. Wishnow, S. Yu, *Multispectrum Analysis of the Oxygen A-Band*, *Journal of Quantitative Spectroscopy & Radiative Transfer*, <http://dx.doi.org/10.1016/j.jqsrt.2016.03.037>.

- [87] N. A. Lavrentiev, M. M. Makogon & A. Z. Fazliev, *Comparison of the HITRAN and GEISA spectral databases taking into account the restriction on publication of spectral data*, Atmospheric and Oceanic Optics, 2011. **24**: p. 436-451.
- [88] N. Jacquinet-Husson, R. Armante, N. A. Scott, A. Chédin, L. Crépeau, C. Boutammine, A. Bouhdaoui, C. Crevoisier, V. Capelle, C. Boone, N. Poulet-Crovisier and others, *The 2015 edition of the GEISA spectroscopic database*, Journal of Molecular Spectroscopy, 2016. **327**: p. 31-72.
- [89] F. Thibault, *Theoretical He-broadening coefficients of infrared and Raman C₂H₂ lines and their temperature dependence*, Journal of Molecular Spectroscopy, 2005. **234**: p. 286–288.
- [90] G. Herzberg, *Molecular Spectra and Molecular Structure II. Infrared and Raman Spectra of Polyatomic Molecules*, Lancaster Press, Inc., Lancaster, 1964.